Two-year moored records of dense-water production and flow through a gap in the Mid-Atlantic Ridge north of Iceland

Silje Skjelsvik

Master's Thesis in Physical Oceanography

Geophysical Institute

January 2020

Abstract

In this master's thesis, I have investigated dense-water production and flow through a channel across the Mid-Atlantic Ridge north of Iceland. The channel connects the East Greenland Current to the west and the central Iceland Sea to the east, and is named Eggvin Offset. Data for this study were obtained from the Eggvin Offset Mooring, three hydrographic/velocity surveys, and an Argo float which was deployed near the mooring. The Eggvin Offset Mooring was deployed on the southern slope of the channel from August 2016 to June 2018, and formed the basis of this study with high temporal hydrographic and velocity measurements.

Air-sea-ice interactions, mixed-layer evolution, and dense-water transports were further investigated in the Eggvin Offset over the two years the mooring was deployed. Hydrographic variability was linked to the sea ice extent, large-scale winds, and atmospheric heat fluxes, which revealed differences between winter 2016-17 and winter 2017-18. The water in the mixed layer the first winter was in general denser and deeper compared to the second winter. Moreover, higher turbulent heat fluxes and stronger northerly winds were found in the area the first winter. The sea ice edge was nearer the mooring the first winter than it was the following year. The observations also revealed that sufficiently dense water ($\sigma_\theta \geq 27.8\,\mathrm{kg/m^3}$) to contribute to the overflows across the Greenland-Scotland Ridge was formed in the channel. Water dense enough to supply the North Icelandic Jet ($\sigma_\theta > 28.03\,\mathrm{kg/m^3}$), and thereby also the densest component of the Atlantic Meridional Overturning Circulation, was, however, not formed in this region.

Transports of two dense-water layers were estimated. One estimation was done for the mixed layer, when the density was higher than the overflow water limit. The second transport was estimated for the depths corresponding to the properties of the North Icelandic Jet transport mode water. The velocities in the channel were generally directed eastward, into the Iceland Sea, in particular at intermediate and greater depths. However, the velocities were low, and so were the transports. Hence, from the available observations, the Eggvin Offset is neither an important pathway, nor source, of dense water to the Denmark Strait Overflow Water.

Acknowledgments

Wow, where to begin. The last two years have gone so fast. It has been hectic, but also very enjoyable. The journey has taken me from arranging a national climate and energy conference with my amazing fellows at "Geofysen" to chasing polar storms in the Iceland and Greenland Seas. And from work with "Værtinnen og Havmesteren" to Harvard, MIT and WHOI. I have met so many good and inspiring people along the way, and I have experienced so much that I will carry with me in life after master's.

Speaking of good people. There are so many I would love to thank for supporting me the last two years. I will start by thanking my supervisor Kjetil Våge, for giving me the opportunity to embark on the two journeys to the Iceland and Greenland Seas, to WHOI and, not to mention, Jan Mayen! I am forever grateful for all the new experiences and for everything I have learned about the sea, seasickness and "spadame". I would also like to thank my co-supervisor Stefanie Semper, for your support and teaching (and for loving hiking and running too).

I would also like to give thanks to Ilker Fer, for helping me out with the data processing, to Helge Bryhni for good talks about the instruments attached to the mooring, and to the OVENS group, for good scientific discussions. Thank you Ailin Brakstad for helping me out with the Seaguard. Thanks to Chris Barrell, Annic Terpstra and Denis Sergeev for helping me out with atmospheric data and good talks about polar storms. Thank you, Øyvin Paasche and several others from UiB, for making my trip to Boston and Harvard possible. Thank you, Helge Drange, for being a source of inspiration, for your support with all the ongoing projects and for proof-reading my master's thesis.

I would also like to thank friends and family, and all my fellow study mates. Life in general would not be the same without you! Thanks to everyone in the About Tomorrow Foundation, for trying to make the world a little greener and better every day. A special thanks to my partner in crime, Even. I really appreciate your humor, your good cooking skills, and for always believing in me. Finally, thank you Eplehuset AS, for equipping me with a (recycled) MacBook, such that I could do all the hard core programming (nearly) without problems.

Contents

Abstract i

Acknowledgments iii

1 Introduction **2**

2 Background **4**

2.1 The Nordic Seas 4

2.1.1 Circulation in the Nordic Seas 6

2.1.2 Sources and pathways of overflow water 8

2.2 The meandering Polar Front 9

2.3 Air-sea-ice interaction in the Iceland Sea 10

3 Data and methods **13**

3.1 The Eggvin Offset Mooring 13

3.2 Additional data 14

3.3 Current data 17

3.4 Calibration 18

3.5 Synthetic salt data 22

3.6 Mixed-layer depth 23

3.7 Transport estimates 26

4 Results **30**

4.1 On the hydrography of the Eggvin Offset 30

4.1.1 Atmospheric forcing 46

4.1.2 The impacts of sea ice 58

4.2 Flow through the Eggvin Offset 60

5 Discussion **68**

5.1 On the hydrography of the Eggvin Offset 68

5.2 Evolution of the mixed-layer depth 70

5.3 Comparison of winter 2016-17 and winter 2017-18 71

5.4 Dense water transport through the Eggvin Offset 73

6 Conclusion **75**

7 Future work **77**

Bibliography **79**

Chapter 1

Introduction

The target area of this thesis is the Eggvin Offset, a gap in the Mid-Atlantic Ridge in the northwestern Iceland Sea (Fig. 2.1). This is a small area in the Nordic Seas where deep-water formation takes place. The dense water formed in the Nordic Seas spills over the Greenland-Scotland Ridge (GSR) into the North Atlantic and maintains the lower limb of the Atlantic Meridional Overturning Circulation (AMOC). Changes in strength and pattern of the AMOC impact global climate, as it is a major distributor of heat from lower to higher latitudes (Scheffer *et al.*, 2001; Lenton *et al.*, 2008; Furevik *et al.*, 2007). It is therefore of interest to investigate the largest and densest component to the North Atlantic Deep Water (NADW), which is the Denmark Strait Overflow Water (DSOW; Dickson and Brown, 1994).

Several hypotheses on the origin and pathways of the DSOW have been proposed. Today we know that there are two major currents that transport dense water to the sill at Denmark Strait: the East Greenland Current (EGC) and the North Icelandic Jet (NIJ; Fig. 2.1). The EGC is the western branch of the cyclonic boundary current system around the Nordic Seas (Mauritzen, 1996), and carries modified Atlantic-origin Water and Polar Surface Water (PSW) southward. Dense water transported by the EGC is responsible for about two thirds of the total dense-water transport (Harden *et al.*, 2016). The NIJ, on the other hand, is a current along the northern slope of Iceland (Semper *et al.*, 2019), which transports the densest water to Denmark Strait (Våge *et al.*, 2011). The locations where these waters are formed and their pathways to the NIJ are, however, still being investigated.

The deepest and densest mixed layers in the Iceland Sea occur in the northwestern part (Våge *et al.*, 2015). However, details about the deep-water formation and circulation in this region are unclear as the region is sparsely sampled, especially during winter. This is due to sea ice cover and rough weather conditions. The lack of observations in this area was the motivation to deploy a mooring in the Eggvin Offset, which consisted of 25 hydrographic and velocity instruments, resulting in a data set with high temporal and vertical resolution. The mooring was deployed over two years from August 2016 to June 2018, and the data set provids the basis for this study.

Hydrographic variability in the upper ocean has been linked to sea ice extent and to regional and local atmospheric forcing. Analyses of the hydrographic properties, the mixed-layer evolution, and seasonal variability have been conducted to address the importance of the Eggvin Offset. Is atmospheric driven open-ocean convection in the Eggvin Offset an important source to the NIJ, and hence, to the lower limb of the AMOC? Is the channel an important pathway of dense-water transport between the Greenland and Iceland Seas?

Chapter 2

Background

2.1 The Nordic Seas

The Nordic Seas occupy the region between Greenland in the west, Norway in the east, Svalbard in the north and the GSR in the south (black line in Fig. 2.1). The area encompasses the Norwegian, Greenland, and Iceland Seas, and represents approximately 1% of the area of the world's ocean (Furevik *et al.*, 2007). The Nordic Seas connect with the Arctic Ocean through the Barents Sea and Fram Strait to the north, and with the North Atlantic to the south. As such, the Nordic Seas enable cold and fresh Polar Water to mix with warm and saline Atlantic Water (AW). Moreover, the blending of different origin water masses and the presence of extremely cold air temperatures during winter and sea ice make the Nordic Seas of key importance for the AMOC (Chafik and Rossby, 2019).

The northern branch of the Mid-Atlantic Ridge stretches from the Icelandic shelf to Fram Strait, and separates the Iceland and Greenland Seas to the west from the Norwegian Sea to the east. The Iceland and Greenland Seas are characterized by a pronounced cyclonic circulation due to the large-scale wind pattern (the westerlies and the polar easterlies). The cyclonic circulations in the Iceland and Greenland Seas are known as gyres, which are separated from each other by the West Jan Mayen Ridge. The gyre circulation is stronger in the Greenland Sea than in the Iceland Sea, due to stronger atmospheric forcing and steeper bathymetry (Voet *et al.*, 2010;

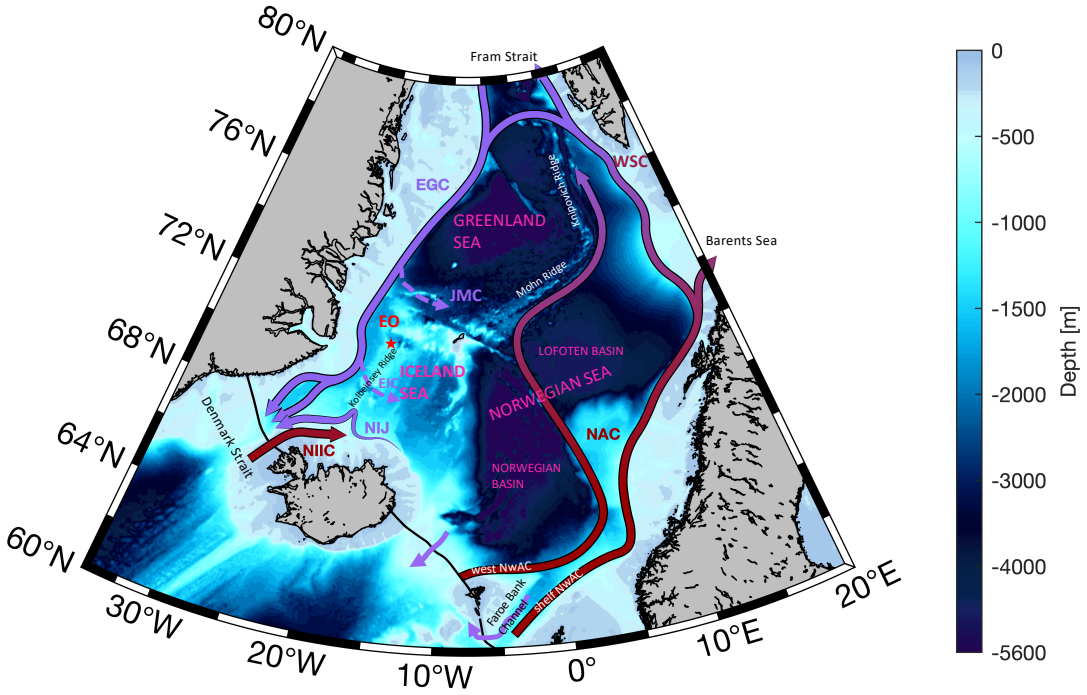

Figure 2.1: Map of the bathymetry and general circulation in the Nordic Seas. Red colors represent inflow of warm Atlantic Water and purple colors represent cold and dense waters flowing southward. The red star is the location of the Eggvin Offset Mooring. The acronyms are the Eggvin Offset (EO), the North Icelandic Irminger Current (NIIC), the North Icelandic Jet (NIJ), the East Icelandic Current (EIC), the Jan Mayen Current (JMC), the West Spitsbergen Current (WSC), the East Greenland Current (EGC), the western and eastern ('shelf') branch of the Norwegian Atlantic Current (NwAC), and the North Atlantic Current (NAC). The color shading is the bathymetry from ETOPO1.

Moore *et al.*, 2015). This favors the Greenland Sea as the prime location of deep-water formation compared to the Iceland Sea, which is in general shallower, less stratified, and more dependent on the sea ice edge to allow for deep-water formation.

From Iceland to Jan Mayen the Mid-Atlantic Ridge is known as the Kolbeinsey Ridge, and it separates the westernmost part of the Iceland Sea from the central and eastern parts. Two major gaps exist across the Kolbeinsey Ridge: the Eggvin Offset and the Spar Offset, often referred to as the Spar Fracture Zone, (Fig. 2.2a). The Eggvin Offset, which is the focus of this study, is located between the mid- and northern part of the Kolbeinsey Ridge. The northern part of the Kolbeinsey Ridge is known in literature as the Eggvin Bank (Fig. 2.2b) and is located west of the Jan Mayen Micro Continent (Tan *et al.*, 2017).

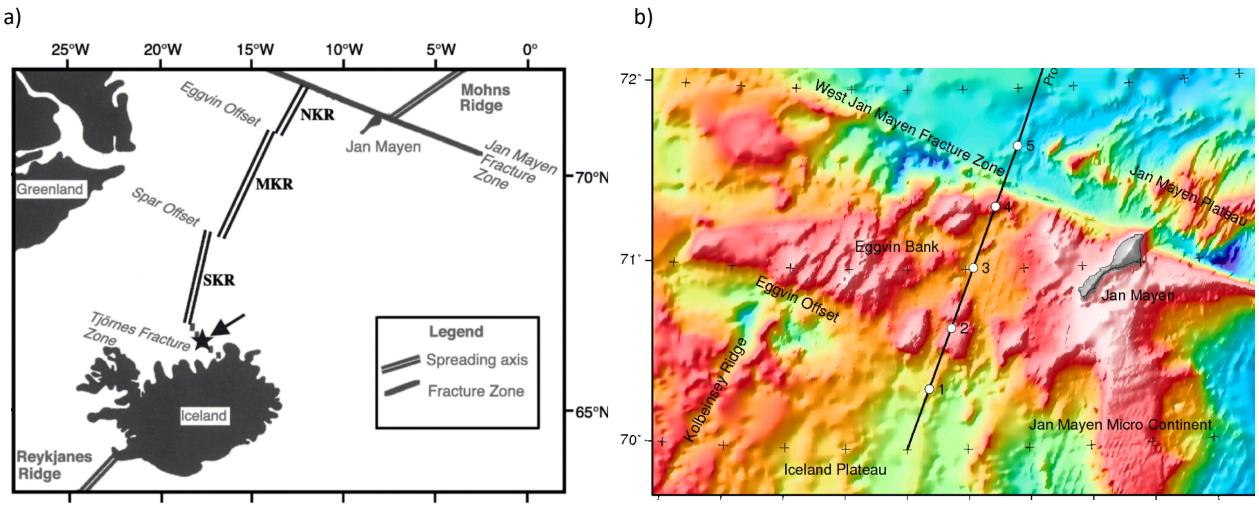

Figure 2.2: An overview of the northern branch of the Mid-Atlantic Ridge on the Iceland Plateau and its major, zonal gaps. a) From south, the South Kolbeinsey Ridge (SKR), Mid Kolbeinsey Ridge (MKR) and the North Kolbeinsey Ridge (NKR) are shown. b) Bathymetry of the Eggvin Offset region. Figures by courtesy of Thibaut Barreyre, University of Bergen, KG Jebsen Centre for Deep Sea Research, 2018.

2.1.1 Circulation in the Nordic Seas

Warm and saline AW enters the Nordic Seas east and west of Iceland. The largest inflow enters in the surface layer in the Faroe Bank Channel east of Iceland and is carried poleward by the northern extension of the Gulf Stream, named the North Atlantic Current (Østerhus *et al.*, 2019). This current separates into two branches before reaching the Nordic Seas (Fig. 2.1). While the western Norwegian Atlantic Current (NwAC) follows the western rim of the Norwegian Basin towards the Mid-Atlantic Ridge north of Jan Mayen (Mohn and Knipovich Ridges), the east NwAC continues along the Norwegian coast. The AW is modified on its way northward by strong heat loss to the atmosphere and from mixing with colder water masses (Mauritzen, 1996). One branch of the east NwAC veers off into the Barents Sea north of Norway, before it circulates the Arctic Ocean. The rest continues northward along western Svalbard as West Spitsbergen Current (WSC). One portion of the WSC continues into the Arctic Ocean when reaching Fram Strait. The other portion subducts under less dense PSW and joins the EGC southward at intermediate depths.

The EGC flows along the Greenland continental slope from Fram Strait to Denmark Strait. The current consists of three branches: the shelfbreak EGC situated close to the Greenland shelf

break, the Polar Surface Water Jet flowing on the continental shelf, and the outer EGC located near the mid-to-deep continental slope (Håvik *et al.*, 2017). By use of two shipboard surveys in summer 2012, Håvik *et al.* (2017) observed that velocities north and south of Jan Mayen in the outer branch of EGC were directed eastward, toward the Iceland and Greenland Seas (Fig. 2.3). This indicates that water from the EGC could flow through the Eggvin Offset and into the Iceland Sea, which is the topic of investigation in this study.

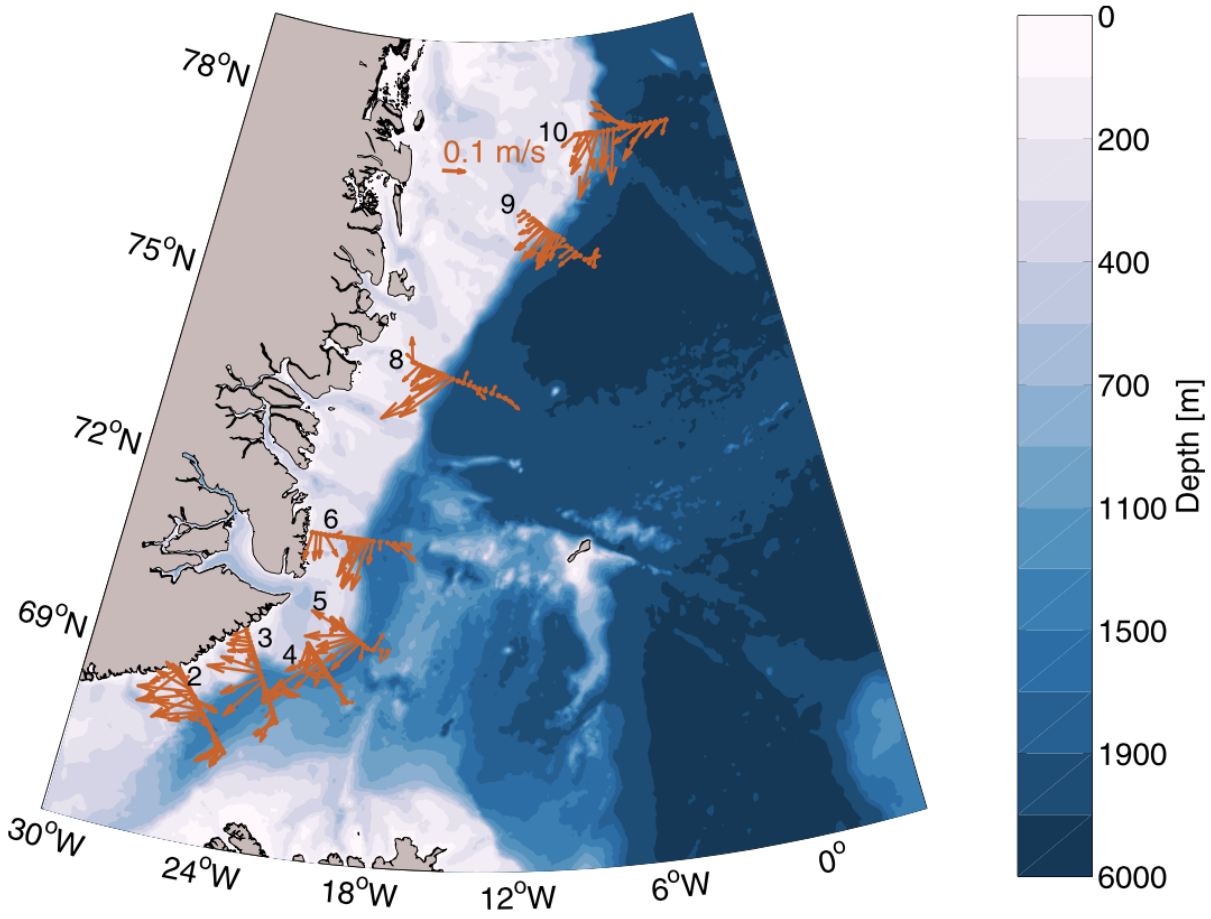

Figure 2.3: Depth-integrated velocity vectors for the upper 500 m (red arrows) and water depth (color shading). Data were collected from a shipboard survey in summer 2012. Section number 6 shows flow towards the Eggvin Offset (Fig. 5 from Håvik *et al.*, 2017).

Upstream of Denmark Strait, at the northern tip of the Blosseville Basin, the EGC bifurcates into a shelfbreak branch and a separated branch. The former continues along the Greenland shelf break, while the latter flows along the eastern rim of the Blosseville Basin and continues

southward along the base of the Iceland slope, through Denmark Strait. East in Denmark Strait, a less significant portion of AW enters the Nordic Seas in the North Icelandic Irminger Current (NIIC). This current follows the western Icelandic continental slope, and is hypothesized to be the upper limb of a local overturning cell (Våge *et al.*, 2011). The lower limb of this cell is the NIJ, which flows along the northern Iceland continental slope towards Denmark Strait.

2.1.2 Sources and pathways of overflow water

Water sufficiently dense to contribute to the overflow water east and west of Iceland are formed in the Nordic Seas. Overflow water is identified by a lower potential density limit of $\sigma_\theta = 27.8\,\mathrm{kg/m^3}$ (Dickson and Brown, 1994). DSOW accounts for approximately half of the overflow water that spills over the GSR and encompasses the largest portion of the densest overflow water. The other half spills over the ridge east of Iceland, where the largest plume is the Faroe Bank Channel Overflow Water (FBCOW). The FBCOW accounts for one third of the total overflow transport (Hansen *et al.*, 2016; Østerhus *et al.*, 2019). The formation and circulation of these overflow waters are important for the global climate, as they feed the lower limb of the AMOC (Harden *et al.*, 2016; Østerhus *et al.*, 2019; Chafik and Rossby, 2019).

Most of the NADW is formed in the Nordic Seas (Gebbie and Huybers, 2010). Today we know that this happens in two ways. One is the modification of AW that circulates cyclonically around the periphery of the Nordic Seas (Mauritzen, 1996; Rudels *et al.*, 2002; Tanhua *et al.*, 2005; Köhl *et al.*, 2007; Eldevik *et al.*, 2009). The resulting product is referred to as Atlantic-origin Water (Våge *et al.*, 2011) and comprises the largest contribution to the DSOW, and hence the NADW (Harden *et al.*, 2016). The other major contribution to the DSOW is the Arctic-origin Water. This is water formed by open-ocean convection in the Greenland and Iceland Seas (Swift *et al.*, 1980; Mastropole *et al.*, 2017), and is carried toward Denmark Strait primarly by the NIJ (Jonsson and Valdimarsson, 2004; Våge *et al.*, 2011; Semper *et al.*, 2019).

Several hypotheses of the origin and pathway of DSOW have been proposed through time, and the importance of the Iceland Sea has been debated. Water sufficiently dense to contribute to the DSOW is ventilated throughout the Iceland Sea gyre. The densest component was, on the

other hand, not observed ventilated, but rather found at intermediate and great depths (Våge *et al.*, 2015). This indicates that the product of wintertime convection in the Iceland Sea may not be a significant source of the densest portion to the DSOW. It further implies that this water must be formed somewhere else and transported to the Iceland Sea gyre to supply the NIJ.

Dense-water transport by the NIJ can account for approximately one third of the total DSOW and does also constitute the densest portion of the DSOW ($\sigma_\theta \geq 28.03\,\mathrm{kg/m^3}$; Våge *et al.*, 2011; Harden *et al.*, 2016). However, Semper *et al.* (2019) argues that the contribution of water from the NIJ to the Denmark Strait overflow is higher than previously estimated. Such dense water has been observed in the Greenland Sea gyre at intermediate depths in winter (Brakstad *et al.*, 2019), which strengthens the hypothesis that the densest portion of the DSOW is formed in the Greenland Sea and transported to the Iceland Sea (Våge *et al.*, 2015; Pickart *et al.*, 2017). This is further supported by Messias *et al.* (2008), who found evidence of a rapid connection between the basins through tracer experiments. More details of how and where this dense water is transported to the Iceland Sea, and hence to the NIJ, is yet to be revealed.

2.2 The meandering Polar Front

The Nordic Seas encompasses three domains, from west: the Polar, the Arctic, and the Atlantic domains (Swift and Aagaard, 1981). The inflows of warm, saline water to the east, and fresh, cold water to the west result in large zonal temperature and salinity gradients across the Nordic Seas. These characteristics have been used to define the different domains. The Arctic domain consists of the Iceland and Greenland Seas, and is separated from the Atlantic domain by the Arctic Front. The Polar and Arctic domains, on the other hand, are separated by the Polar Front, which is defined by the 34.5 isohaline (converted to 34.66 g/kg as Absolute Salinity is used further on in this study; Swift and Aagaard, 1981).

Langehaug *et al.* (prep) investigate a relationship between the fluctuations in the total freshwater transport, large-scale wind stress, and surface salinity in the Arctic domain. They have found that the seasonal variations of freshwater transport to the deep basins are dominated by variations in the sea ice transport, which are related to large-scale wind stress in the area. The

northerly winds are stronger than normal during fall and winter, and the freshwater transport reaches its largest value in winter (as the main freshwater transport is sea ice through Fram Strait). During spring and summer, the northerly winds weaken and the freshwater transport is in general low, as less sea ice enters the Nordic Seas from the Arctic Ocean (Langehaug *et al.*, prep).

The lateral extent of freshwater in the western Nordic Seas is related to the seasonal migration of the Polar Front, and is found to be controlled by large-scale winds (Langehaug *et al.*, prep). During summer, when the northerly winds are relatively weak, the Polar Front is located at its most easterly position. The northerly winds strengthen during fall and winter, which forces the Polar Front to migrate westward, toward Greenland (Våge *et al.*, 2018). The migration of the Polar Front is of interest in this study, as the lateral cycle of its position periodically brings a large amount of freshwater to the Iceland and Greenland Seas. More freshwater spreading into the deep basins leads to enhanced stratification and is thereby expected to influence the formation of dense water in this area, and hence DSOW (Brakstad *et al.*, 2019; Langehaug *et al.*, prep).

2.3 Air-sea-ice interaction in the Iceland Sea

Air-sea-ice interactions are important to understand and investigate in order to locate the formation regions of the DSOW. When cold, dry air moves over relatively warm water, extremely strong air-sea heat fluxes occur. These occurrences are called cold-air outbreaks, and are observed where polar air masses discharge over more temperate areas, such as in the Nordic Seas (Papritz and Spengler, 2017). This leads to intense cooling of the ocean and deep-water formation. The Nordic Seas is ideally situated for such strong heat fluxes, due to the combination of warm AW, sea ice and polar air. Furthermore, the air-sea heat fluxes are largest near the ice edge, as this is where the coldest air meets the much warmer ocean (Renfrew and Moore, 1999; Våge *et al.*, 2015; Papritz and Spengler, 2017).

The sea ice edge in the western Nordic Seas has, however, retreated towards Greenland during the past century, with an enhanced retreat over the past decades (Moore *et al.*, 2015; Våge

et al., 2018). The winter mean open-ocean heat flux[1] from the Iceland Sea gyre has been substantially reduced from 1995 (140 W/m^2) to 2014 (50 W/m^2; Moore *et al.*, 2015). This is a result of the retreat of the sea ice edge, which causes a smaller temperature gradient between the atmosphere and ocean, and hence, weaker heat flux. The ongoing global warming will therefore most likely weaken the formation of Arctic-origin Water, and thereby also the AMOC (Condron and Renfrew, 2013).

The deepest and densest mixed layers in the Iceland Sea are formed in the northwestern region, on the outskirts of the gyre, where the largest air-sea heat fluxes are found (Våge *et al.*, 2015; Pickart *et al.*, 2017). Fresh, low-density water occupies the surface in this region in summer (Swift *et al.*, 1980; Våge *et al.*, 2013), which is known to inhibit wintertime convection (Dickson *et al.*, 1988; Malmberg and Jónsson, 1997). These arguments were based on sparse wintertime data in the western Nordic Seas, especially for the western Iceland Sea. However, Våge *et al.* (2018) showed that this fresh surface layer that dominated the western Iceland Sea in summer was gone by late fall, which preconditioned the water column for winter convection. They hypothesized that this was caused by intense northerly winds in fall and winter, that led to Ekman transport of the fresh surface layer toward Greenland.

The climate of the Iceland Sea region is largely dominated by the Icelandic low, which is the northern part of the North Atlantic Oscillation. When the Icelandic low is deep (strong low-pressure), extratropical cyclones brings relatively warm air from south/southeast over the Iceland Sea and northward (Renfrew *et al.*, 2019). Such an event occured in December 2015, which caused a record warming of the North Pole (Moore, 2016). The temperature adjacent to the North Pole raised by 26°C in 24 hours, and a strong reduction of sea ice in the northern Nordic Seas and Arctic Ocean was observed. However, when the Icelandic low is shallow (weak low-pressure), other synoptical weather systems dominate the reagion. For example, a deep Lofoten low can bring polar air from the north over the Iceland and Greenland Seas, and a southwestern Icelandic low can force barrier winds off the cost of Greenland over the Iceland Sea (Harden *et al.*, 2011; Renfrew *et al.*, 2019).

[1] Ocean heat flux, $\Delta H = \frac{\rho * C_p * \Delta T * V}{\Delta t}$, is the change in heat over a unit square meter between time $t+1$ and time t.

Deep-water formation in the Iceland Sea is therefore a result of a complex air-sea-ice system. Papritz and Spengler (2017) stated that deep-water formation in the Iceland Sea occurs during a few intense cold-air outbreaks, rather than by continuous heat loss during weak cold-air outbreaks. These authors further proposed that the pathways of polar air masses were crucial for the resulting atmospheric heat fluxes[2] over the ocean, hence the large-scale wind pattern is a contributing factor. The mean winter wind field in the Nordic Seas is dominated by northerly winds in the northern part, along east Greenland, and over the western and central Iceland Sea, and with southerly winds on the eastern side (Moore, 2012). Changes in this wind pattern is important to understand and predict, in order to understand the deep-water formation in the Iceland Sea (Papritz and Spengler, 2017; Renfrew *et al.*, 2019). This study aims to address some of the uncertainties regarding the formation of dense water in the Iceland Sea and transport of dense water toward Denmark Strait.

[2]Atmospheric heat flux is in this thesis referred to the turbulent heat flux (thf; latent + sensible heat fluxes).

Chapter 3

Data and methods

3.1 The Eggvin Offset Mooring

Data for this study were obtained from the Eggvin Offset Mooring, which was located in the Eggvin Offset (70.6°N, 15.6°W), in the northwestern Iceland Sea. The mooring was deployed from 28 August 2016 to 7 June 2018. Its purpose was to measure dense-water formation and flow through the offset, where the deepest and densest mixed layers in the Iceland Sea were expected to be found according to Våge *et al.* (2015). The location of the mooring was intended to be ice free in winter, still sufficiently close to the ice edge, in order to be exposed to the most intense cold-air outbreaks.

The mooring was equipped with 25 point hydrographic instruments, current meters and temperature loggers: five Sea-Bird Electronics 56 (SBE56) measuring temperature every 30 seconds, four Sea-Bird Electronics 37 (SBE37) measuring temperature, salinity, and pressure every 15 minutes, eleven Sea-Bird Electronics 39 (SBE39) measuring temperature and pressure every 15 minutes, one Seaguard measuring temperature, salinity, pressure, and point velocity every 30 minutes, one Rotor Current meter (RCM-07) from Aanderaa, which measured velocity every second hour, and three Acoustic Doppler Current Profilers (ADCP, two work horses and one long ranger), measuring velocity every hour and every second hour, respectively (Fig. 3.1; Tab. 3.1).

A closer look at the pressure data revealed that the instruments that measured pressure had

undergone a drift. From the deployment in August 2016, the pressure sensors at each depth available showed a trend in reduced pressure until November 2016. Moreover, the Eggvin Offset Mooring must have been deployed a bit farther to the south on the slope, such that it covered the entire water column from 8 m (instead of 50 m as planned) in the surface layer to the bottom depth at 1200 m.

3.2 Additional data

Additional hydrographic and velocity data used in this study were obtained from three shipboard conductivity-temperature-depth (CTD) sections across the Eggvin Offset from R/V *Håkon Mosby* (August 2016), R/V *Alliance* (February 2018), R/V *Kristine Bonnevie* (June 2018), and an Argo float (ID: 3901988, Fig. 3.2).

The shipboard hydrographic and velocity surveys sampeled the Eggvin Offset three times while the mooring was deployed. The first cruise was related to the deployment of the Eggvin Offset Mooring and crossed the channel, from south to north, in late August 2016. The second survey was during the winter cruise with the Iceland Greenland Seas project (Renfrew *et al.*, 2019), which crossed the Eggvin Offset at the end of February and beginning of March 2018. The last section was taken in June 2018, during the recovery of the mooring. Hydrographic and velocity measurements obtained from CTD casts, lowered Acoustic Doppler Current Profilers (LADCPs) and ship-mounted instruments on these three cross-sections of the channel have been used in this study to supplement the mooring data. The hydrographic fields from the CTD sections were used to compute the geostrophic shear via the thermal wind relation. These geostrophic velocities were then referenced with the shipboard ADCP data to obtain absolute geostrophic velocities, following the method by Semper *et al.* (2019). Here, velocities are positive towards the east.

The Argo float was deployed 2 km from the Eggvin Offset Mooring at the end of February 2018. The float profiled to approximately 1000 m every day and drifted through the channel at 200 m depth until 16 May 2018. At that time, the float was near the eastern end of the channel,

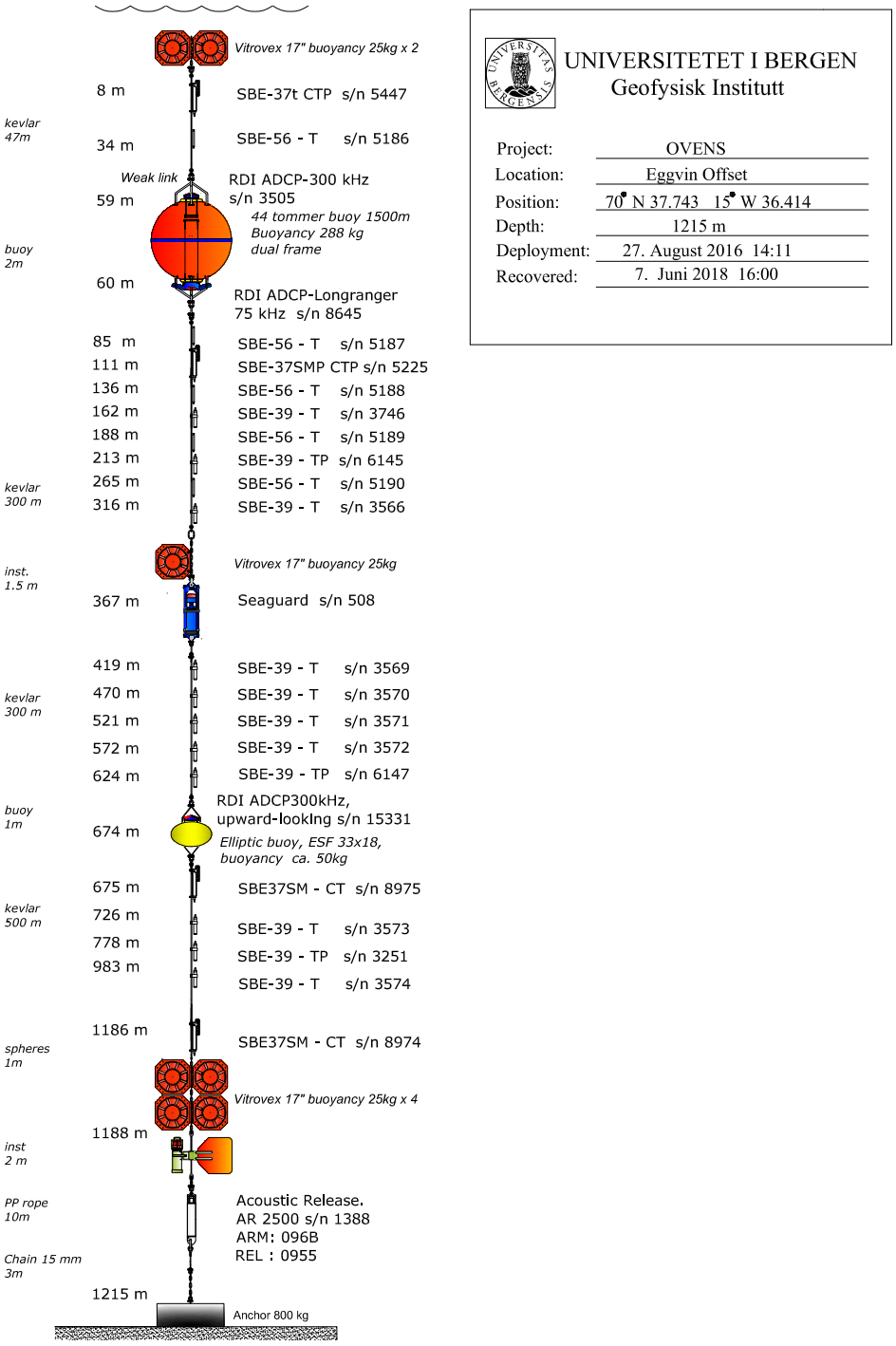

Figure 3.1: The instrumentation of the Eggvin Offset Mooring, schematic by Helge Bryhni, December 2019, University of Bergen.

and started profiling every fifth day and drifting at 1000 m instead. The Argo float was equipped with hydrographic sensors and its velocity through the Eggvin Offset was estimated and compared to the mooring data, by use of its positions and time.

Due to the lack of salinity data, the in-situ temperature data were used in the analysis, while for the cruise and Argo data, Conservative Temperature was used. Subsequently, the word 'in-situ temperature' refers to the actual measured temperature from the mooring, and 'temperature' refers to the Conservative Temperature from the cruises and Argo float. 'Salinity' in the text refers to Absolute Salinity and 'density' is always potential density anomaly. The TEOS-10 global seawater toolbox was used for all conversions (McDougall and Barker, 2011).

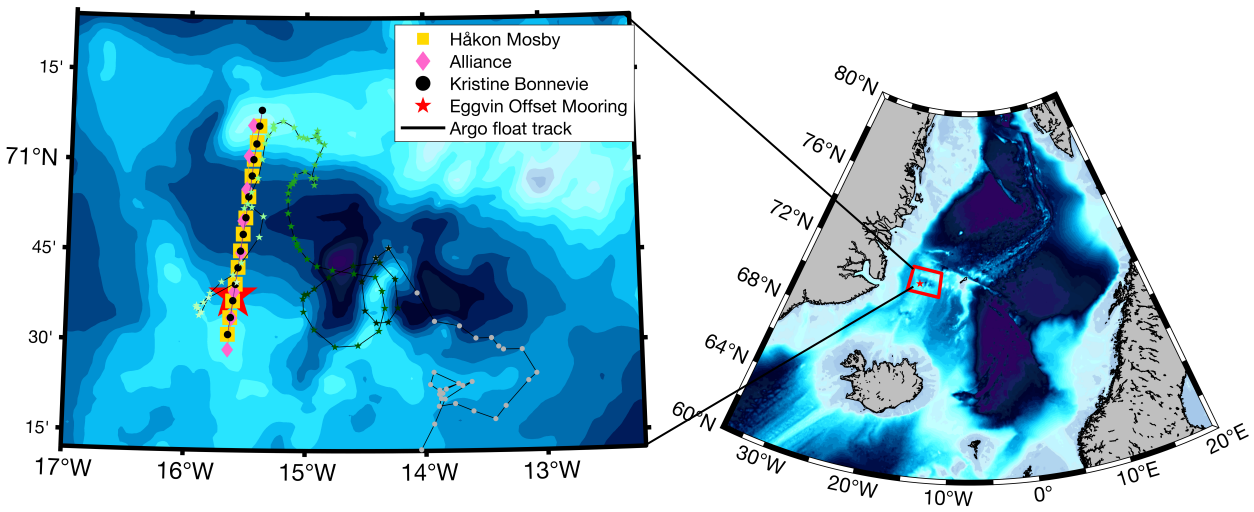

Figure 3.2: Map of CTD stations from the three cruises, the Argo track and the location of the Eggvin Offset mooring (red star). Yellow squares are from R/V *Håkon Mosby* in August 2016, purple diamonds are from R/V *Alliance* in February 2018, and black dots are from R/V *Kristine Bonnevie* in June 2018. The black line represents the track of the Argo float, which was deployed 2 km west of the mooring on 28 February 2018. The Argo drift is shown by colored dots, from light green to dark green (28 February to 16 May) to grey (16 May to 21 September). In this period the float profiled down to 1000 m every day and drifted at 200 m depth. The float started to dive every fifth day and drifted at a depth of 1000 m. Color shading is ocean depth.

The atmospheric and sea ice data were obtained from the latest climate reanalysis data, ERA5, a product from the European Centre for Medium-Range Weather Forecasts (Copernicus Climate Change Service (C3S), 2017). The data were downloaded to cover the area of interest

[65°N – 80°N, 35°W – 20°E] in the time period the mooring was deployed. The ERA5 data set provides hourly fields on single pressure levels. The fields included in this study were the 2 m atmospheric temperature, 10 m wind, mean sea level pressure, sea ice concentration, sensible and latent heat fluxes, mean shortwave radiation, and mean long wave radiation.

3.3 Current data

The Eggvin Offset Mooring was well equipped with instruments measuring current velocity. Attached to the mooring were three ADCPs, one Seaguard current meter, and one RCM measuring flow velocity and direction. One work horse ADCP at 59 m was facing upward and sampled all the way to the sea surface with a beam frequency of 300 kHz. Another ADCP was attached at 60 m and faced downward. This was a long ranger and reached all the way down to 663 m. The last ADCP was sampling the depth range from 680 m to 544 m, faceing upward as well. The Seaguard measured the velocity and direction at one point, at 367 m depth. The ADCPs had a resolution of 0.1 cm/s and a range of ± 500 cm/s, while the Seagurad RCM had a resolution of 0.01 cm/s and a range of 0-300 cm/s. The RCM-07 at great depth had a problem with the rotor container, such that the velocity data were not possible to recover.

The velocities were rotated into a coordinate system aligned with the mean flow and the contours of constant depth in the Eggvin Offset. These two methods resulted in an east/northeastward flow of 3° ("mean flow-method") and 5° ("bathymetry-method") in the Eggvin Offset (Fig. 3.3), where 0° was east. The bathymetry-method was used further in this study, as the geometry in the channel was used in later calculations.

Moreover, the significance of the velocity data was addressed. This was done by calculating the standard mean error of the rotated along-stream velocities over the whole time period averaged over four depth intervals: 10 m – 100 m, 100 m – 300 m, 300 m – 500 m and 500 m – 700 m (Fig. 3.4). High sampling frequency over a continuous time period gave the measurements a type of memory (auto correlation), which means that a sample at time *t+1* is a function of the sample at time *t*. The standard mean error was computed by considering the integral time scale

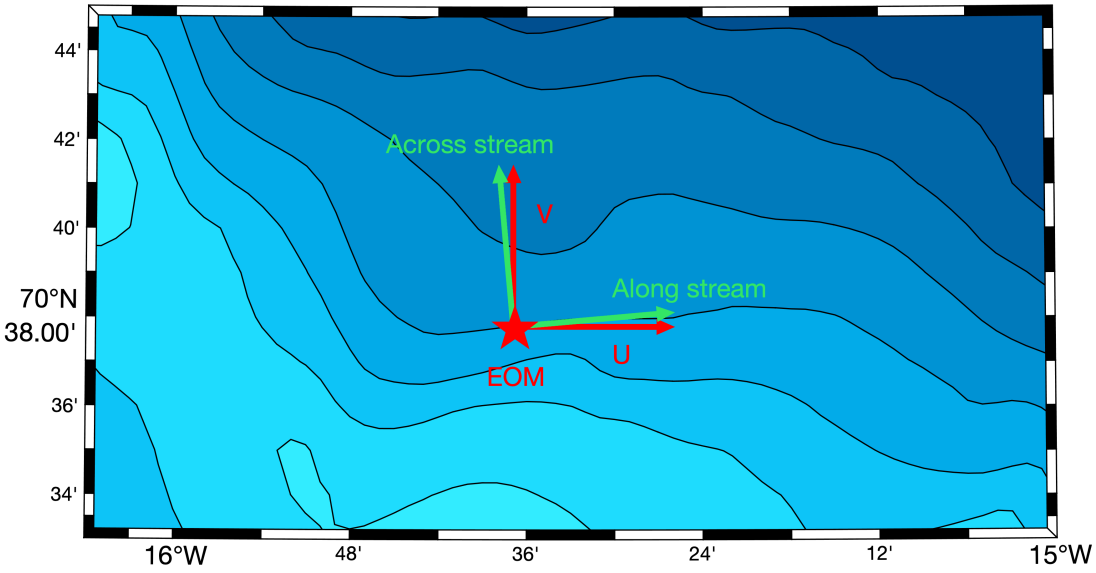

Figure 3.3: The location of the Eggvin Offset mooring (red star) and direction of un-rotated (red) and rotated currents (green) in the Eggvin Offset. Black lines are depth contours and color shading is ocean depth.

of the time series, which is the sum of squared auto correlation functions.

The velocities were weak and the error ellipses were larger than the mean velocities (Fig. 3.4). This means that the velocities were not significant in magnitude, but they had a preferred direction. Despite large fluctuations in the upper layer, the velocities at intermediate and greater depths were all directed to the east. The angle of the ellipse depended on the covariance of the U (east-west) and V (north-south) components of the flow. The magnitude, on the other hand, depended on the variance of the velocity data. The length of the axes of the ellipses were determined by the standard mean error in the along- and across-stream directions.

3.4 Calibration

After the recovery of the mooring in June 2018, the data were inspected for spikes, drifts, and other issues. The hydrographic data set was overall very good, except for one troublesome con-

ductivity sensor at 1198 m and a fault with the rotor container on the RCM-07 that measured current velocity at 1200 m. Data from these two sensors were therefore excluded from the analysis.

The rest of the measurements were calibrated by comparing the time series of in-situ temperature and conductivity with the three surveys that crossed the channel in the time period the mooring was deployed. Data from the nearest station to the mooring from each survey were used. The distances were 1.7 km, 1.1 km, and 1.6 km between the mooring and the nearest station on R/V *Håkon Mosby*, R/V *Alliance*, and R/V *Kristine Bonnevie*, respectively. The values used for comparison from the CTD stations were averaged over a depth interval, ± 10 m the depth of the moored instrument. The calibration points from the mooring were averaged over a time interval, which was $\pm$ 1 day from the time of the CTD casts. Standard deviations for each calibration value were added, and visual inspection of each time series from the mooring was done to validate the data. If the calibration points were not inside the limits of the standard deviations, corrections were made.

Most of the time series passed the above criteria and recorded throughout the 2-year deployment. Only four time series had to be calibrated (Table 3.1). The calibration adjustment was either done by adding a constant, if the measurements were only off by a constant, or by multiplying with a linear function if the problem was a linear drift in the sensors. An example of the first method is illustrated below (Fig. 3.5).

Table 3.1: An overview of the different instruments at the Eggvin Offset Mooring, accuracy of the instruments, and whether the measurements had to be adjusted for drifts/offsets. The abbreviations are: D (depth), accuracy (Acc.), calibration (Cal.), in-situ temperature (T), conductivity (C) and velocity (vel). Green color indicates that the data were not calibrated, while red color means that the data were calibrated. "Yes, linear" means that the data set was corrected by a linear function and the "yes, constant" means that the data set was corrected by adding a constant.

Instrument	**D [m]**	**Acc. *T***	**Acc. *C***	**Acc. vel**	**Cal. *T***	**Cal. *C***	**Cal. vel**
SBE37 sn5447	8	± 0.002 °C	± 0.003 mS/cm		no	no	
SBE56 sn5186	34	± 0.002 °C			no		
ADCP sn3505	59	± 0.4 °C		± 0.5 cm/s	no		no
ADCP sn8645	60	± 0.4 °C		± 0.5 cm/s	no		no
SBE56 sn5187	85	± 0.002 °C			no		
SBE37 sn5225	111	± 0.002 °C	± 0.003 mS/cm		no	no	
SBE56 sn5188	136	± 0.002 °C			no		
SBE39 sn3746	162	± 0.002 °C			no		
SBE56 sn5189	188	± 0.002 °C			no		
SBE39 sn6145	213	± 0.002 °C			no		
SBE56 sn5190	265	± 0.002 °C			no		
SBE39 sn3566	316	± 0.002 °C			no		
Seaguard sn508	367	± 0.03 °C	0.002 mS/cm	± 0.15 cm/s	no	yes, constant	no
SBE39 sn3569	419	± 0.002 °C			no		
SBE39 sn3570	470	± 0.002 °C			no		
SBE39 sn3571	521	± 0.002 °C			no		
SBE39 sn3572	572	± 0.002 °C			yes, linear		
SBE39 sn6147	624	± 0.002 °C			no		
ADCP sn15331	674	± 0.4 °C		± 0.5 cm/s	yes, constant		no
SBE37 sn8975	675	± 0.002 °C	± 0.003 mS/cm		no	no	
SBE39 sn3573	726	± 0.002 °C			no		
SBE39 sn3251	778	± 0.002 °C			no		
SBE39 sn3574	983	± 0.002 °C			no		
SBE37 sn8974	1186	± 0.002 °C	± 0.003 mS/cm		no	unrecoverable	
RCM-7 sn10909	1188	± 0.05°C		± 0.15 cm/s	yes, constant		unrecoverable

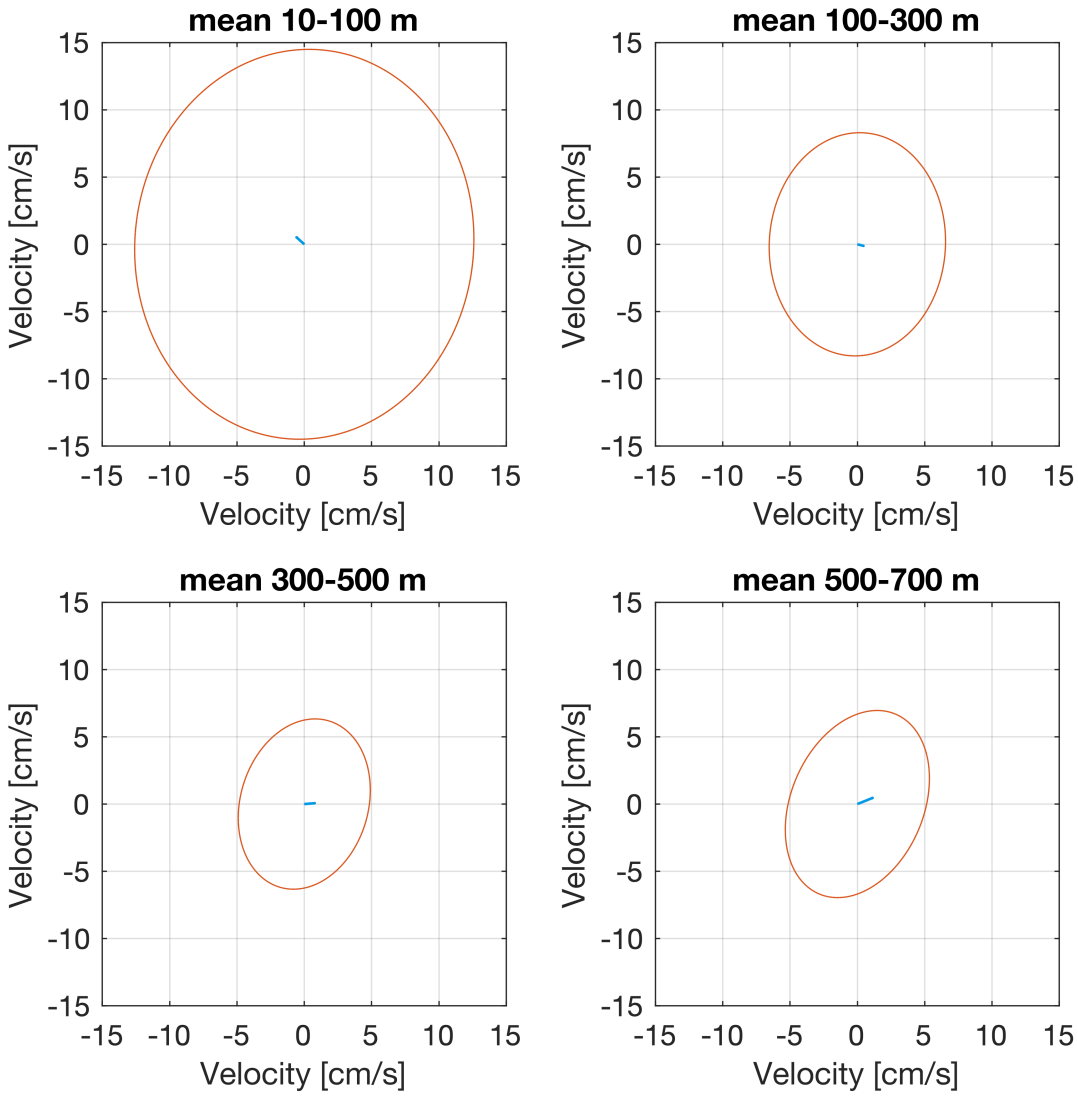

Figure 3.4: Error ellipses of velocity data from the Eggvin Offset Mooring over the whole time period (August 2016 to June 2018). The ellipses represent the standard mean error of the velocity data from the four depth intervals presented. The blue arrows represent the direction and magnitude of the mean flow. When error ellipses are larger than the arrows, the velocity is not significantly different from zero. Additionally, more circular ellipses indicate that the flow does not have a very steady direction.

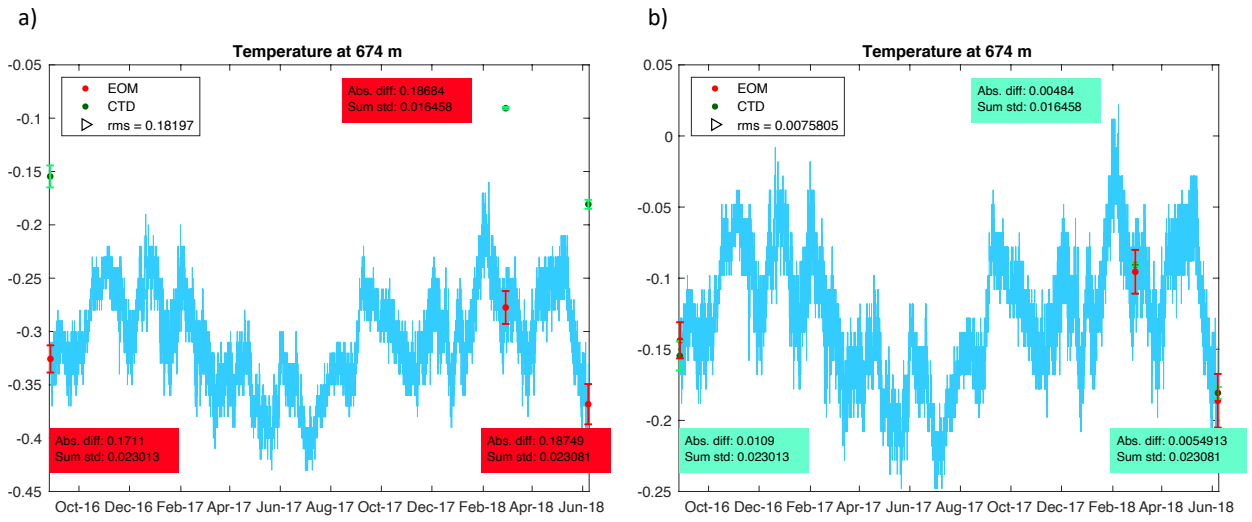

Figure 3.5: Time series of un-corrected **(a)** and corrected **(b)** in-situ temperature from the ADCP at 674 m. Calibration points are from the mooring (red dots) and the nearest station to the mooring at the three cruises (green dots), with error bars explained in the text above.

3.5 Synthetic salt data

Salinity data were only available at four depths: 8 m, 111 m, 367 m, and 675 m. One method was therefore attempted to calculate salinity from in-situ temperature and conductivity data, to investigate salinity and density variations in the Eggvin Offset. A tight one-to-one relationship was identified between moored in-situ temperature and conductivity at the four depth the instruments measured both parameters. This one-to-one relationship gave motivation to try to construct synthetic salinity data for the entire water column. Linear and polynomial calculations of conductivity as a function of in-situ temperature and depth were then conducted, with measurements from the mooring and the three CTD stations, following the approach of Darelius *et al.* (2011). The resulting linear functions were quite distinct from each other, due to different in-situ temperature ranges at different depths. Thus, it was not possible to apply one-to-one correlations between in-situ temperature and conductivity at each depth throughout the entire water column. This was also confirmed by the CTD casts near the mooring (Fig. 3.6). These measurements indicated that the density change with depth was dominated by salinity, not temperature (Fig. 3.7). Hence, salinity and density data at all depths from the Eggvin Offset Mooring could not be estimated.

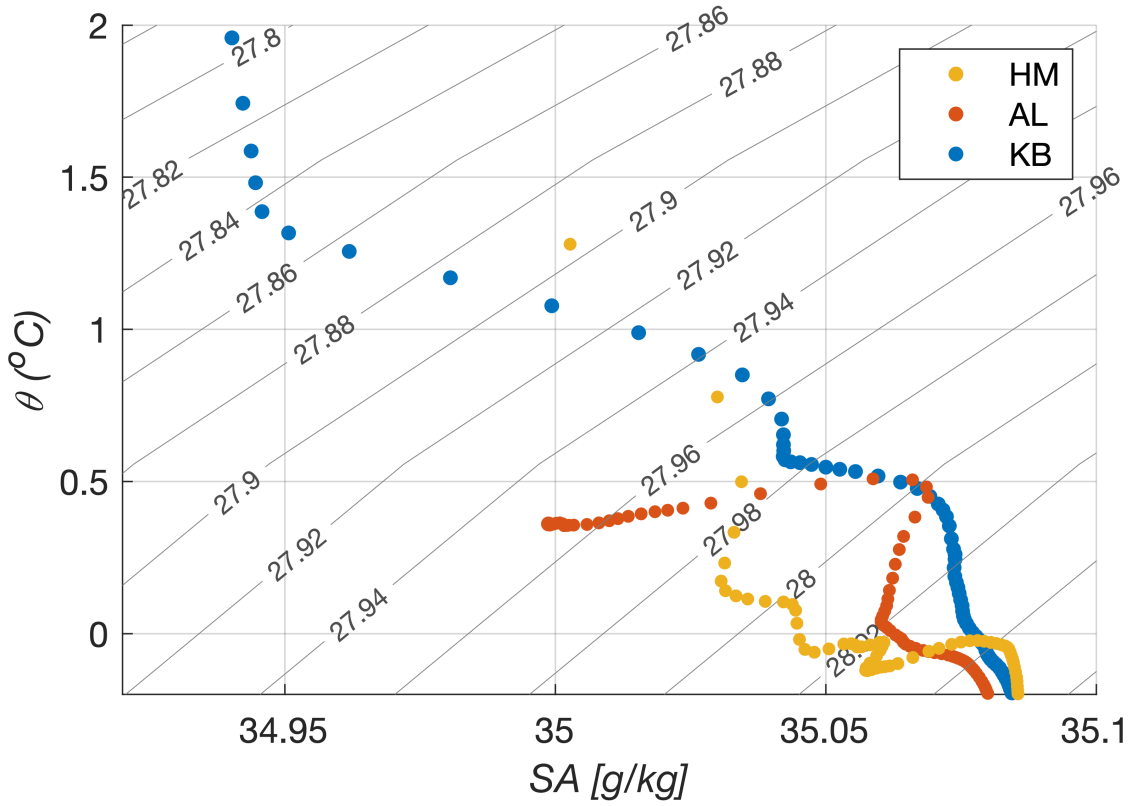

Figure 3.6: Temperature (blue), density (black), and salinity (red) from the nearest CTD stations to the Eggvin Offset Mooring at the three cruises R/V *Håkon Mosby* (HM), R/V *Alliance* (AL), and R/V *Kristine Bonnevie* (KB). None of the three profiles are one-to-one.

3.6 Mixed-layer depth

The high vertical resolution of in-situ temperature made it possible to estimate the mixed-layer depth from a temperature difference criterion (Fig. 3.8, Nilsen and Falck, 2006; Våge *et al.*, 2015). While Nilsen and Falck 2006 used a temperature difference of $\Delta T = 0.8$°C in the Greenland Sea, Våge *et al.* (2015) found that $\Delta T = 0.2$°C was a better fit to the less stratified Iceland Sea. In this study, $\Delta T = 0.15°$ was the best estimate, chosen after visual inspection of several temperature differences. The stratification of the water column and lower in-situ temperature resolution than the hydrographic profiles considered by Våge *et al.* (2015) might have been the reason why a smaller ΔT was better in the Eggvin Offset.

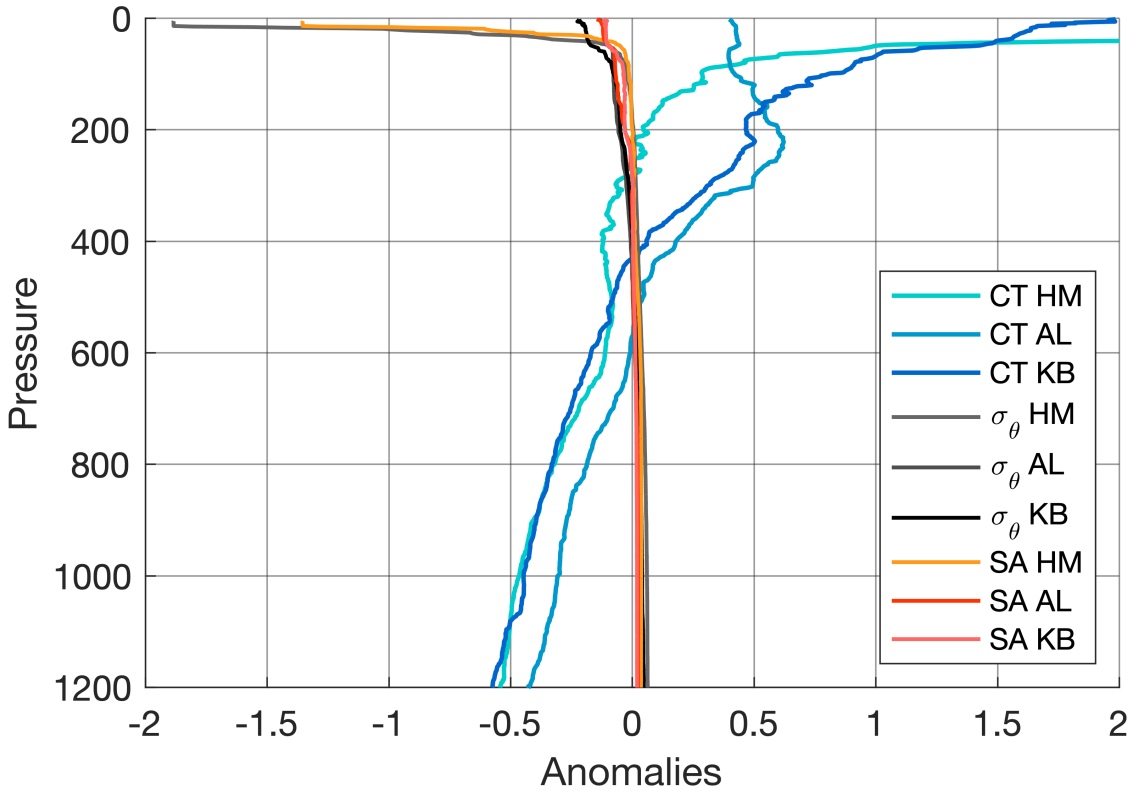

Figure 3.7: Anomalies in temperature (blue), density (black) and salinity (red) from the nearest CTD stations to the Eggvin Offset Mooring at the three cruises R/V *Håkon Mosby* (HM), R/V *Alliance* (AL), and R/V *Kristine Bonnevie* (KB). The density profiles follows the salinity profiles, not the temperature profiles.

The difference criterion method was applied using an autonomous temperature algorithm, where a reference time series of in-situ temperature was chosen. The uppermost instrument at 8 m was the natural reference, but during the convection period, November through April, this method resulted in too shallow mixed layers. Hence, the algorithm was divided into summer and convective seasons. The convective season was further divided in three stages, where the reference time series were set to 36 m in stage 1, 111 m in stage 2, and 162 m in stage 3 (gray shading in Fig. 4.3). Stage 3 was only observed the first winter from 5 April to 5 May 2017. The mixed-layer depth was then estimated to be the depth of the instrument where the reference temperature plus the temperature difference reached ($T_{ref} + \Delta T$). The resulting mixed layers were still too shallow due to the separation distance of the instruments (25 m in the upper 300 m and 50 m between 300 m and 800 m depth). This was corrected by adding 12.5 m to the mixed-

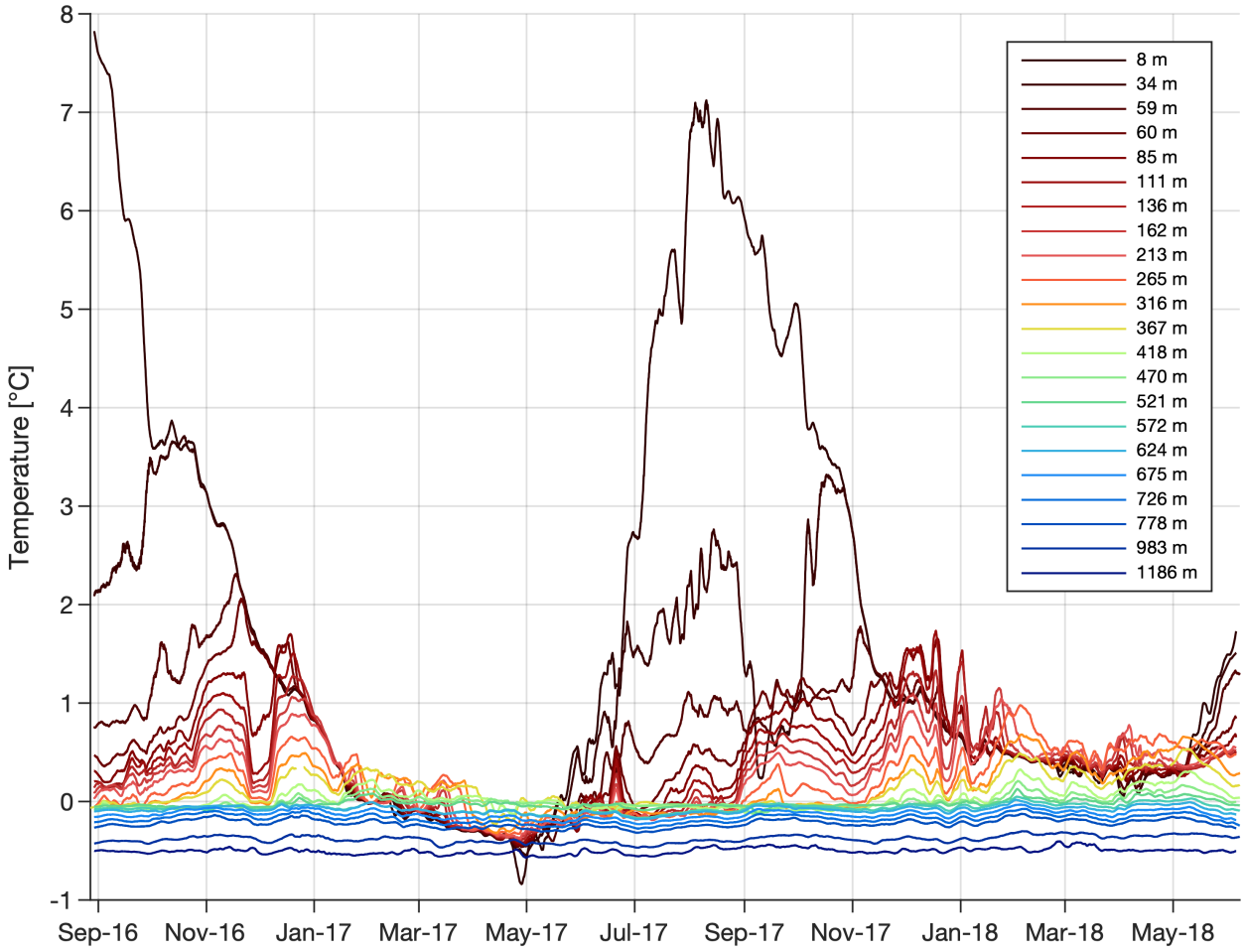

Figure 3.8: In-situ temperature time series from every instrument attached to the Eggvin Offset Mooring. Colors from red to blue indicate the depth of the records, from the surface to the bottom. The depth of the mixed layer can be inferred by studying the depth of the deepest instrument when the time series converge.

layer time series in the upper 300 m and 25 m for depths between 300 m and 800 m.

A density-difference criterion was conducted with the density data from the Argo float when it drifted on the southern slope in the Eggvin Offset. The same method as for the temperature-difference criterion was used, and the resulting time series was compared with the mixed-layer time series from the mooring and from the temperature-difference criterion used on the temperature data from the Argo float. This comparison was done to strengthen the representation of the mixed-layer time series from the mooring data.

3.7 Transport estimates

An interest in this study was to see whether the Eggvin Offset was an important pathway of overflow water into the Iceland Sea. Transports through the Eggvin Offset were therefore estimated for two different layers of dense water. One was the mixed layer, when the water was sufficiently dense ($\sigma_\theta \geq 27.8\,\mathrm{kg/m^3}$) to contribute to the overflow across the GSR. The second was the dense water at greater depths corresponding to the NIJ transport mode (Semper *et al.*, 2019). The bulk hydrography of the NIJ is $-0.29°\mathrm{C} \pm 0.16°\mathrm{C}$ and $35.075\,\mathrm{g/kg} \pm 0.006\,\mathrm{g/kg}$, which corresponds to a density of approximately $28.05\,\mathrm{kg/m^3}$ (Tab. 3.2; Semper *et al.*, 2019). The densities of the freshest and warmest water, and the saltiest and coldest water, were used to estimate a density span for the NIJ transport mode ($\pm 0.01\,\mathrm{kg/m^3}$). The resulting range was then $28.04\,\mathrm{kg/m^3}$ to $28.06\,\mathrm{kg/m^3}$ and was used to estimate the depth interval of deep, dense water in the Eggvin Offset: 550 m – 850 m (Fig. 3.9).

Table 3.2: Properties of the NIJ transport mode (Semper *et al.*, 2019). Corresponding depth (Corr. depth) is the depth in the Eggvin Offset where the properties of NIJ transport mode water are found.

	Temperature [°C]	Salinity [g/kg]	σ_θ [kg/m^3]	Corr. depth [m]
Mode	-0.29 ± 0.16	35.075 ± 0.006	28.05	672
Max.	-0.45	35.081	28.063	851
Min.	-0.13	35.069	28.037	548
Diff.	-0.32	00.012	00.026	303

The geometry of the Eggvin Offset was studied in order to determine the region the Eggvin Offset Mooring could represent, which in turn was used in the transport estimates. The offset is a zonal gap with sloping bathymetry (shallower water) to the north and south (Fig. 2.2), and the Eggvin Offset Mooring was deployed on the southern slope, in a steep terrain (Fig. 3.10). It was therefore assumed that the mooring could represent the southern slope, from the southern point where the slope begins and to the local maximum depth 21 km farther north. This had to be argued for, and hence the steepness and some dynamics of this slope and channel were

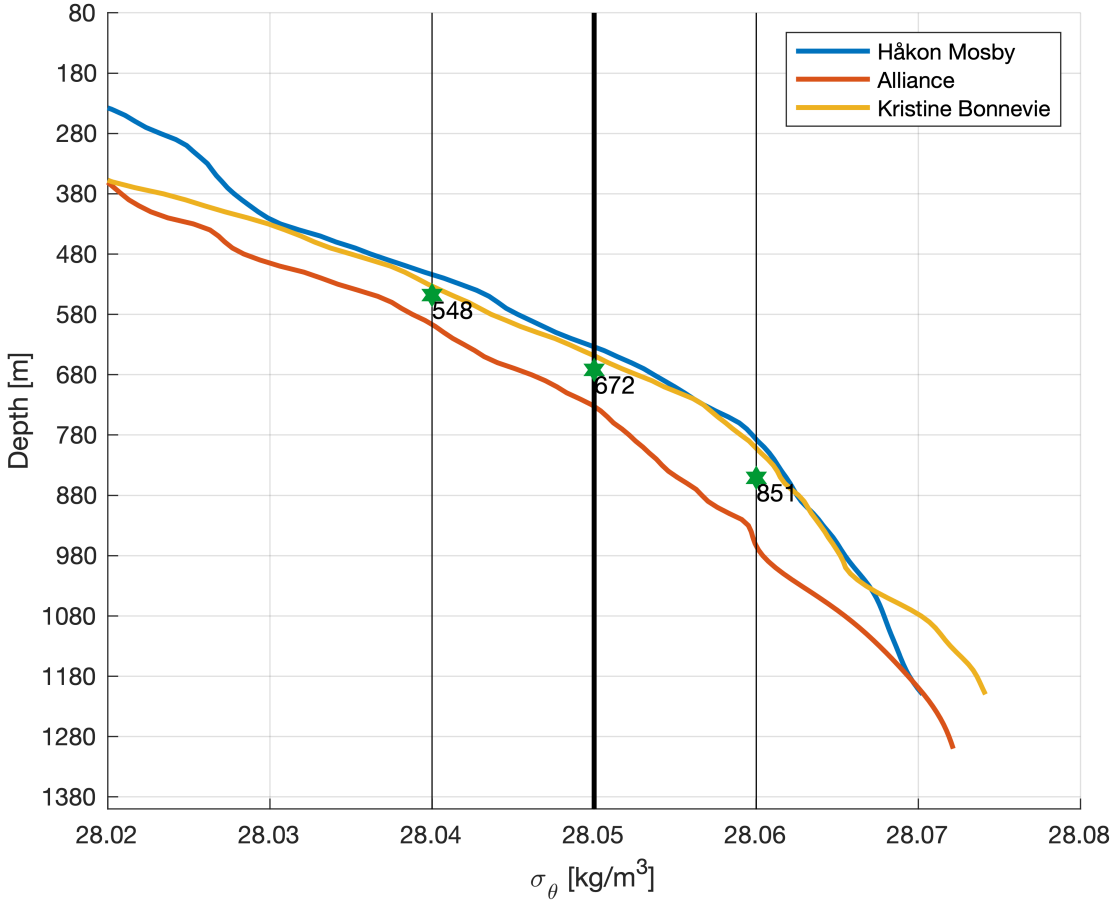

Figure 3.9: Depths estimated from the densities obtained from the nearest CTD stations of the three surveys (R/V *Håkon Mosby*, R/V *Alliance*, and R/V *Kristine Bonnevie*). The densities correspond to the North Icelandic Jet transport mode. Green hexagons indicate the mean depth of the three CTD casts at the different densities.

investigated.

The southern slope could be divided into two sections based on the bathymetry of the slope. The slope was steeper toward the south and less steep toward the north. The southernmost 11 km were in approximately the same steepness range, and the northernmost 10 km were in another, less steep range (Fig. 3.10). The Eggvin Offset Mooring was therefore assumed to at least represent the southernmost 11 km, and at most the entire slope presented in Fig. 3.10. Furthermore, these maximum and minimum widths were used together with maximum and minimum depths and velocities to estimate the range of maximum and minimum transports.

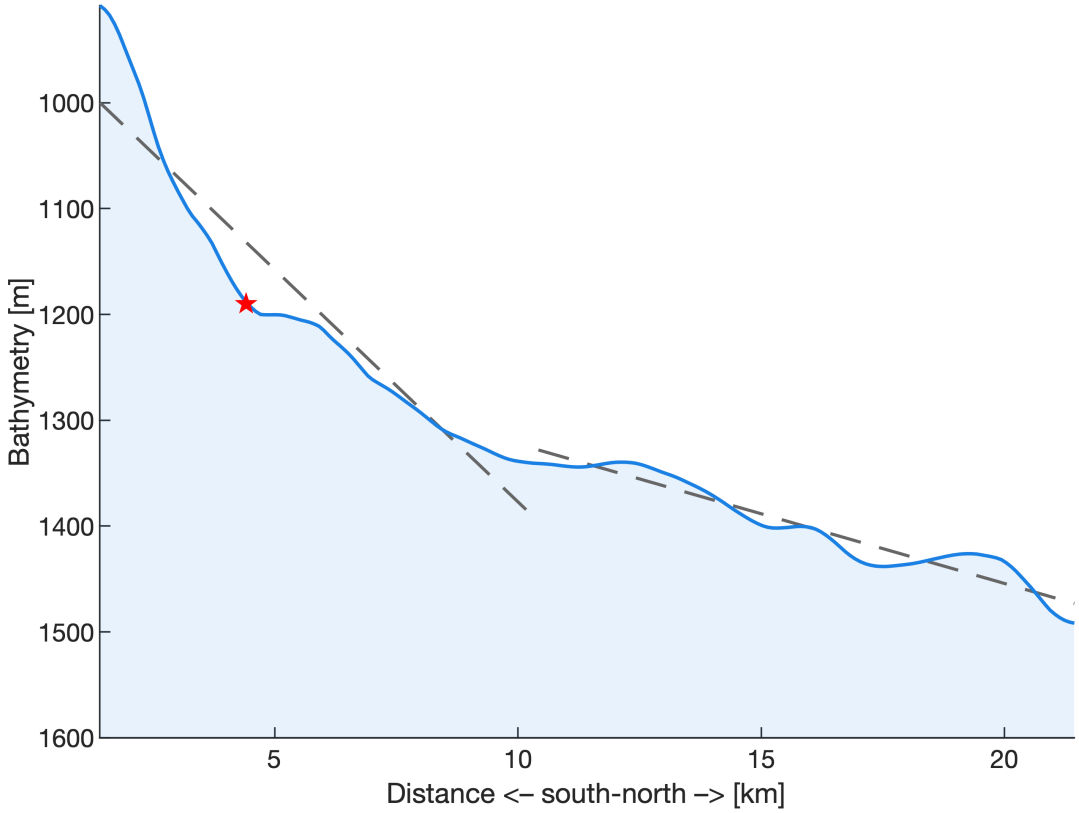

Figure 3.10: Bathymetry of the southern slope in the Eggvin Offset (thick blue line). The red star is the location of the Eggvin Offset Mooring, and the dashed lines are the least square lines of the bathymetry to indicate regions of similar steepness.

Additional assumptions for geostrophic flow were considered: Friction at the bottom and at the surface were neglected, uniform flow along the southern slope (Fig. 4.25), the water was shown to be horizontally homogenous (flat isopycnals: Figs. 4.11, 4.12, and 4.13), and the flow was assumed to be non-divergent and with no vertical shear. The water was therefore not allowed to climb up or down the slope. Furthermore, the theory of geostrophic flow says that the flow turns right at Northern Hemisphere. Additionally, the circulation will follow the potential vorticity contours ($f/h = constant$), where f is the Coriolis parameter and h is depth, in the case where barotrophic flow is evident, as for the Eggvin Offset (equation 10-22 in Marshall and Plumb, 2016). The flow will therefore follow the contours of constant depth (isobaths).

The Rossby Number, hence the relation between lateral advection and the Coriolis force,

was estimated to be much lower than 1, by use of a mean velocity over intermediate to great depths (0.011 m/s) and a length scale covering the southern slope of the Eggvin Offset. Based on these assumptions, the mooring is considered representative of the flow along the southern slope of the Eggvin Offset, that spans over 21 km, from [70.6°N, 15.6°W] to [70.9°N, 15.6°W]. The transports were then estimated for the two dense-water layers, together with transport ranges from minimum to maximum transports.

Chapter 4

Results

Data from the Eggvin Offset Mooring, combined with shipboard measurements and an Argo float, have been investigated to answer the questions for this study (Chapter 1). The aim was to find whether wintertime convection occured in the Eggvin Offset, and the depths and densities of the mixed layers. Were the mixed layers sufficiently dense to contribute to the overflow water at Denmark Strait? Or, was dense water formed another place and transported through the Eggvin Offset?

4.1 On the hydrography of the Eggvin Offset

The two-year in-situ temperature record from the Eggvin Offset Mooring showed that the upper layer was dominated by a pronounced seasonal signal, with relatively warm summers and cold winters (Fig. 4.1). The surface layer started to freshen in May and June 2017. The fresh water was most pronounced in August 2017, with a salinity much lower than 34.66 g/kg, which is the definition of the Polar Front in the Nordic Seas (Section 2.2; Swift and Aagaard, 1981; Langehaug *et al.*, prep). In October 2017, the surface water was substantially more saline, and by November 2017 there was no longer a well-defined surface layer, but a mixed-layer depth of 75 m (Figs. 4.1, 4.2a, and 4.3). The water column was thereby well preconditioned for open-ocean convection, which agrees with observations west of the Eggvin Offset in winter 2015-16 (Våge *et al.*, 2018). Surface cooling continued from December through April in winter 2016-17, and from December through March in winter 2017-18. The continued cooling led to further deepening of the mixed

layer (Figs. 4.1 and 4.3).

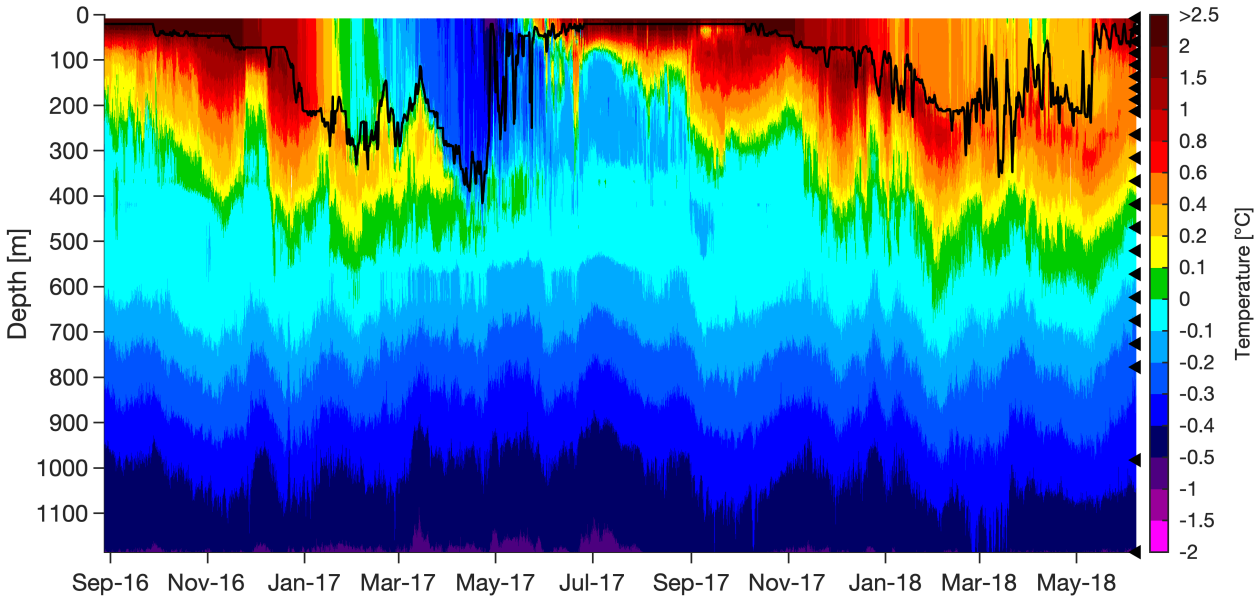

Figure 4.1: In-situ temperature time series from the Eggvin Offset Mooring, with observations from 22 depths (black triangles) and a time step of every second hour. The black line represents the mixed-layer depth calculated from the algorithm described in Section 3.6.

The seasonal variability differed at greater depths (Fig. 4.2a, c, and d). The most pronounced seasonal signal was observed at the surface, as expected, and decreased with depth (Figs. 4.2 a–d). For example, the salinity range at 8 m was [33.56-35.04] g/kg, at 111 m it was [34.99-35.065] g/kg, and at 367 m the range was [35.045-35.075] g/kg. The temperature range also became narrower with greater depths. Moreover, the temperature increased from summer until the end of December at 111 m and over the whole winter at 367 m (Figs. 4.2a, c, and d). During those periods the surface was cooling.

The cooling and densification started at the end of December for both winters at 111 m depth and in winter 2016-17 at 367 m, much later than at the surface (Figs. 4.4, 4.5, and 4.6a). This implies that two different mechanisms, atmospheric cooling and ocean advection, regulated the hydrographic change from May to December at the surface and at depth, respectively.

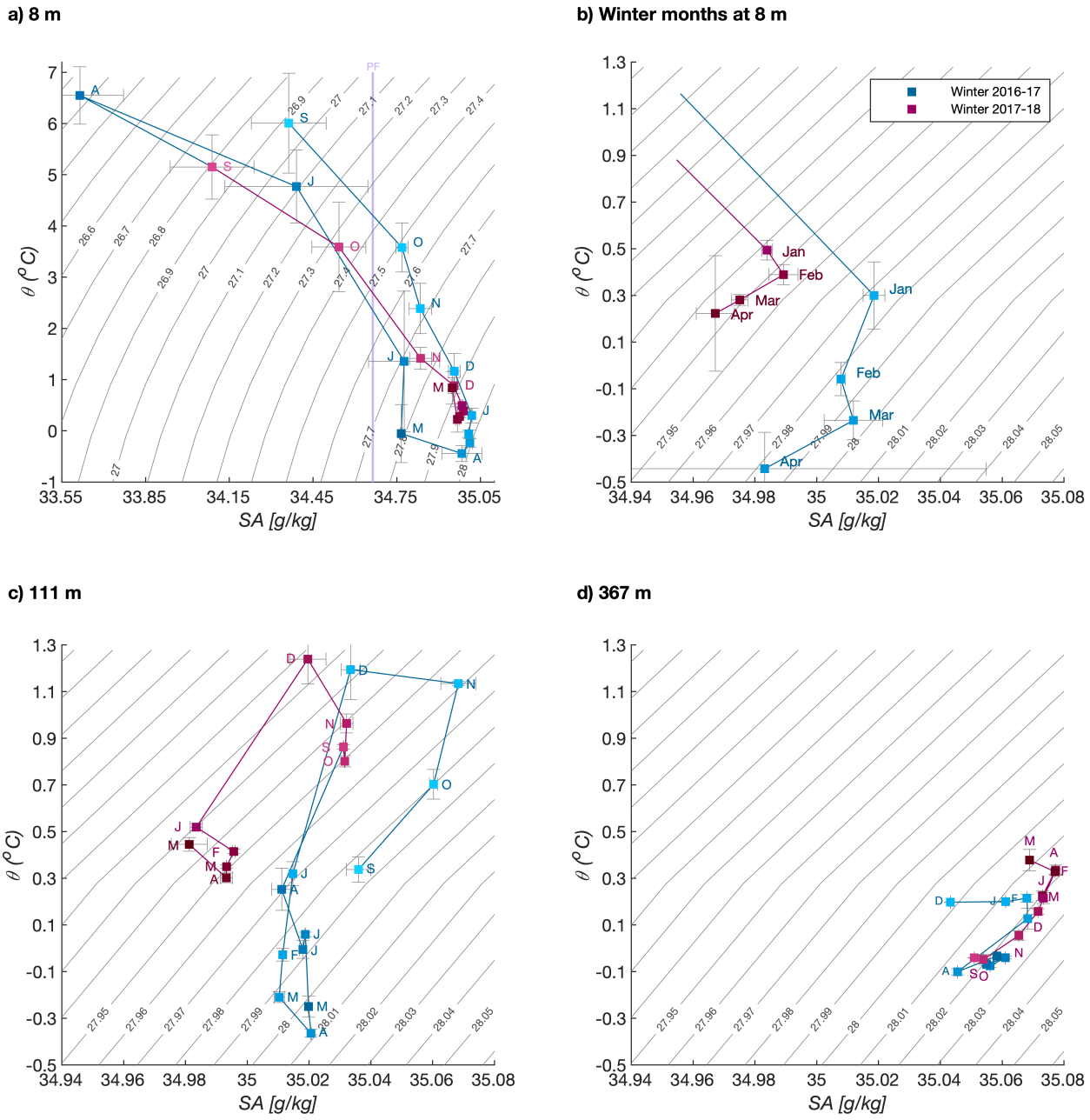

Figure 4.2: Temperature versus salinity, with isopycnals in gray. **a)** Monthly averaged temperature/salinity over the whole time period, with blue colors illustrating 2017 and red colors 2018, from September (light shading) to August (dark shading). **b)** Monthly averaged temperature/salinity at the surface over the two winters, **c)** Monthly averaged temperature/salinity over the whole time period at 111 m, and **d)** monthly averaged temperature/salinity at 367 m. The error bars represent the standard mean error of temperature and salinity. Note the different axes in a).

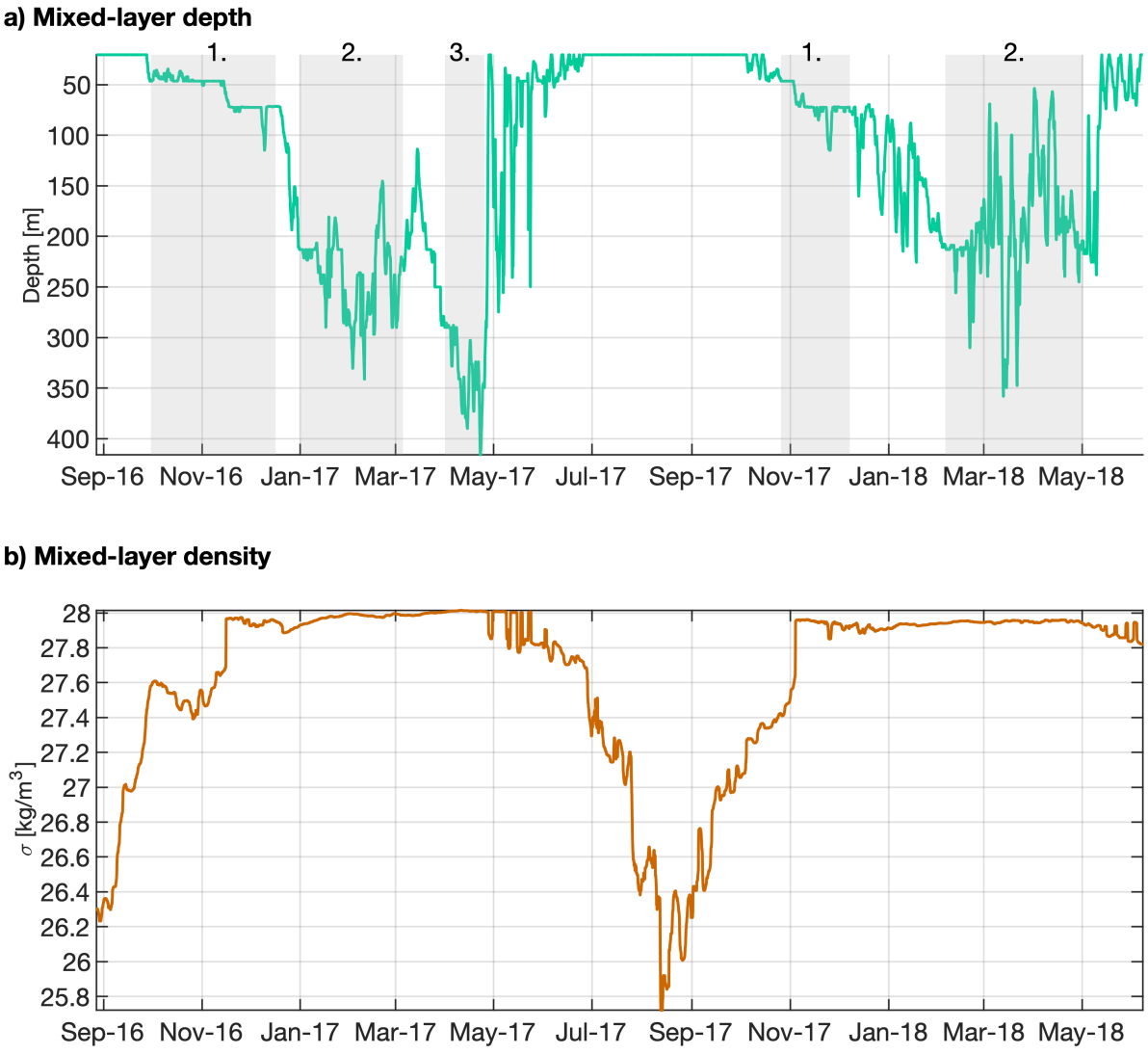

Figure 4.3: Evolution of the **a)** mixed-layer depth and the **b)** mixed-layer density in the Eggvin Offset. The shading and numbers indicate the different stages (Subsection 4.1.1).

The cooling and densification of the water masses at 111 m depth (Fig. 4.5) coincided with mixed layers deeper than 111 m. When the water at 111 m was cooled, the mixed-layer depth was equal to, or deeper than, 111 m (Fig. 4.6c). The observations also revealed that the density at 367 m equaled that of 111 m and 8 m the first week in February 2017 and nearly throughout April 2017 (light red shading in Fig. 4.6). This implies that the mixed layer reached at least 367 m in winter 2016-17, which supports the mixed-layer evolution inferred from in-situ temperature data only (Fig. 4.1).

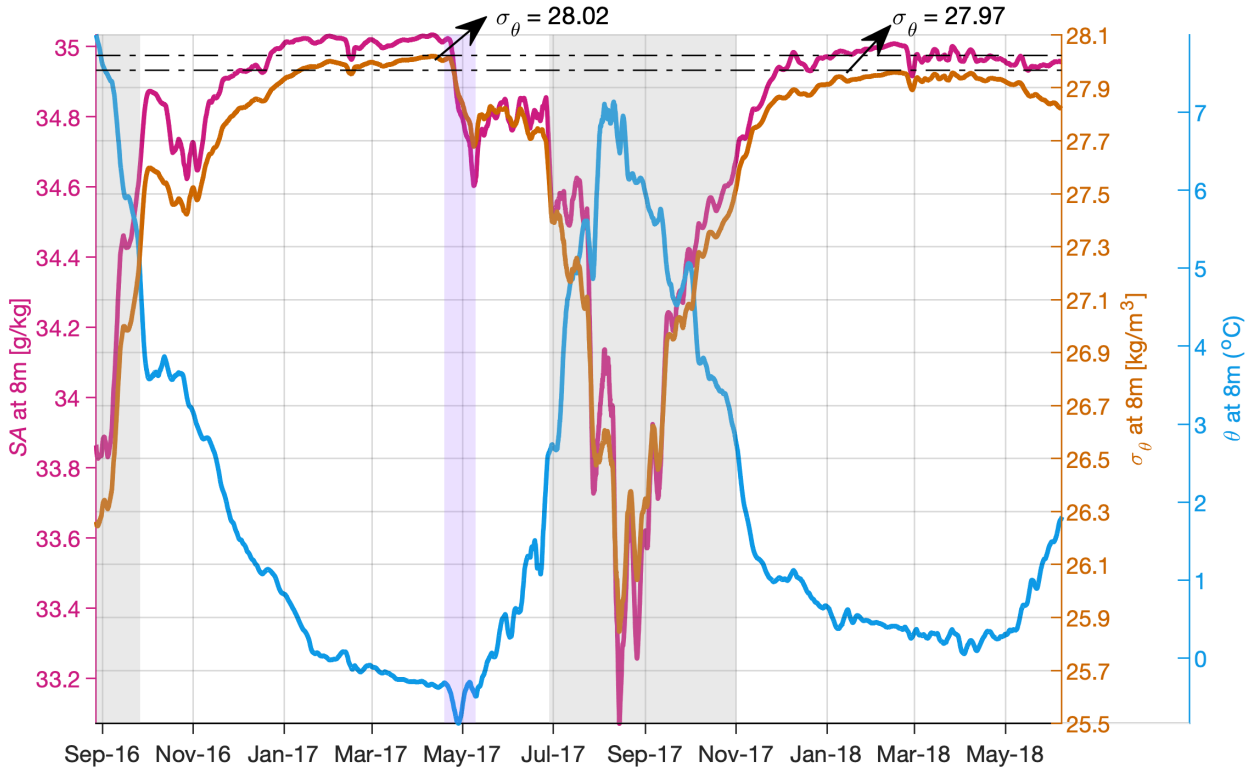

Figure 4.4: Time series of temperature (blue), salinity (red), and density (orange) from the instrument at 8 m attached to the Eggvin Offset Mooring. The purple shading represents when the mooring was covered by sea ice, and the gray shading represents when the Polar Front was east of the mooring. The black dash-dotted lines mark the maximum densities of winters 2016-17 and 2017-18.

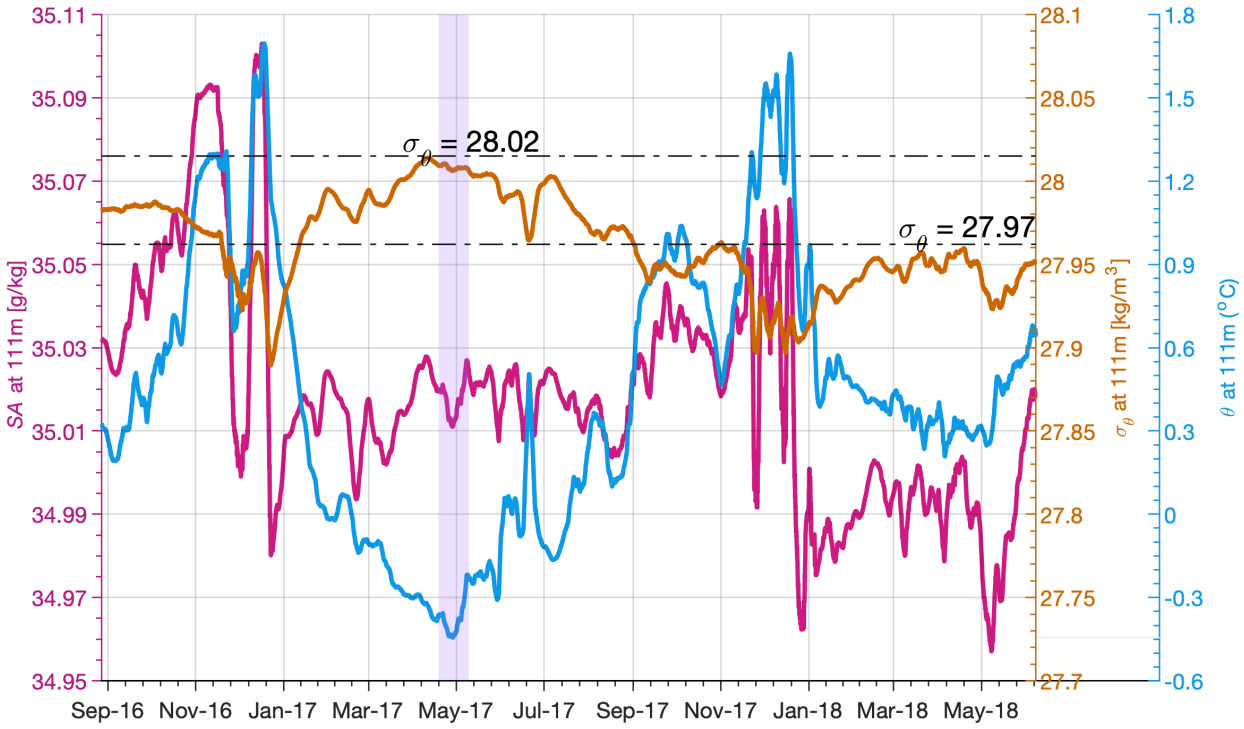

Figure 4.5: Time series of temperature (blue), salinity (red), and density (orange) from 111 m depth from the Eggvin Offset Mooring. The black dash-dotted lines represent the highest densities from winter 2016-17 and winter 2017-18.

The density change differed between the two winters and with depth (Fig. 4.7). While the water in the first winter was densified over the entire water column through the whole winter (December to April), the water in the second winter was only observed to densify at 8 m and 111 m in that time period. At 367 m and 675 m the water actually became less dense during winter 2017-18. A warming at 111 m led to decreased density from summer until the end of December in both winters, and at 367 m in winter 2016-17. Densities in the first winter were generally higher than in the second winter.

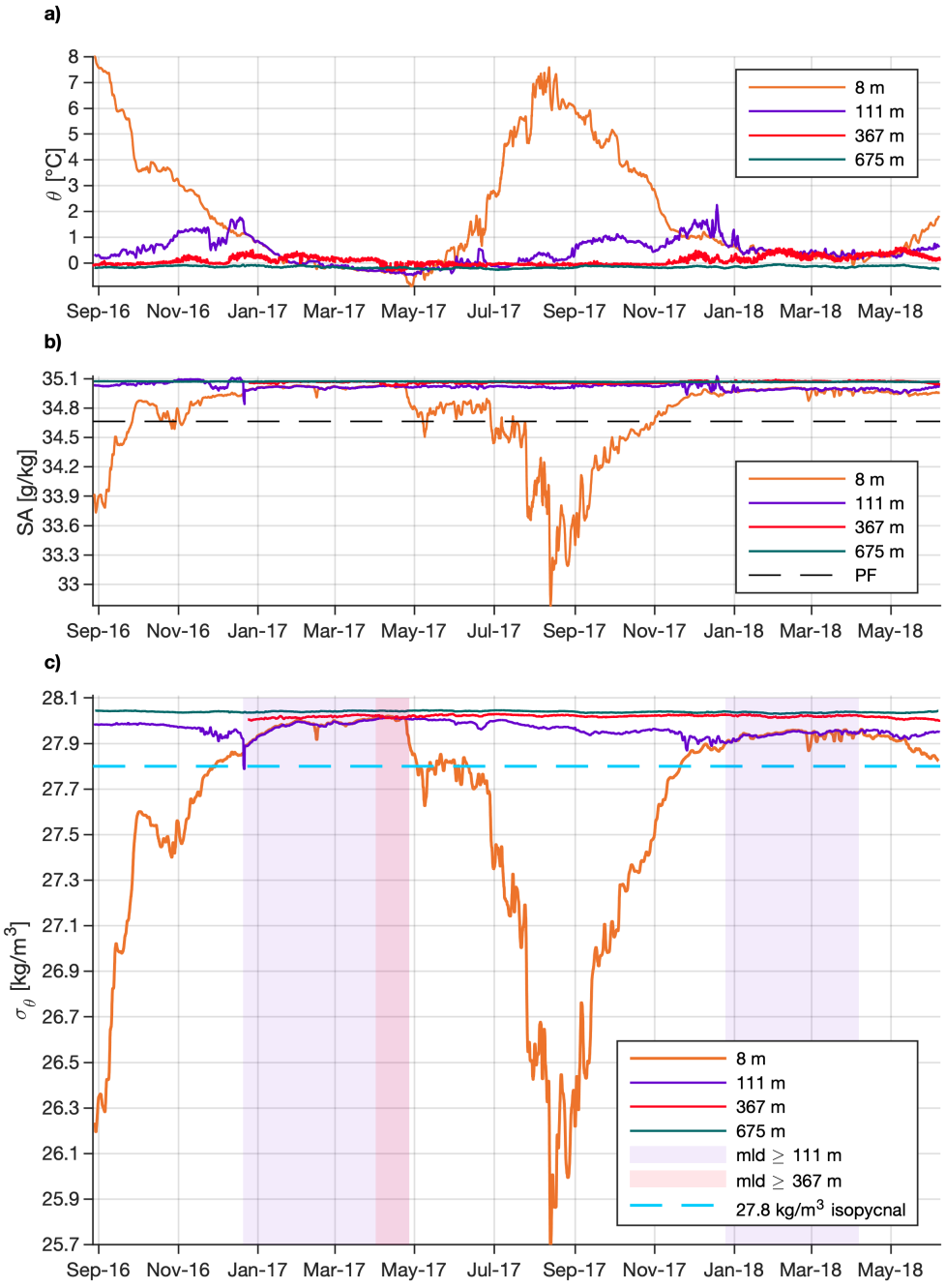

Figure 4.6: Temperature **(a)**, salinity **(b)**, and density **(c)** at the four depths: 8 m (orange), 111 m (purple), 367 m (red), and 675 m (green). The black dashed line in (b) represents the 34.66 g/kg isohaline (the Polar Front), the light purple shading in (c) represent the time period when the mixed-layer depth (mld) was equal to, or deeper than, 111 m, and the light red shading represent the time period when the mixed-layer depth (mld) was equal to, or deeper than, 367 m.

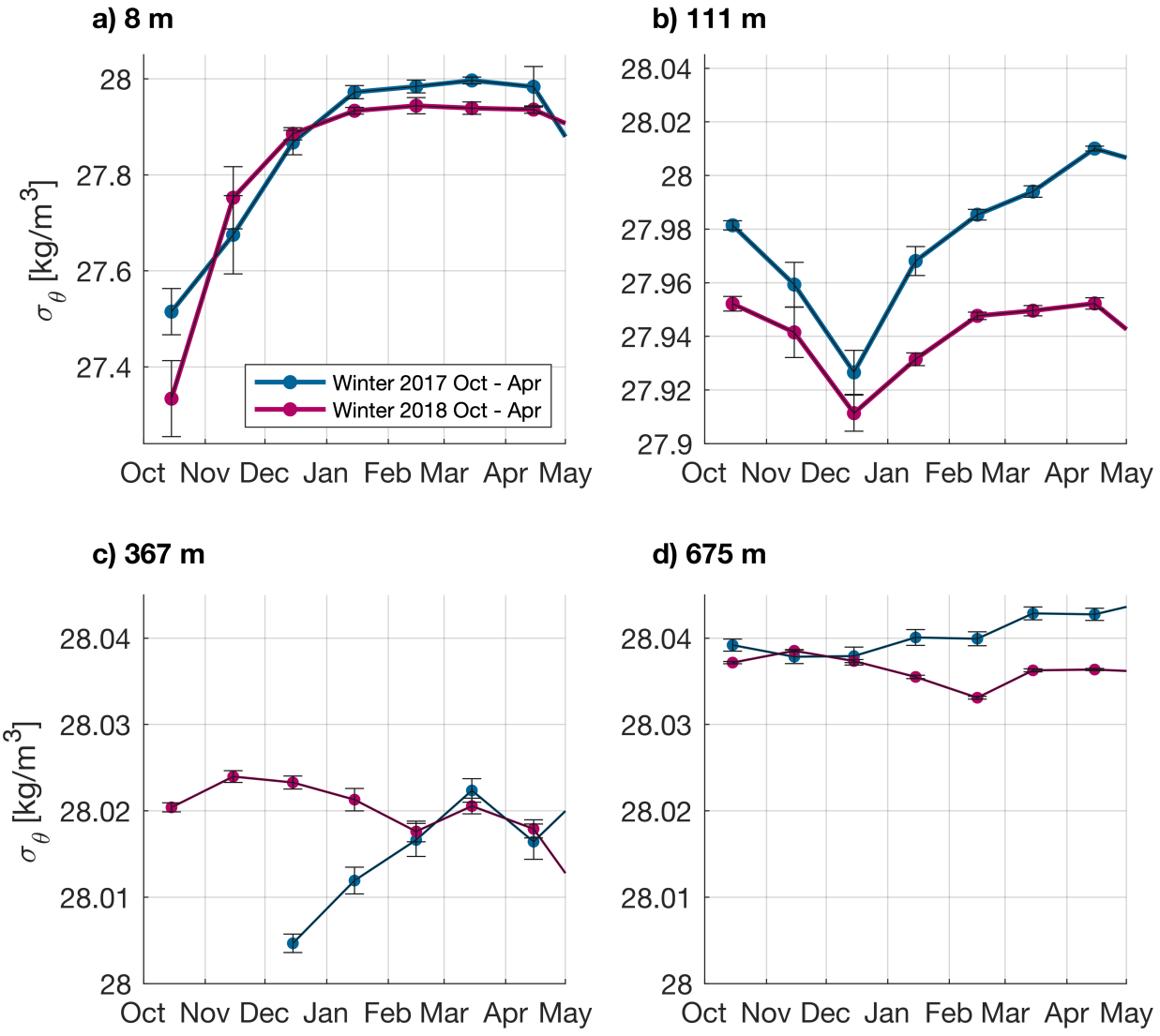

Figure 4.7: Monthly mean density at the four depths with salinity measurements, **a)** 8 m, **b)** 111 m, **c)** 367 m, and **d)** 675 m, from October to April. Winter 2016-17 is represented by the blue line, while winter 2017-18 is represented by the red line. The error bars represent the standard mean error.

The mixed-layer evolution nearly mirrored the seasonal hydrographic signal (black line in Fig. 4.1). The mixed layer was shallow in summer when warm, fresh water occupied the surface, and deepened when the Polar Front migrated westward and the water was cooled in winter. The winter convection period started at the beginning of November, due to intensive surface cooling from September to February (Figs. 4.4 and 4.15). The cooling of the water continued from February to April. At the end of April 2017, the deepest mixed layers were observed. They

reached down to approximately 400 m (Fig. 4.3). Fig. 4.4 also shows that the coldest, saltiest, and densest water ($\sigma_\theta = 28.02\,\mathrm{kg/m^3}$) was seen at the end of April 2017. This was observed immediately before the mooring was completely covered by sea ice, which happened in two pulses (not shown).

The first pulse occurred 27 to 29 April 2017, before the sea ice retreated for almost a week. Then the second pulse of sea ice reached the mooring location on 4 May 2017 and stayed for six days before it migrated towards Greenland. The water masses observed at the mooring, below the sea ice, were classified as cold, fresh, and light Polar Surface Water (purple shading in Fig. 4.4; Swift and Aagaard, 1981; Rudels *et al.*, 2005). These were the only times the mooring was completely covered by sea ice during the two years. However, a tongue of sea ice came near the mooring in mid-February 2017 (not shown), which was recognized as a drop in temperature and salinity at 8 m depth (Fig. 4.4).

In winter 2017-18, the deepest mixed layers occurred at the end of March and reached down to approximately 300 m (Fig. 4.3). This winter was in general warmer than the first winter, and the coldest, saltiest, and densest water was found at the end of March ($\sigma_\theta = 27.97\,\mathrm{kg/m^3}$). Hence, despite the differences, the mixed layers in both winters became more than sufficiently dense to supply the overflow water through Denmark Strait ($\sigma_\theta \geq 27.8\,\mathrm{kg/m^3}$). However, the isopycnal considered a lower limit for the densest portion of the overflow water ($\sigma_\theta = 28.03\,\mathrm{kg/m^3}$) was only nearly ventilated in the Eggvin Offset during winter 2016-17.

The Argo float that was deployed at the end of February 2018 during the R/V *Alliance* cruise (Fig. 3.2) was directly compared with the mooring data over the same time period. The general temperature variability on the southern slope of the Eggvin Offset was relatively similar to the temperature record from the Argo float in winter 2017-18 (Figs. 4.8 and 4.9). The mixed-layer depths determined from both temperature and density criteria from the Argo float were also comparable with the mixed-layer depths estimated from the mooring data. Mixed-layer depths from the float reached approximately 200 m in the first week of March 2018, while the Argo float was located on the southern slope of the channel, less than 12 km away from the mooring (Fig. 4.10). This suggests that the mixed-layer depths estimated from the in-situ temperature from

the mooring are representative for the Eggvin Offset.

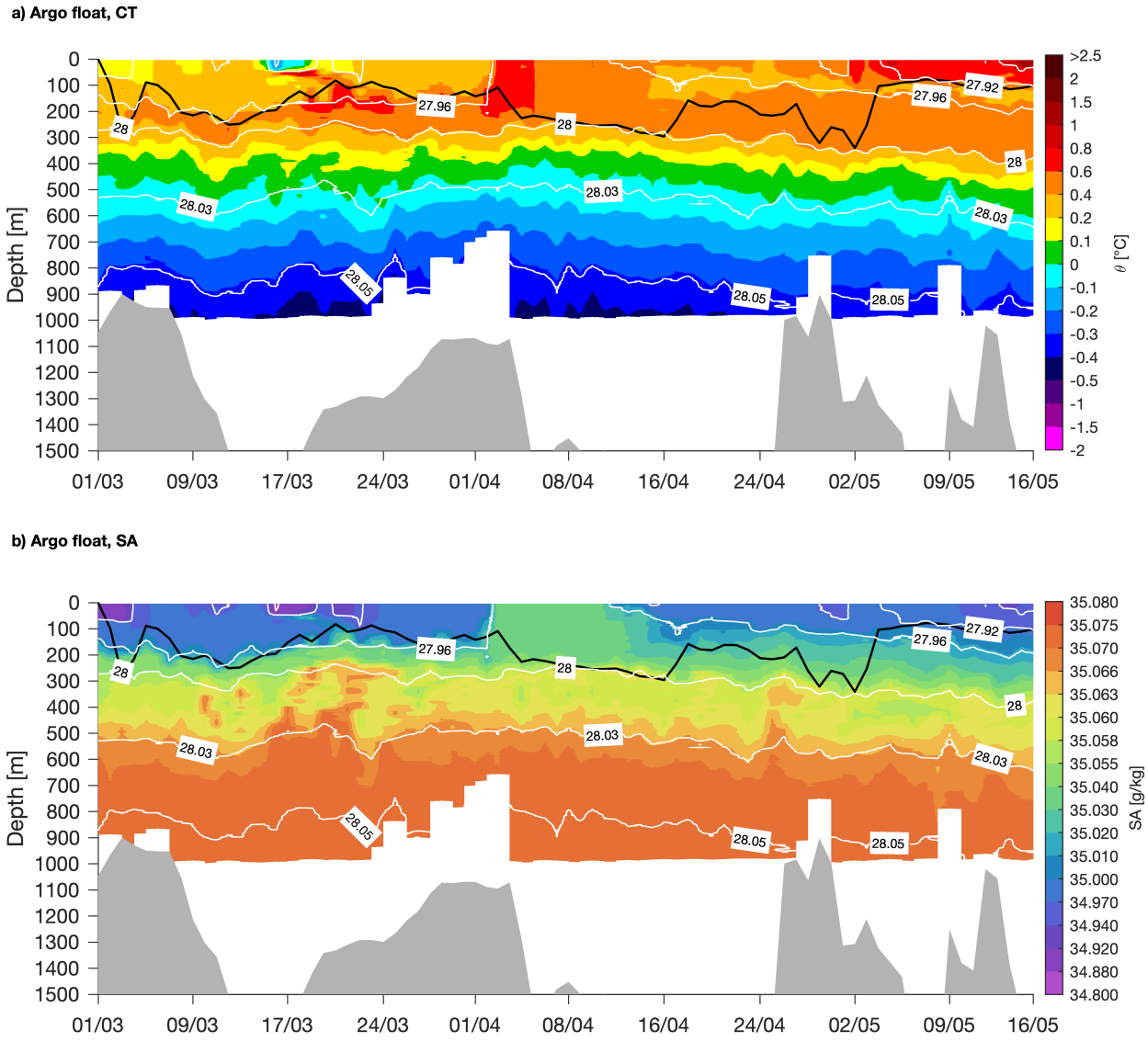

Figure 4.8: Temperature (color shading in **a)** and salinity (color shading in **b)** from the Argo float. White contour lines are density, and the black line represents the mixed-layer depth estimated with the temperature algorithm from the Argo float. Gray patches are bathymetry from ETOPO1 (Amante and Eakins, 2009).

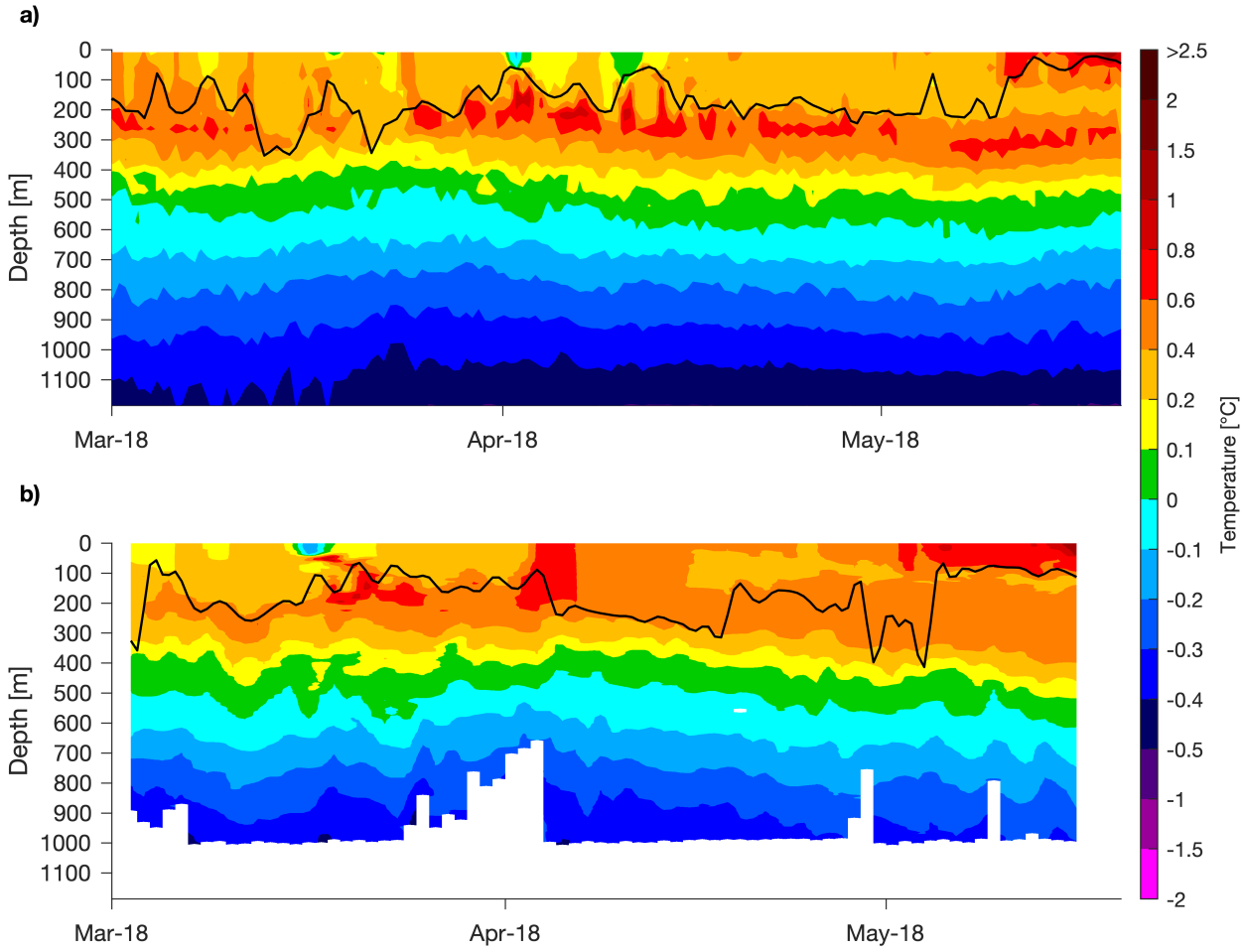

Figure 4.9: In-situ temperature (color shading) and mixed-layer depths (black line) from the Eggvin Offset Mooring **(a)** and the Argo float **(b)**, for the time period from 28 February 2018 to 16 May 2018.

The three cruises that occupied a section across the Eggvin Offset showed that the water was in general horizontally homogeneous. This was seen in the temperature, salinity, and density measurements (flat isopycnals in Figs. 4.11, 4.12, and 4.13). Similarly showed the Argo float, that circulated in the channel before it drifted into the Iceland Sea, that the whole channel in general was relatively horizontally homogeneous (Fig. 4.8).

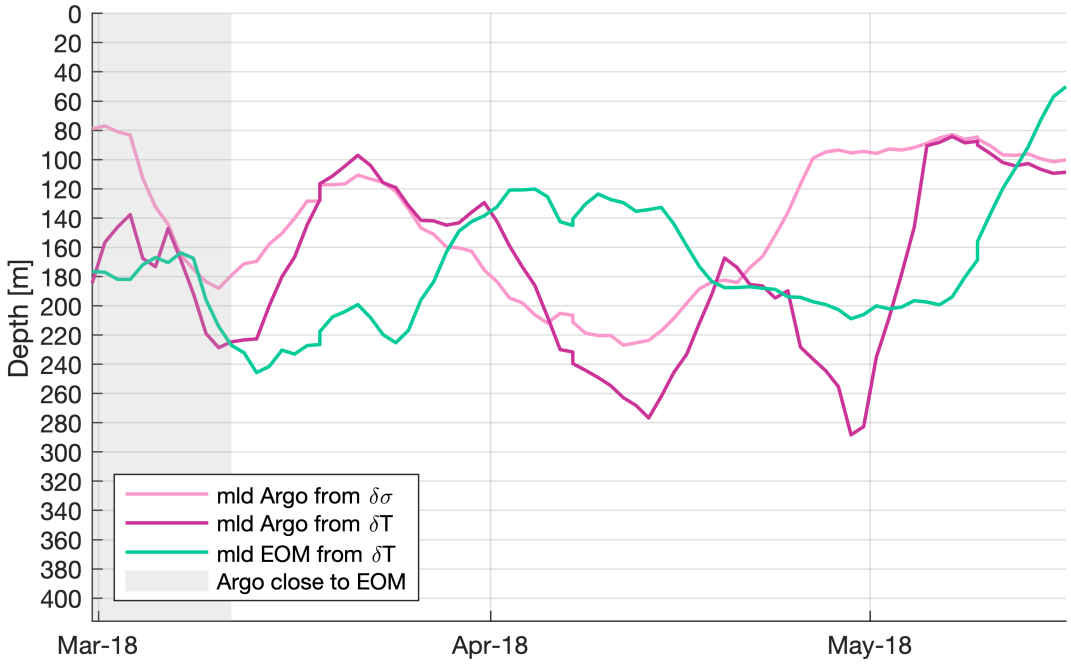

Figure 4.10: Time series of mixed-layer depth (mld) from the Eggvin Offset Mooring (EOM, green) and the Argo float (red and pink). The green and red lines are calculated using the temperature algorithm, while the pink line is calculated from the density method (Section 3.6). The shading indicates where the Argo float was relatively close to the Eggvin Offset Mooring (3 km – 12 km away).

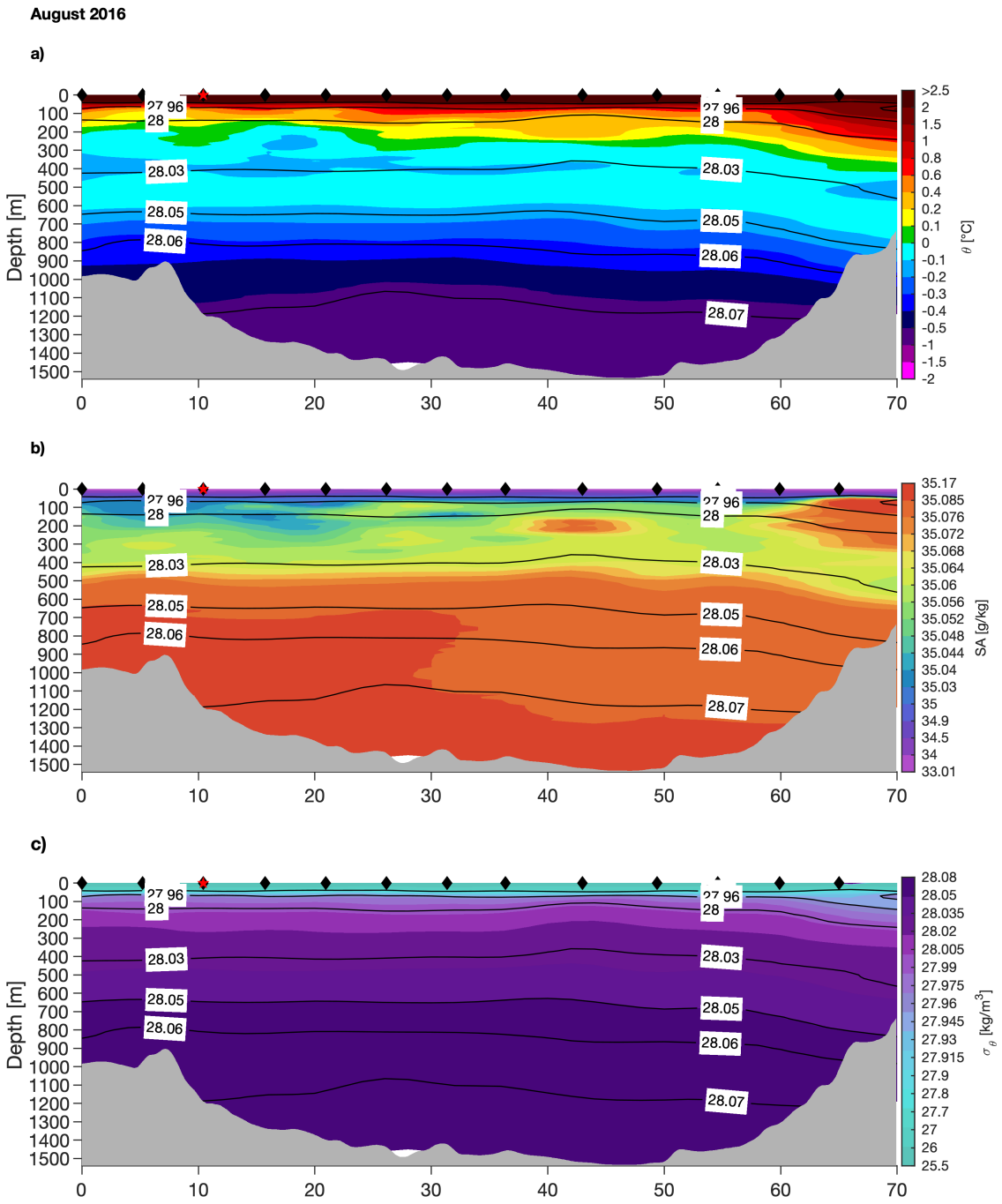

Figure 4.11: Temperature **(a)**, salinity **(b)**, and density **(c)** across the Eggvin Offset, with data collected from R/V *Håkon Mosby* in August 2016. The cross-section (in km) is from south (left) to north (right). The numbers and black contours are density. The black diamonds show the different CTD stations. The red star is the location of the Eggvin Offset Mooring.

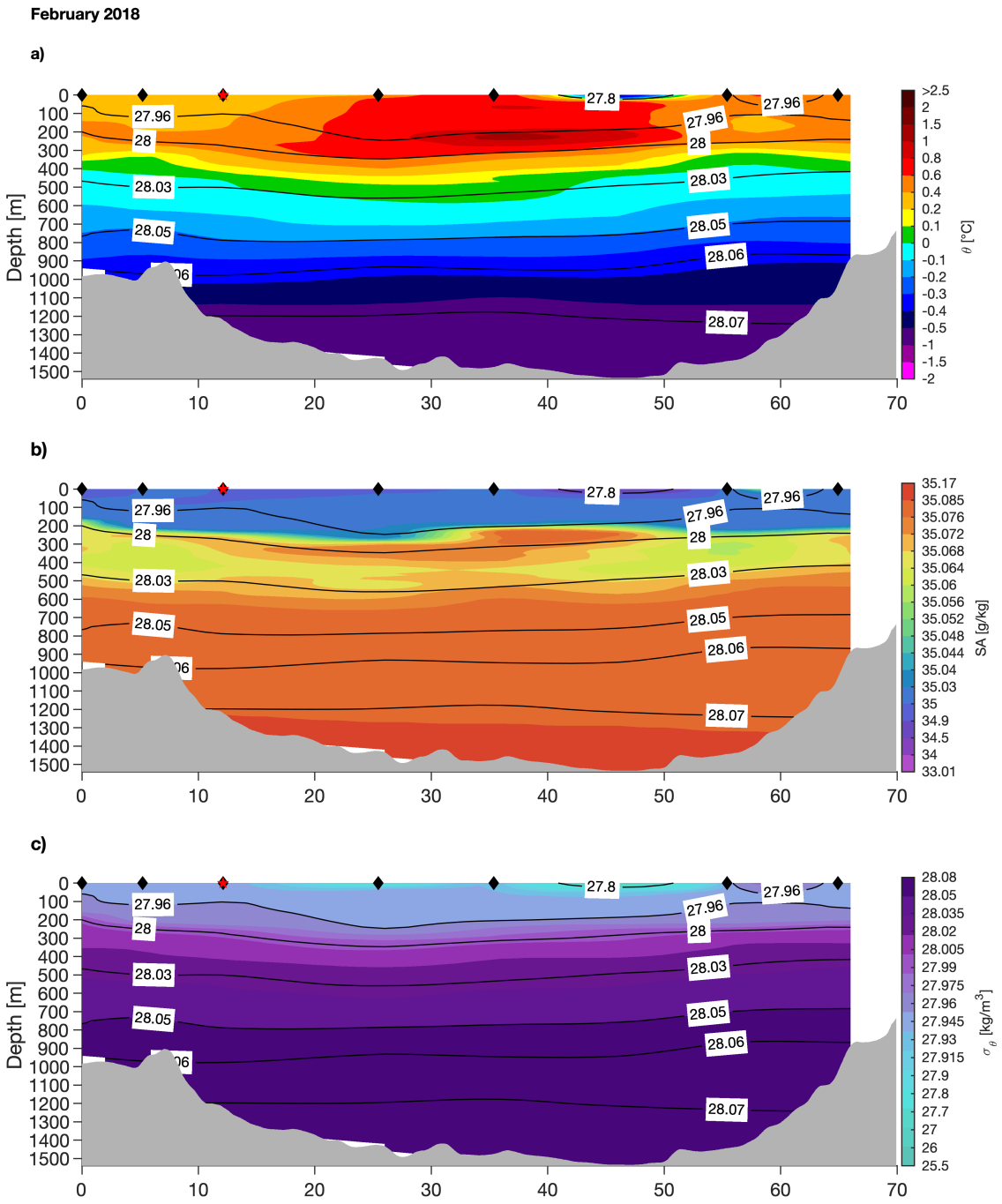

Figure 4.12: Temperature **(a)**, salinity **(b)**, and density **(c)** across the Eggvin Offset, with data collected from the R/V *Alliance* in February 2018. The cross section (in km) is from south (left) to north (right). The numbers and black contours are density. The black diamonds show the different CTD stations. The red star is the location of the Eggvin Offset Mooring.

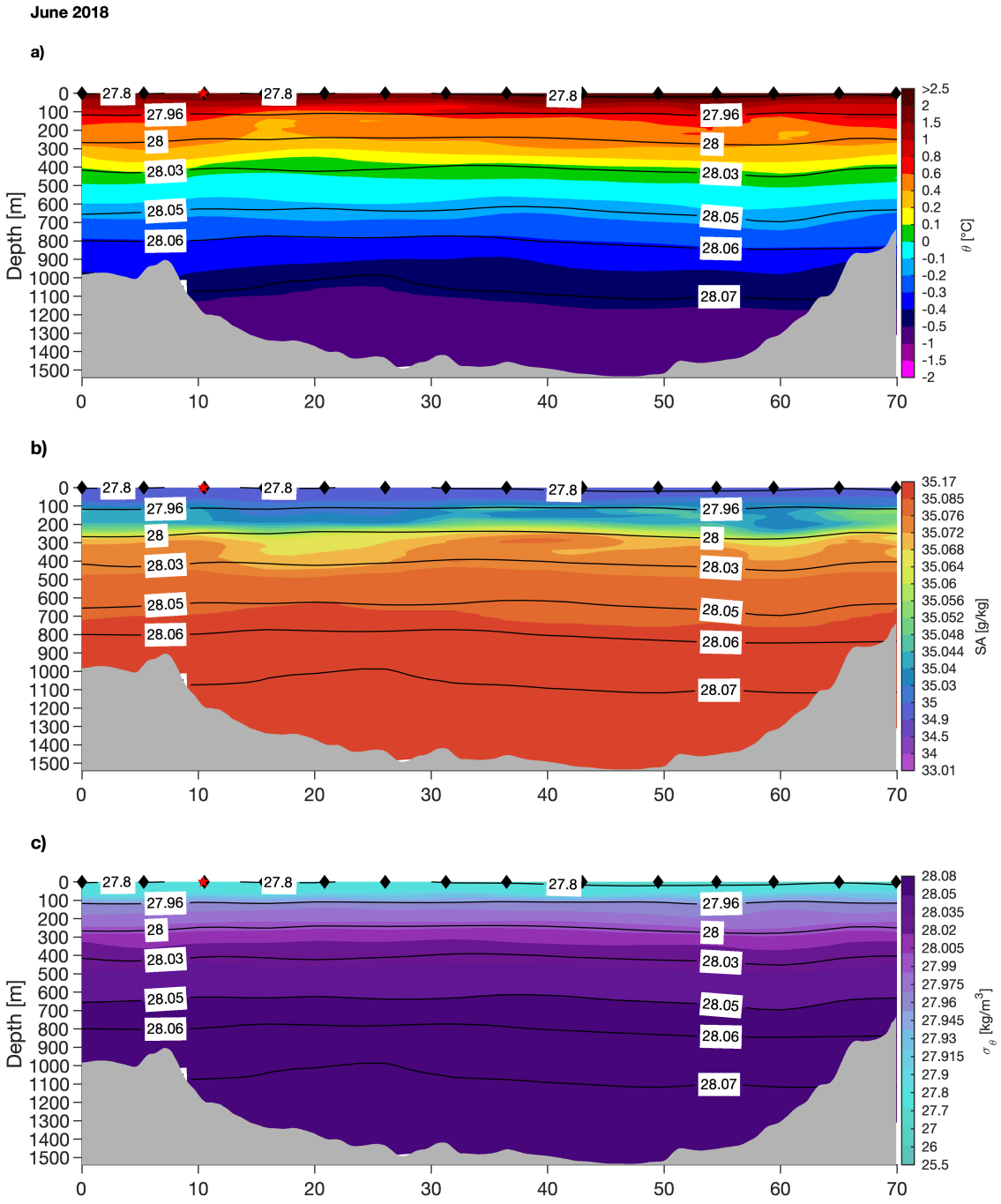

Figure 4.13: Temperature **(a)**, salinity **(b)**, and density **(c)** across the Eggvin Offset, with data collected from the R/V *Kristine Bonnevie* in June 2018. The cross section (in km) is from south (left) to north (right). The numbers and black contours are density. The black diamonds show the different CTD stations. The red star is the location of the Eggvin Offset Mooring.

4.1.1 Atmospheric forcing

The two winters in the Eggvin Offset were quite different. The hydrographic measurements revealed that winter 2017-18 was in general warmer than the previous winter, and that the mixed-layer depths were shallower and the mixed-layer densities were lower. There are two ways the water can be cooled, either by atmospheric forcing or by advection of colder water masses. This subsection focuses on the regional and local atmospheric conditions. Could late-winter atmospheric forcing explain the differences of the hydrography between the two winters?

The mean atmospheric turbulent heat fluxes were twice as high (more negative) in winter 2016-17 (-95 W/m^2) than winter 2017-18 (-56 W/m^2, Figs. 4.14a, b, and 4.15a, b). Hence, a much stronger cooling was observed in the ocean surface in winter 2016-17 than in winter 2017-18. Additionally, the 50% and 15% sea ice edge were much closer to the Eggvin Offset Mooring in winter 2016-17 than in winter 2017-18 (Figs. 4.14a and b). The highest heat fluxes were found near the ice edge, as expected, which in part explains the higher heat fluxes in winter 2016-17 than the following winter at the mooring location (Fig. 4.14a and b).

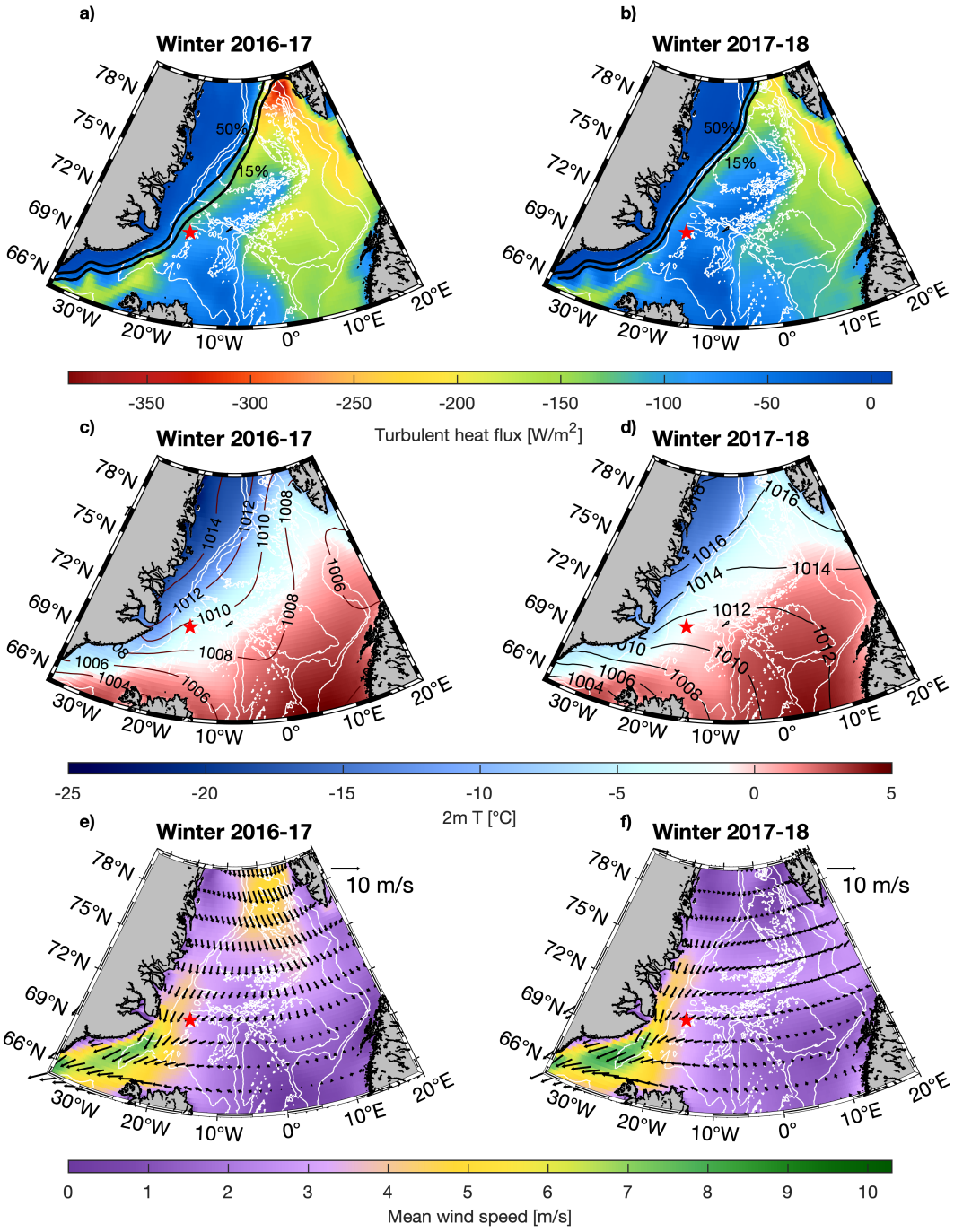

Figure 4.14: ERA5 reanalysis data, averaged over the late-winter months (February-April). The left column shows winter 2016-17 and the right column shows winter 2017-18. The red star is the location of the Eggvin Offset Mooring. **a)** and **b)** show the turbulent heat flux with bathymetry as white contour lines. The thick black lines are the 50% and 15% sea ice concentration contours. **c)** and **d)** show 2 m atmospheric temperature, with black contours of mean sea level pressure. **e)** and **f)** show the wind speed, with black arrows representing the strength and direction of the wind. The white contours are bathymetry from ETOPO1 (Amante and Eakins, 2009).

The mean 2 m atmospheric temperature was three times as cold in the first winter than the following (-3°C versus -1°C, Figs. 4.14c and d). While winter 2016-17 was always below 0°C, winter 2017-18 had periods of positive temperatures. These positive temperatures were found during February 2018, when strong and warm southerly winds dominated the entire Nordic Seas and north of Fram Strait (Fig. 4.16). Simultaneously as this warming, the 15% sea ice concentration edge retreated towards Greenland.

The Eggvin Offset was also exposed by southeasterly winds in February 2017, but they were weaker, and additionally, northerly winds occupied the Nordic Seas north of 70° W and along the ice edge of east Greenland (Fig. 4.16). The late-winter mean northerly winds were in general stronger in the first winter compared to the second (Figs. 4.14e and f).

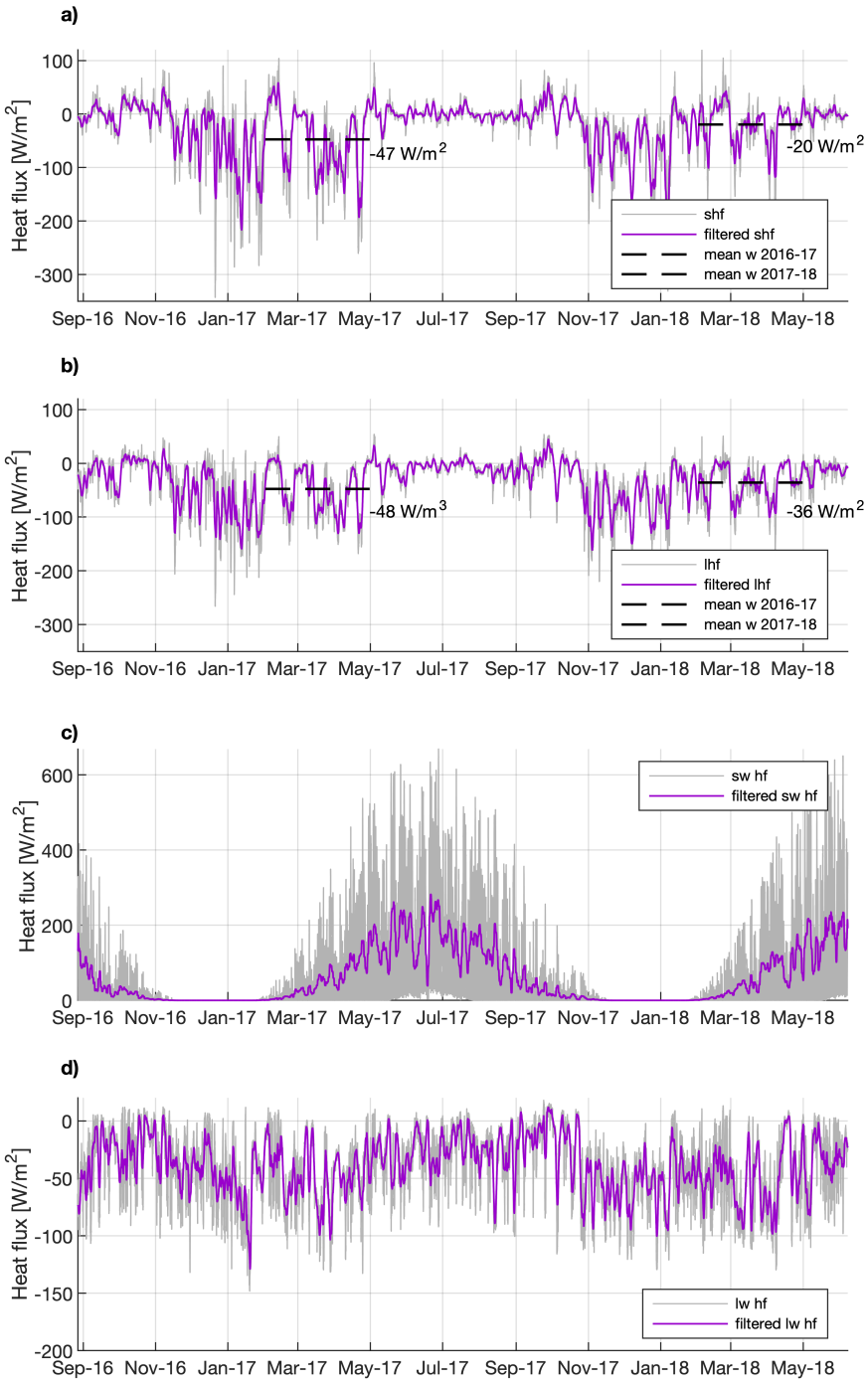

Figure 4.15: Atmospheric heat fluxes from ERA5 reanalysis data. The purple lines are 2-day filtered data, while the gray lines are unfiltered, hourly data. **a)** shows sensible heat fluxes (shf), **b)** latent heat fluxes (lhf), **c)** shortwave radiation (sw hf), and **d)** long wave radiation (lw hf). Negative values are defined as heat going from the ocean to the atmosphere (upward). The thick, black dashed lines and numbers are late-winter means.

The atmospheric differences of the two winters were investigated more closely, in order to better understand the oceanic differences (Fig. 4.17). The differences in turbulent heat flux, 2 m atmospheric temperature, and wind speed and direction between the two winters are presented in Fig. 4.17. Firstly, these show that the atmospheric heat fluxes were much higher in the Eggvin Offset the first winter, and were located along, or near, the ice edge. Secondly, the 2 m atmospheric temperatures were much lower the first winter than the following winter over the whole region. Finally, the northerly winds were stronger in the Eggvin Offset, and along the ice edge, in winter 2016-17 than winter 2017-18 (green color in Fig. 4.17c).

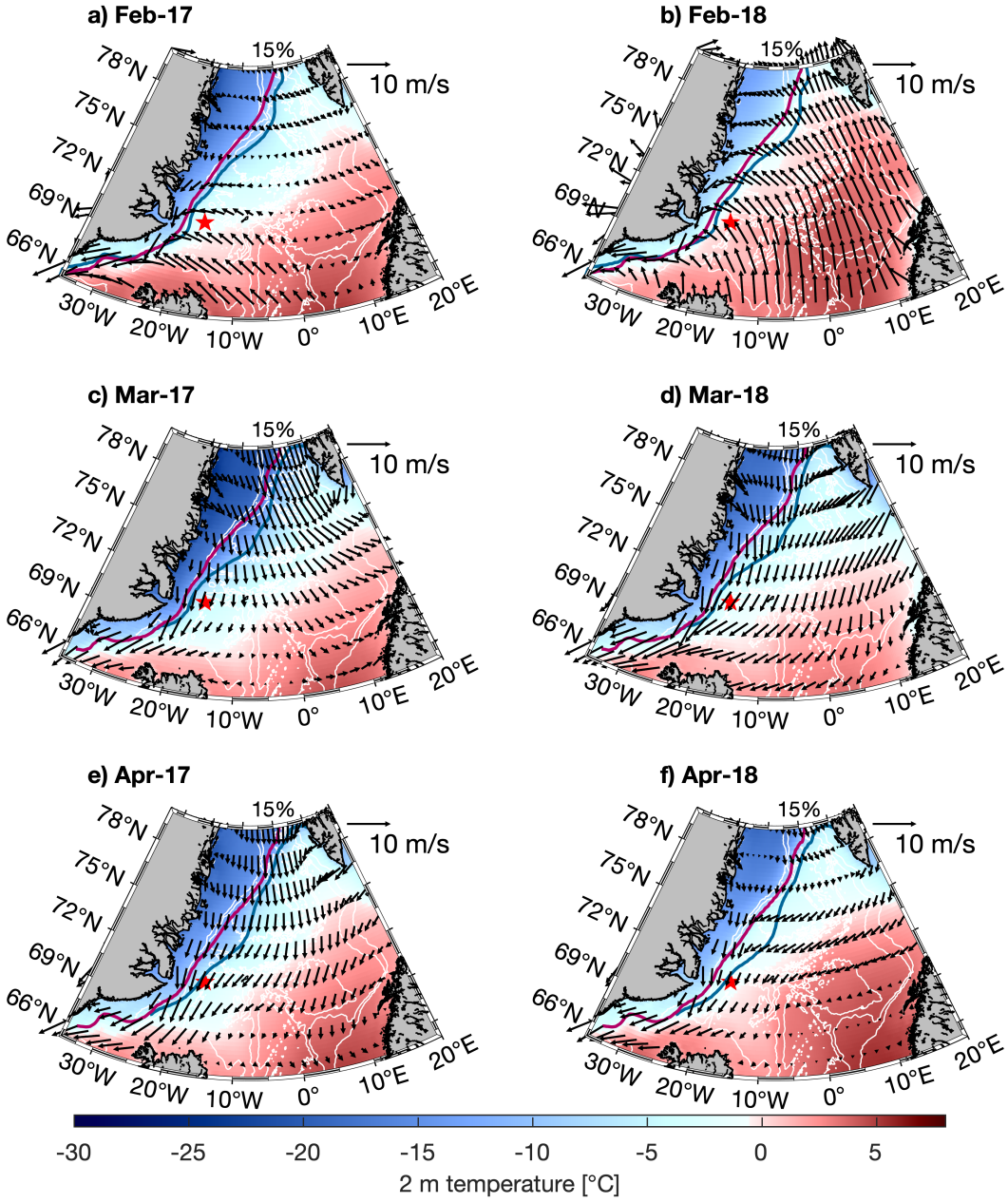

Figure 4.16: Monthly mean 2 m atmospheric temperature (color shading), wind speed and direction (black arrows), and 15% sea ice edge (blue contours for winter 2016-17 and red contours for winter 2017-18). The white contours are bathymetry from ETOPO1 (Amante and Eakins, 2009) and the atmospheric data are from Copernicus Climate Change Service (C3S) (2017).

To further investigate the interaction between the atmosphere and the ocean, different time periods with relatively constant mixed-layer depths (gray shading in Fig. 4.3a) were studied more closely together with atmospheric turbulent heat fluxes (Figs. 4.18 and 4.19). This method made it possible to compare the generally much higher ocean heat flux with the atmospheric heat flux. These periods are hereafter called stages, and the very high temporal resolution of the moored measurements made it possible to cover cold-air outbreak events (Section 2.3; Renfrew *et al.*, 2019).

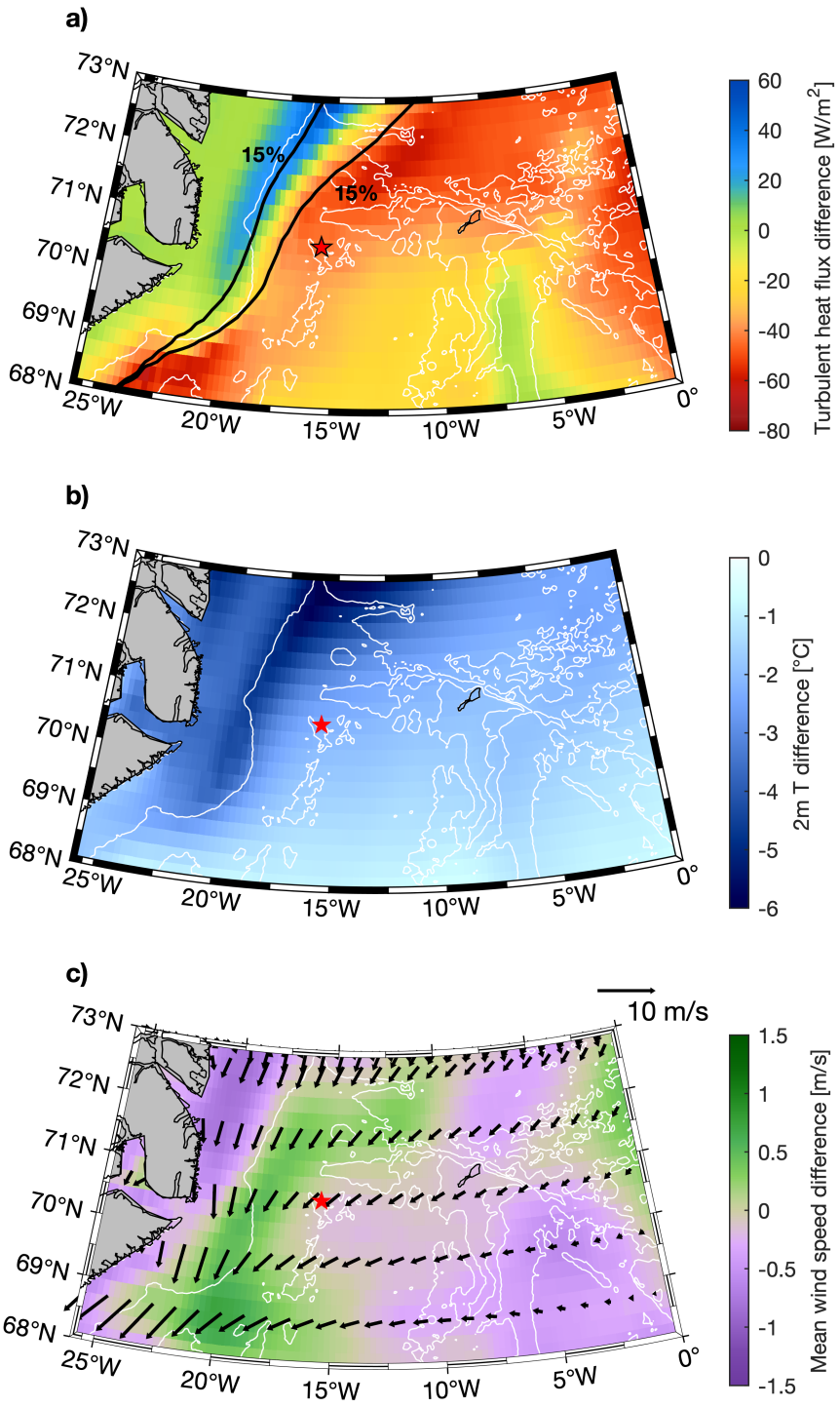

Figure 4.17: Late winter (February-April) differences between winter 2016-17 and 2017-18 (first winter minus second winter). **a)** Difference in turbulent heat flux (color shading) and late winter mean sea ice extent (black contours, winter 2016-17 to the east and winter 2017-18 to the west). **b)** Difference in 2 m atmospheric temperature (color shading). **c)** Difference in wind strength (color shading) and mean wind direction (black arrows). The red star is the location of the Eggvin Offset Mooring.

In winter 2016-17, several cold-air outbreak events were observed in all three stages. In stage one, two examples are from 15 to 17 November and from 6 to 8 December (Fig. 4.18a). In stages two and three, the turbulence heat fluxes were in general higher, and some cold-air outbreak events were observed from 11 to 13 January and 21 to 23 April. The following winter was quite different. Only two stages were observed, as the mixed layer was not made sufficiently dense to penetrate deeper in the water column (Fig. 4.19). However, the atmospheric turbulent heat fluxes in November were relatively high, but not sufficiently high to deepen the mixed layer. In fact, the atmospheric heat flux and the ocean heat flux were strongly anti-correlated in this time period, which means that another mechanism must impact the hydrography in the upper ocean.

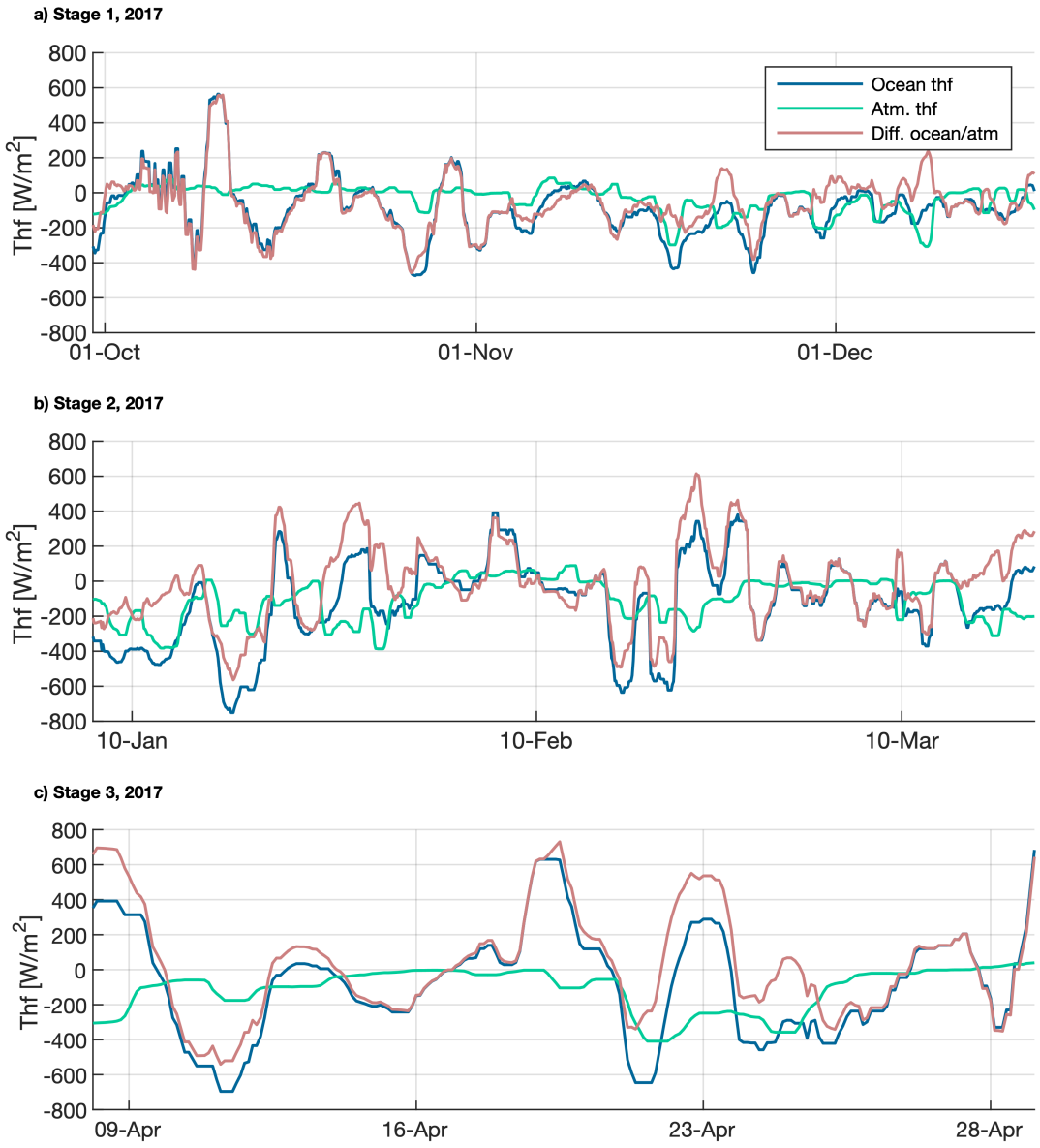

Figure 4.18: Atmosphere (green) and ocean (blue) heat fluxes during three different stages indicated in Figure 4.3, in winter 2016-17. The red line represents the difference between the ocean and atmosphere heat fluxes (ocean minus atmosphere). Note the different time axes of the three panels.

The difference between the oceanic heat flux and the atmospheric heat flux (light red line in Figs. 4.18 and 4.19) followed the oceanic heat flux most of the time, which means that the atmospheric heat flux was low compared to the ocean heat flux. In general for winter 2016-17, the atmospheric heat flux increased in magnitude from stage 1 to stage 3, from ca. $-50\,\mathrm{W/m^2}$ to $-130\,\mathrm{W/m^2}$. In winter 2017-18, on the other hand, the atmospheric heat flux decreased in magnitude from stage 1 to stage 2, from ca. $-140\,\mathrm{W/m^2}$ to $-60\,\mathrm{W/m^2}$. Note, these numbers deviate from the mean late-winter values mentioned above, as these values represent the mean of the first and last stages.

The atmospheric forcing had a pronounced effect on the mixed-layer depth. As such, the stronger atmospheric heat fluxes in 2017 contributed to deeper mixed layers, and oppositely, the weaker atmospheric heat fluxes in 2018 caused shallower mixed layers than the first winter (Fig. 4.20). Note that the strongest atmospheric heat flux in the beginning of March 2018 corresponds to the cold-air outbreak observed during the Iceland Greenland Seas project field campaign (Renfrew *et al.*, 2019). This event lasted for more than 10 days, until 12 March 2018, which is seen from the relatively strong atmospheric heat flux period in the ERA5 data in this study (Fig. 4.20b). This event led to a rapid deepening of the mixed layer, approximately 200 m.

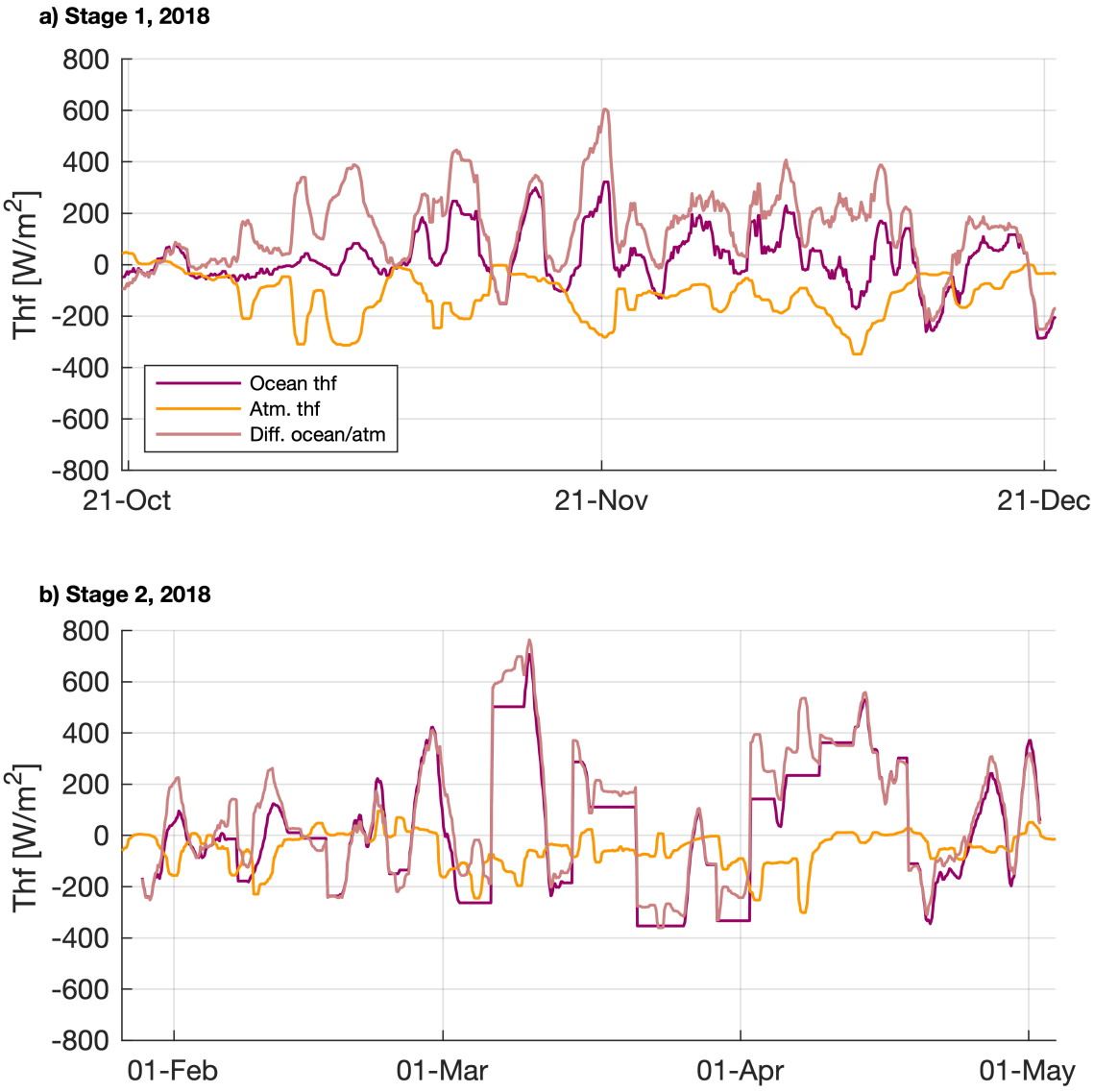

Figure 4.19: Atmosphere (orange) and ocean (dark red) heat fluxes during the two stages indicated in Figure 4.3, in winter 2017-18. The light red line represents the difference between the ocean and atmosphere heat fluxes (ocean minus atmosphere). Note the different time axes of the three panels.

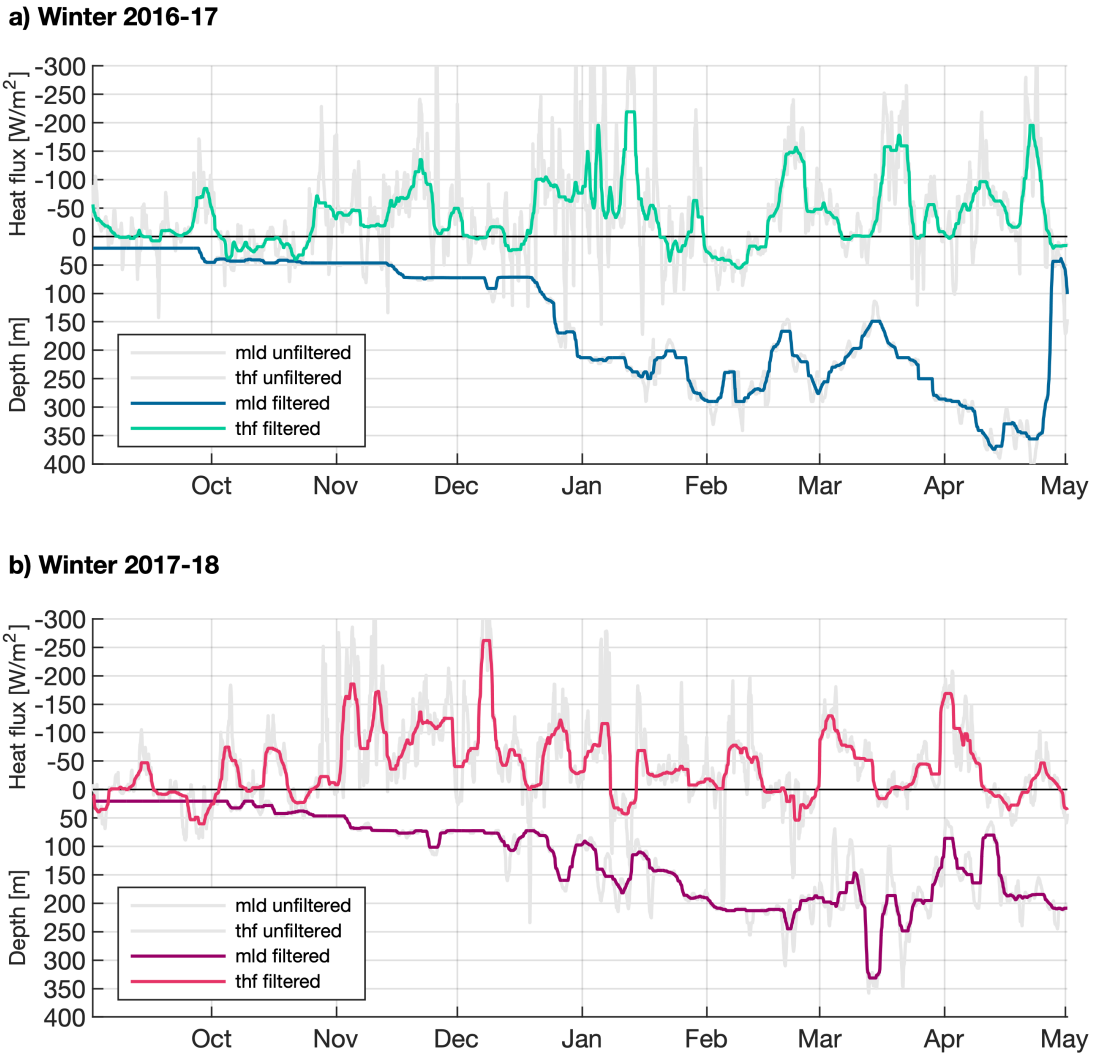

Figure 4.20: Atmospheric heat fluxes (thf) and mixed-layer depths (mld). **a)** Filtered atmospheric turbulent heat fluxes (green) and filtered mixed-layer depths (blue), both for winter 2016-17. **b)** Filtered atmospheric turbulent heat fluxes (light red) and filtered mixed-layer depths (dark red) for winter 2017-18. The light gray lines are unfiltered time series.

4.1.2 The impacts of sea ice

Sea ice is another important factor that can impact the mixed-layer depth. The strongest heat fluxes are found in the vicinity of the ice edge (Section 2.3; Figs. 4.14a and b; Marshall and Schott, 1999; Renfrew and Moore, 1999; Våge *et al.*, 2015 and Papritz and Spengler, 2017), due to

discharge of cold polar air masses over the relatively warm ocean surface.

Sea ice concentration from ERA5 were used to investigate the effect of the proximity of the sea ice edge to the mooring location on the mixed-layer evolution in the Eggvin Offset (Fig. 4.21). In the first winter (February-April), the 15% sea ice concentration edge was 70 km west of the Eggvin Offset Mooring. In the second winter, this 15% sea ice concentration edge was 125 km west of the mooring, much closer to the Greenland coast. Furthermore, the sea ice advanced towards the mooring during winter 2016-17, while it was closest to the mooring at the beginning of the following winter and retreated towards Greenland with time (Fig. 4.22). This was in line with the wind observations, where the northerly winds strengthened during winter 2016-17, and were in general weak during winter 2017-18 (Fig. 4.16).

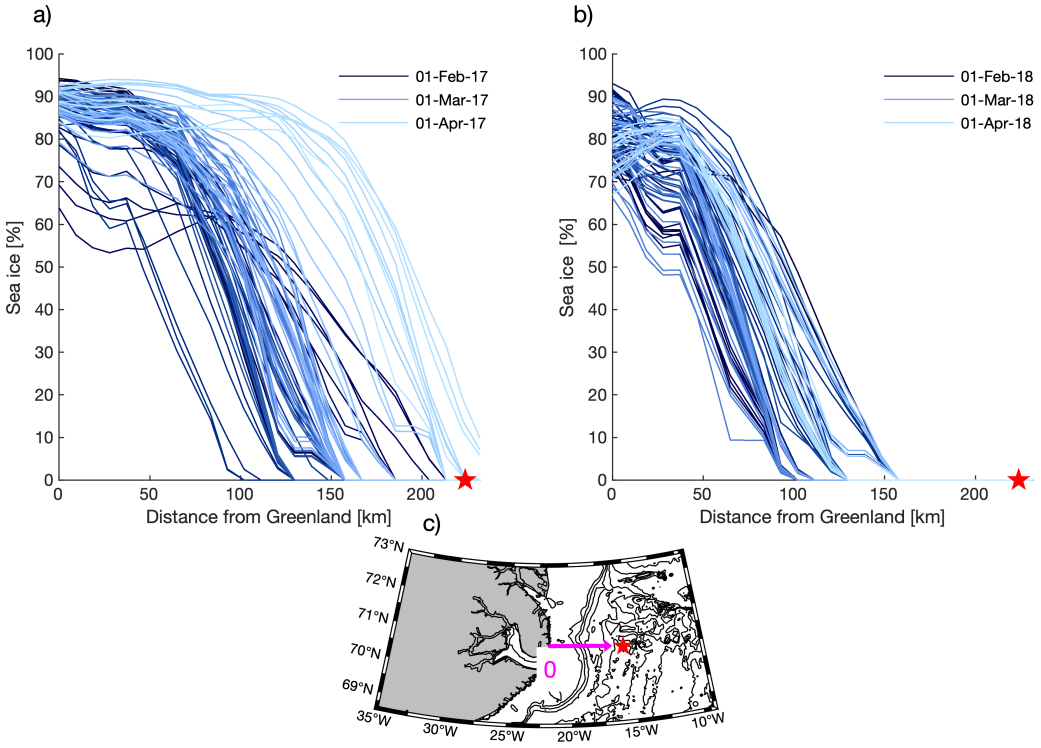

Figure 4.21: Sea ice concentration as a function of distance between Greenland and the Eggvin Offset Mooring, during winter 2016-17 **(a)** and winter 2017-18 **(b)**. The color shading represents time from February (dark blue) to April (light blue). There are many more lines than observed from this figure, as several are converging due to the lat-lon resolution. The map **(c)** shows the x-axis, which has its origin (the '0') at the Greenland coast at the same latitude as the Eggvin Offset Mooring. The red star is the Eggvin Offset Mooring.

In order to find the dominating factor for deep-water formation in this area, it was of interest to understand the link between the sea ice edge and the atmospheric heat fluxes. The atmospheric turbulent heat fluxes were therefore investigated as a function of the 15% sea ice concentration edge, between Greenland and the Eggvin Offset Mooring (Fig. 4.22). The largest heat fluxes were found at, or near, the ice edge for both winters. The extent of the ice edge was coherent with the peak in heat fluxes for both winters. The differences between the two winters became evident: higher turbulent heat fluxes in the first winter than in the second one.

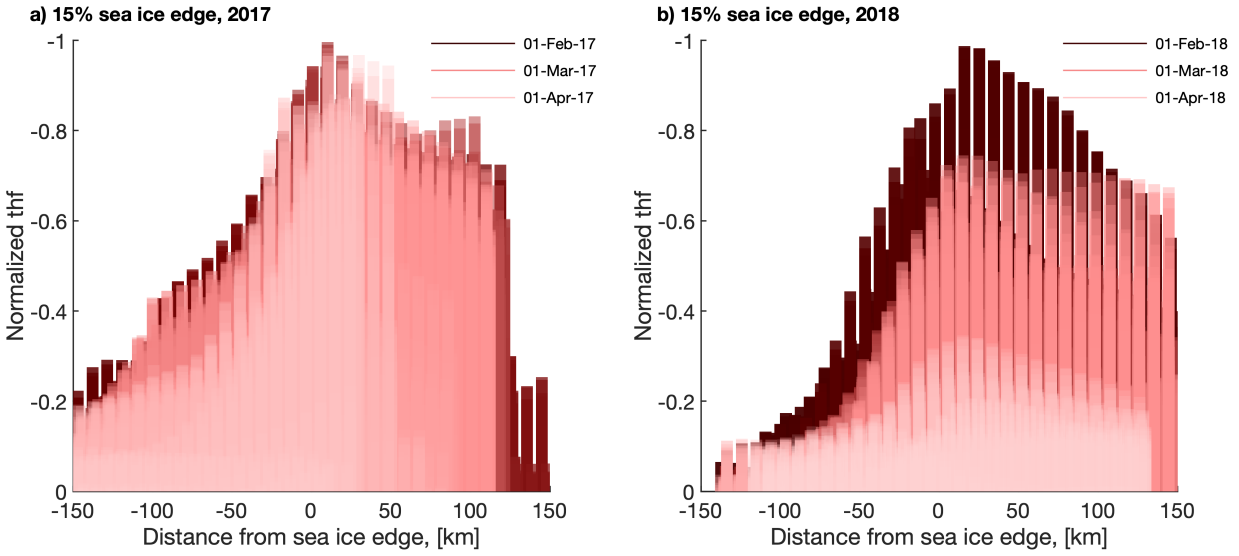

Figure 4.22: Atmospheric turbulent heat fluxes as a function of the sea ice edge for winter 2016-17 **(a)** and 2017-18 **(b)**. The y-axes are normalized heat flux and the x-axes are distance from the ice edge. Negative heat fluxes represent heat loss from the ocean. The color shading is transparent and represents time, from February (dark colors) to April (light colors). The transparency is added to illustrate the large amount of profiles that are plotted.

4.2 Flow through the Eggvin Offset

Observations from this study showed that water sufficiently dense to supply the overflow at Denmark Strait ($\sigma_\theta \geq 27.8\,\mathrm{kg/m^3}$) was ventilated in the Eggvin Offset during both winters. The densities at intermediate and greater depths were also sufficiently dense to supply the densest component of the NIJ, which has a transport mode of 28.05 $\mathrm{kg/m^3}$ $\pm$ 0.01 $\mathrm{kg/m^3}$ (Section 3.7; Semper *et al.*, 2019). The NIJ transport mode was, however, not formed in the Eggvin Offset,

only nearly the first winter. Such dense water could have been transported through the Eggvin Offset. Transports of two dense-water layers were estimated in order to address the importance of the Eggvin Offset to the DSOW: One transport concerned the mixed layer, and the other layer was estimated over the depth interval where densities corresponded to the NIJ transport mode which is 550 m to 850 m in the Eggvin Offset (Fig. 3.9).

The circulation in the Eggvin Offset was hence studied, by use of velocity data from the moor-ing, shipboard data from the three cruises, and the drift of the Argo float (Section 3.3). The time and depth averaged displacement of water in the Eggvin Offset indicated the direction of flow at different depths (Fig. 4.23). The displacement of water varied over time, especially in the surface layer. A northwestward flow was observed in the upper 100 m, while at intermediate and great depths the flow was more or less eastward into the Iceland Sea. This was especially true from January through May for both years (Fig. 4.24). The flow through the channel was in general relatively weak with a pronounced barotropic signal, seen as nearly constant velocities in the vertical (Fig. 4.24).

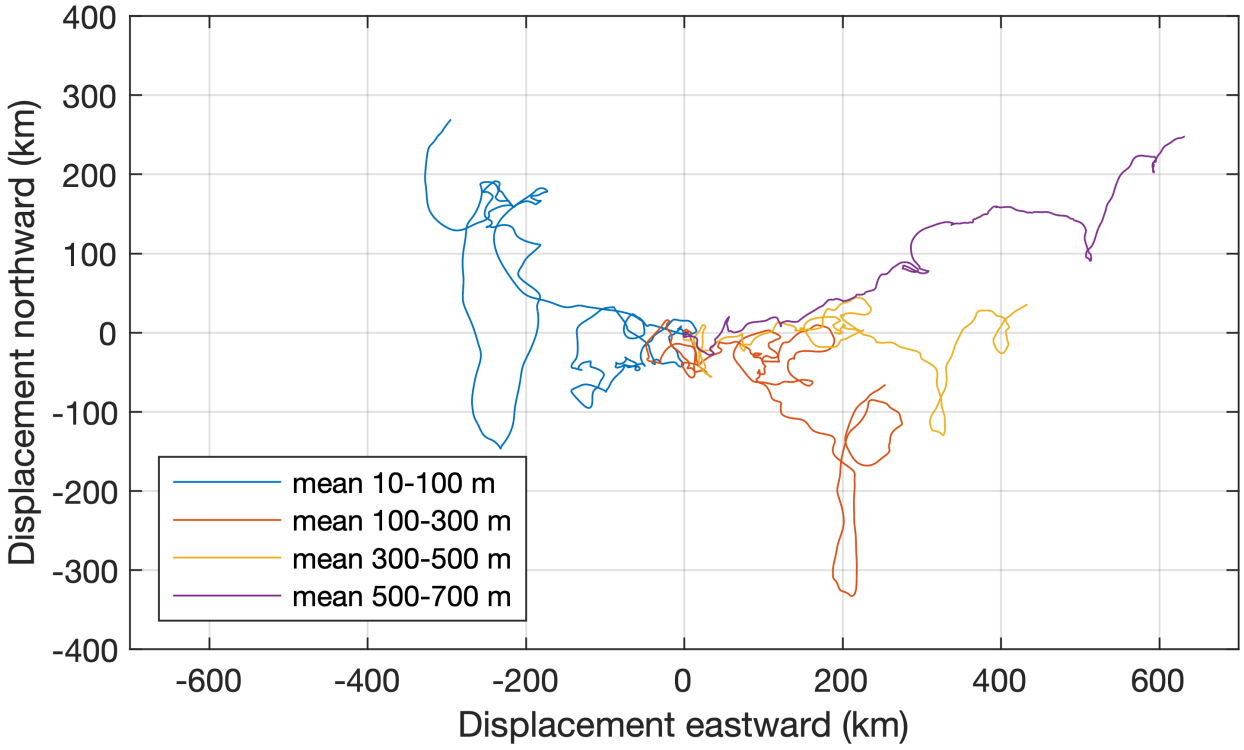

Figure 4.23: Progressive vector diagram of a 5-day low-pass filtered, depth-averaged displacement in the Eggvin Offset, from August 2016 to June 2018.

Sections of absolute geostrophic velocity, constructed from shipboard and ship-mounted measurements from the three cruises (Section 3.2), showed the velocity variation across the channel (Fig. 4.25). The velocities were low, and varied horizontally and from section to section. The velocities were, however, approximately uniform at intermediate and great depths along the southern slope of the channel (Section 3.7; Fig. 3.10).

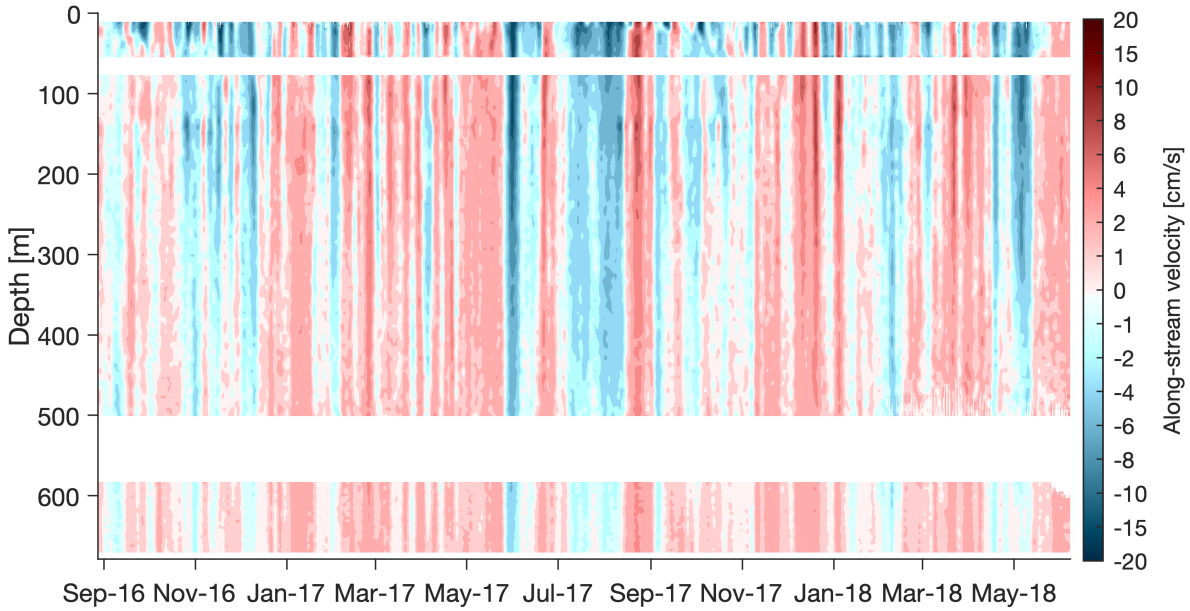

Figure 4.24: Along-stream velocities over the two years. Data are 5-day low-pass filtered and from the three ADCPs that covered the water column from 11 m to 700 m depth (Section 3.3). The instruments are separated by white bands. Red colors indicate eastward flow, toward the Iceland Sea, while blue colors indicate westward flow, toward Greenland. Velocity in cm/s.

The horizontal density variation across the channel was close to zero, observed from the flat isopycnals in Figs. 4.11, 4.12, and 4.13. Based on the assumptions listed in Section 3.7, the resulting geostrophic flow in the channel was permitted to only follow the isobaths (Fig. 4.26). This statement is also supported by the general knowledge of geostrophic flow on the Northern Hemisphere, flowing at right angles to the slope with shallower water on the right-hand side (equation 10-22 in Marshall and Plumb, 2016; Brown, 2016). This implies that water flowing through the Eggvin Offset is going from west to east into the Iceland Sea. Observations from the mooring agreed with this assertion (Fig. 4.24).

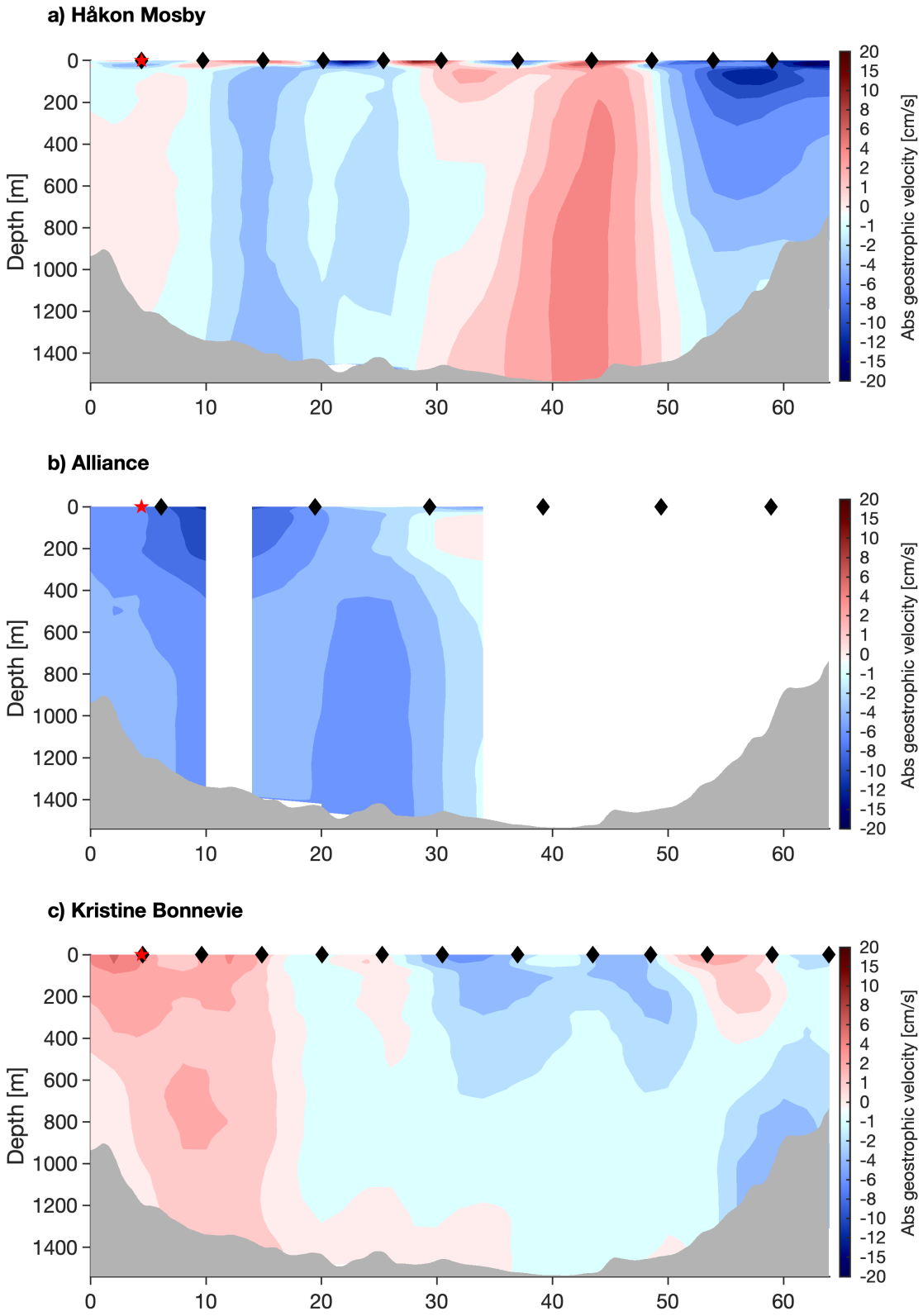

Figure 4.25: Absolute geostrophic velocity across the Eggvin Offset from the three cruises: **a)** R/V *Håkon Mosby*, **b)** R/V *Alliance*, and **c)** R/V *Kristine Bonnevie*. Red colors are eastward velocity into the Iceland Sea, and the blue colors are velocity towards Greenland. Velocities are in cm/s. The black diamonds represent the CTD stations, and the red star is the location of the Eggvin Offset Mooring.

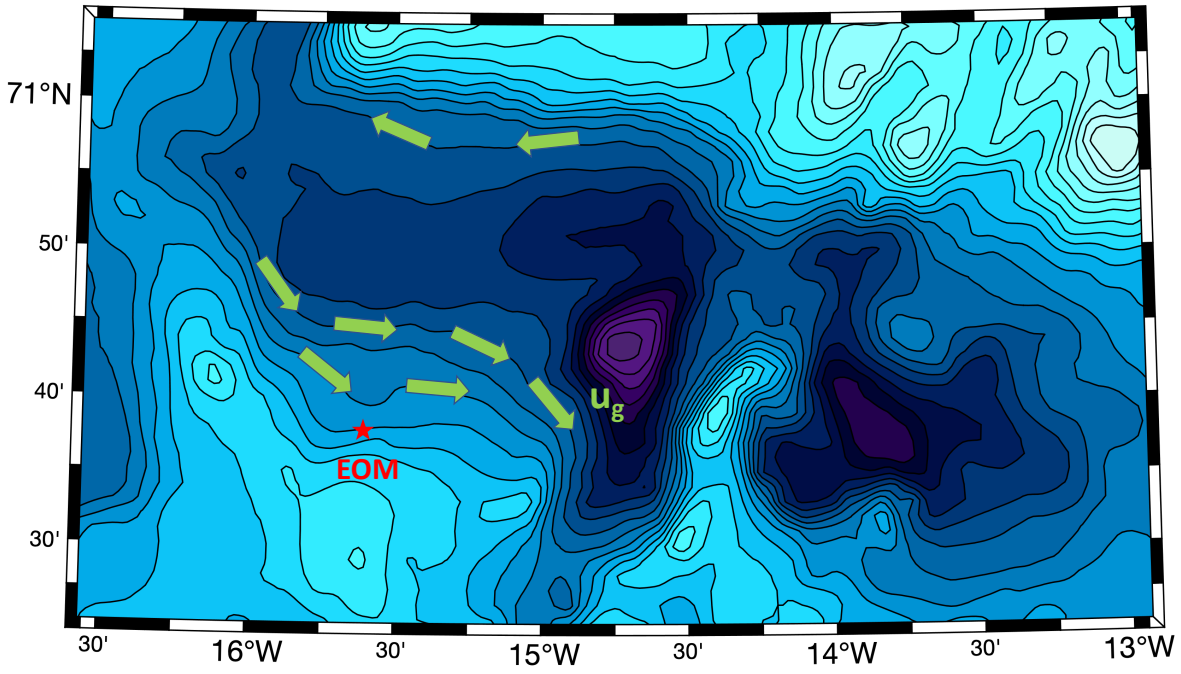

Figure 4.26: Isobaths in the Eggvin Offset (70°N, 15°W). The green arrows (added to the figure) indicate the direction of the geostrophic flow, following the isobaths (black contours). The red star is the Eggvin Offset Mooring (EOM). The colored shading is bathymetry from ETOPO1 (Amante and Eakins, 2009).

Based on these arguments and observations, the transport of dense water in the mixed layer, for periods when the density was higher than 27.8 kg/m^3, was estimated to be 0.013 Sv[1] with a transport range of [0.007 Sv to 0.015 Sv], averaged over the two years (Fig. 4.27). The dense-water transport at depth, on the other hand, was estimated to be 0.072 Sv with a transport range of [0.024 Sv to 0.105 Sv], averaged over the two years (Fig. 4.28). The overall transport, especially at depth, was directed into the Iceland Sea.

[1] Sv = 10^6 m^3/s, and is an oceanographic unit used to measure volumetric transport.

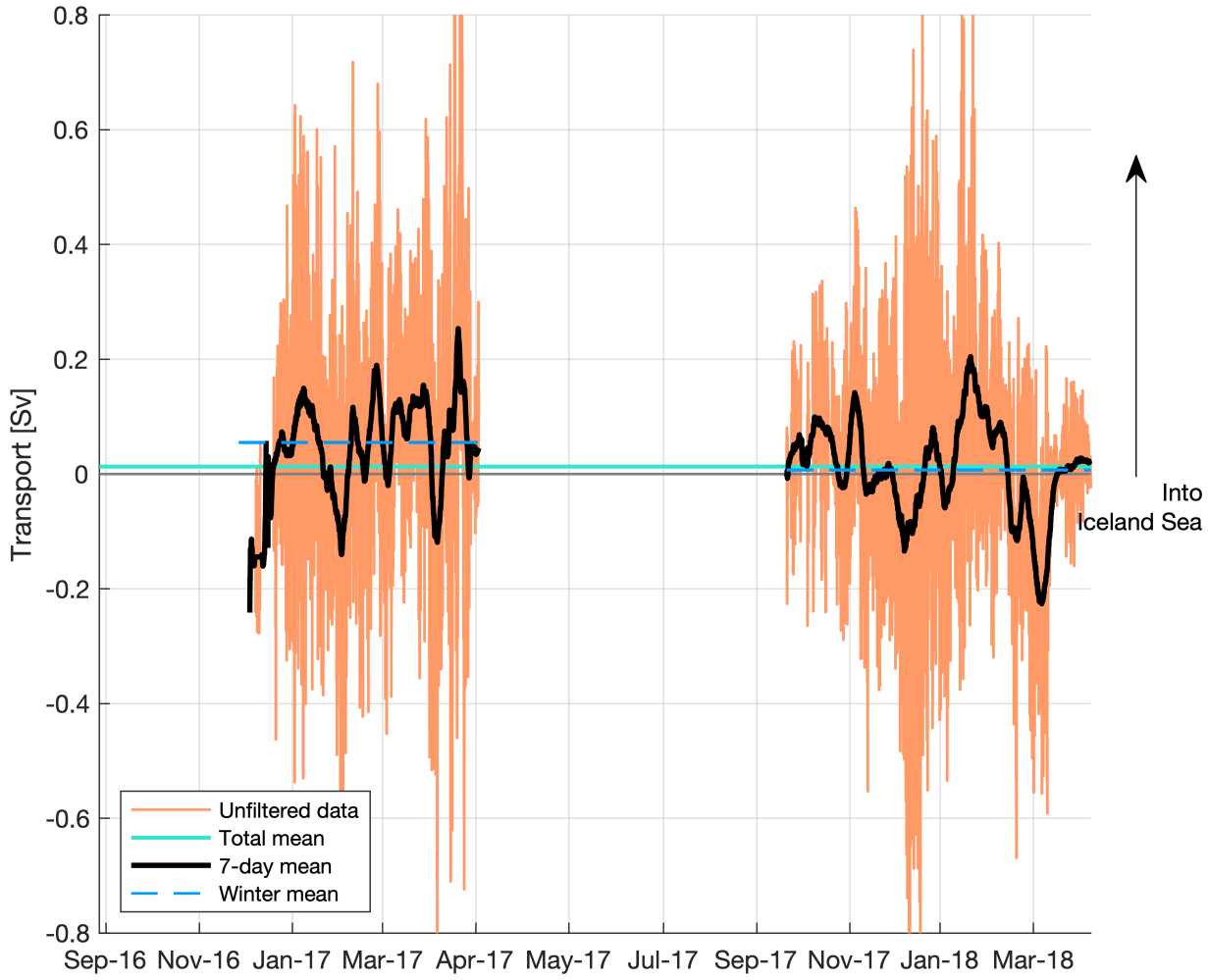

Figure 4.27: Transport in the mixed layer when the 27.8 kg/m^3 isopycnal was ventilated in the Eggvin Offset. Unfiltered transport is shown in orange, the black line is 7-day filtered transport, the gray line is the zero line to indicate when there was eastward or westward flow. Positive transport is directed into the Iceland Sea. The green line is the overall mean transport of 0.013 Sv.

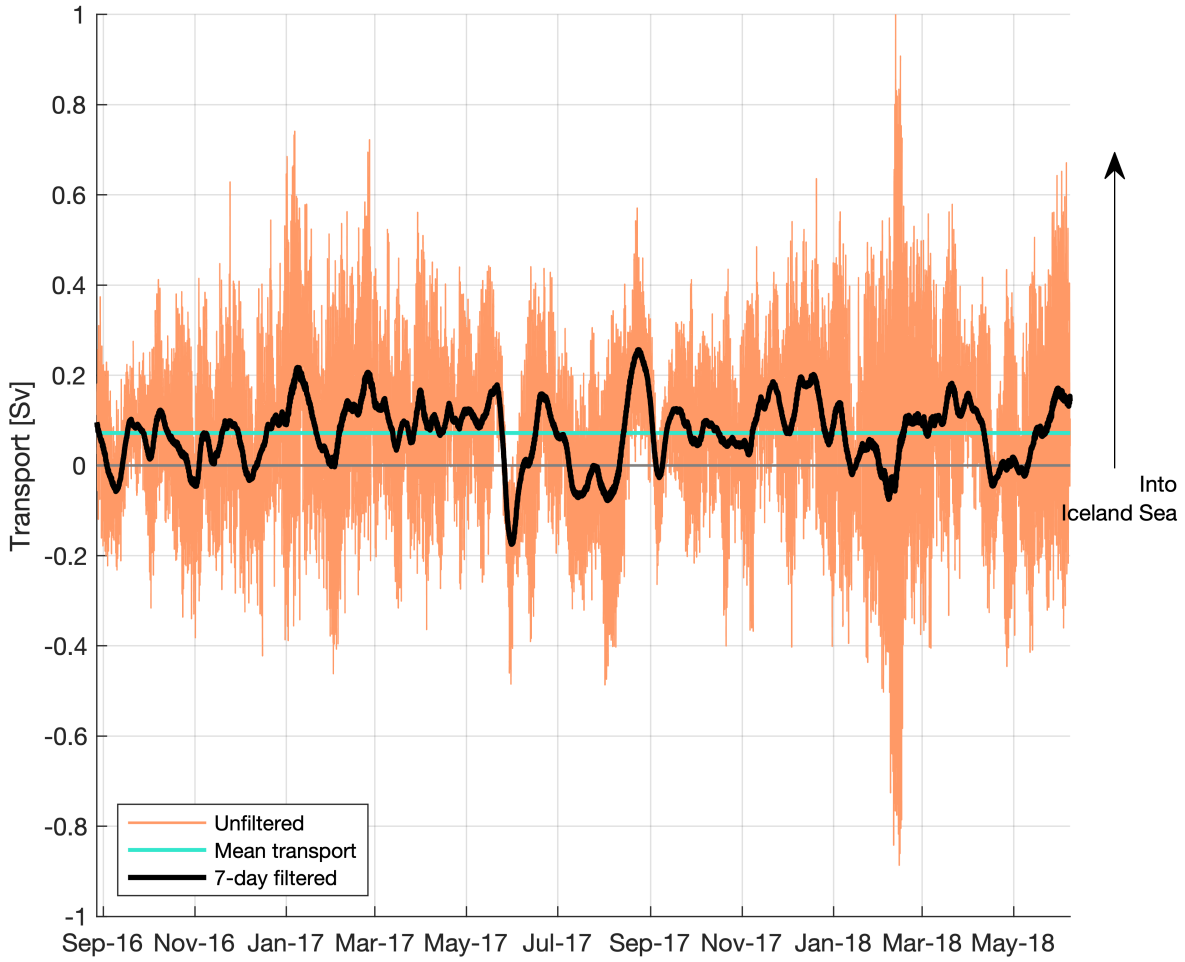

Figure 4.28: Transport of dense water, $28.04\text{kg/m}^3 \leq \sigma_\theta \leq 28.06\text{kg/m}^3$, averaged over 550 m - 850 m depth. The orange line is unfiltered data, the black line is 7-day filtered transport, and the green line is the overall mean transport of 0.072 Sv.

Chapter 5

Discussion

The subject of investigation in this study is the Eggvin Offset, which is the northernmost gap in the Kolbeinsey Ridge that connects the EGC to the west with the Iceland Sea to the east (Fig. 2.1). Analyses of a two-year mooring deployment revealed new findings of winter open-ocean convection and circulation in the northwestern Iceland Sea, where the deepest and densest mixed layers have been found in previous studies (Section 2.3; Våge *et al.*, 2015; Pickart *et al.*, 2017). However, the region was until lately scarcely sampled, because of sea ice cover in the past and harsh weather conditions during winter. Results from this study have therefore enhanced our knowledge of mixed-layer evolution and circulation in the northwestern Iceland Sea, as described below.

5.1 On the hydrography of the Eggvin Offset

The Eggvin Offset Mooring provided observations of seasonal variability in hydrography in the mixed layer (Fig. 4.2). The seasonal variability of salinity can be linked to the migration of the Polar Front, which is defined as the boundary between the Polar and the Arctic domains of the Nordic Seas (Section 2.2).

The observations demonstrated that the Polar Front, and hence the extent of Polar Water, migrated east of the mooring in summers 2016 and 2017, when the salinity at 8 m was observed to be less than 34.66 g/kg (Fig. 4.4). During fall, the surface layer became substantially more

saline as the Polar Front returned toward the west. This seasonal cycle of the Polar Front is closely linked to seasonal changes in large-scale wind stress in the Nordic Seas (Våge *et al.*, 2018; Langehaug *et al.*, prep). The northerly winds were weak in the Eggvin Offset during summer (not shown), which allowed the Polar Water to extend farther to the east. During fall and winter, the northerly winds strengthened and pushed the Polar Front westward (Fig. 4.16). This is in line with glider observations west of the Eggvin Offset in winter 2015-16 (Våge *et al.*, 2018). The lateral migration of the Polar Front is therefore an important factor for preconditioning the water for wintertime open-ocean convection in the Eggvin Offset.

The seasonal signal differed between the surface and greater depths. While the surface was cooling from fall throughout the winter, the measurements from 111 m and 367 m showed a warming until December. When the mixed layers reached 111 m and 367 m, however, the water at 111 m and 367 m started to cool, respectively (Fig. 4.3). This means that two different mechanisms were causing the hydrographic changes at surface and at depth. While the surface was exposed to local, atmospheric cooling, the water at depth was modified by advection of water through the channel. This advected water may come from the outer branch of the EGC, which has been observed to flow southeastward north and south of Jan Mayen, and thus may supply the Eggvin Offset (Bourke *et al.*, 1992; Håvik *et al.*, 2017).

Furthermore, the hydrography in the Eggvin Offset agrees with the water properties observed in the outer EGC in summer. Håvik *et al.* (2017) found that the water masses from the offshore end of two transects differed north and south of Jan Mayen. While the Atlantic- origin Water was present across the entire section in the Greenland Sea, a section toward the Eggvin Offset revealed less saline and colder water masses, distinct from Atlantic- origin Water masses. The temperature and salinity ranges of these water masses are in the same range as measured in the Eggvin Offset, where no maximum salinity and (nearly) no maximum in temperature were found at intermediate depths.

5.2 Evolution of the mixed-layer depth

Mixed-layer depths were determined from an autonomous algorithm applied to the in-situ temperature data, which is based on a difference criterion (Section 3.6; Nilsen and Falck, 2006), and validated by visual inspection. This was possible due to the high vertical resolution, especially in the upper 300 m.

The mixed-layer time series from the mooring was compared to the mixed-layer depths determined using measurements from the Argo float (Figure 4.9). Despite the drift of the float, the mixed-layer depth compared relatively well, especially for the first set of Argo profiles when it was within 12 km from the mooring. The mixed-layer time series from the Argo float were determined from both a temperature-difference criterion and a density-difference criterion. The first method was the same as used for the mooring, and gave the most similar time series (Fig. 4.10). This comparison strengthened the mixed-layer time series estimated from the mooring data.

The mixed layer in winter 2016-17 reached approximately 400 m depth, with a maximum density of $\sigma_\theta = 28.02\,\mathrm{kg/m^3}$, almost sufficiently dense to supply the densest part of the overflow. In winter 2017-18 the mixed layer reached approximately 300 m depth, with a maximum density of $\sigma_\theta = 27.97\,\mathrm{kg/m^3}$. Hence, sufficiently dense water to supply the overflow across the GSR ($\sigma_\theta > 27.8\,\mathrm{kg/m^3}$), and therefore also the deepest limb of the AMOC was ventilated in both winters.

The findings from the first winter agree with observations from glider transects in late February 2016, west of the Eggvin Offset. In this region the mixed-layer depth was estimated to 400 m with a density of $\sigma_\theta = 28.01\,\mathrm{kg/m^3}$ to $28.02\,\mathrm{kg/m^3}$ (Våge *et al.*, 2018), the same as the densest mixed layers observed in the Eggvin Offset the following year. The mixed-layer temperature from February 2016 and winter 2016-17 was also in the same range [-0.2°C to -0.4°C]. The mixed layer in winter 2017-18 was never as cold and dense. Lack of adequate cooling to obtain a higher density in the latter winter may be why it never achieved as deep mixed layers as the previous winters.

5.3 Comparison of winter 2016-17 and winter 2017-18

Among the most visible findings from this study was the differences between the two winters. The water in winter 2016-17 was in general colder and had deeper mixed layers than winter 2017-18. Preconditioning of the upper water layer occured throughout fall in both years, until the mixed layers rapidly deepened early in winter, down to 200 m in the first winter and 100 m in the second winter (Fig. 4.3). The first winter had a substantial cooling period during fall and early winter, while the cooling in that time period for the second winter was more moderate (Fig. 4.4). The strong cooling in winter 2016-17 continued over the late-winter months, from ca. 0.1°C to − 1.0°C, while the mixed-layer temperature in winter 2017-18 was never much colder than 0°C.

The differences became even more evident later in winter. The cooling ended in April the first winter and in March the following year. The water started to warm already in April in the second winter. A result of this difference in cooling/warming was observed in the mixed-layer evolution of the two winters. The rapid cooling seen from January to March resulted in a mixed-layer depth of 300 m the first winter, while the second winter underwent a more moderate cooling, which resulted in a mixed-layer depth of ca. 200 m. The first winter continued to cool from March to April, which caused even deeper mixed layers, ca. 400 m, while the latter winter started to warm and reached shallower depths in the same time period, ca. 175 m (Fig. 4.3).

The cooling/warming and the depths of the mixed layers can be linked to the atmospheric forcing. While strong northerly winds were observed in both years from November to January (not shown), the large-scale wind pattern changed in the second winter. Strong southerly winds dominated, not just the Eggvin Offset area, but the entire Nordic Seas and north of Fram Strait throughout February 2018 (Fig. 4.16b). These southerly winds brought warm subtropical-origin air masses toward the Eggvin Offset. Additionally, the northerly winds were in general weaker this winter compared to winter 2016-17. These factors help explain why winter 2017-18 was warmer, had shallower mixed layers and weaker atmospheric heat fluxes than winter 2016-17.

The unusual wind pattern in February 2018 is comparable with the strong southerly winds

that occupied the central and eastern Nordic Seas during the extraordinary heating event in December 2015 (Section 2.3; Moore, 2016). This event caused a significant warming adjacent to the North Pole over a couple of days and reduced sea ice cover in the area. Moore (2016) suggested that in addition to the long-term warming of the North Pole, other changes have resulted in an easier pathway for cyclones to excess the northern area. These are changes linked to the arctic amplification: enhanced warming at high northern latitudes, causing sea ice loss, warmer and moister air masses, and changes in the large-scale wind pattern in the region. The description Moore (2016) presented can be linked to the reduction of sea ice in the Nordic Seas and the midwinter warming together with southerly winds in February 2018.

In addition to the contribution of the southerly winds to the less extent of sea ice the second winter is the strength of the northerly winds in the northern part of the Nordic Seas. These large-scale winds are suggested to be related to the sea ice transport from the Arctic Ocean into the Nordic Seas (Langehaug *et al.*, prep). Weak northerly winds in this area during the winter 2017-18 are therefore considered to partly explain the less sea ice extent.

All of these factors contributed to the difference between the two winters, and they are all linked together. To understand the importance of the sea ice, its distance to the mooring was investigated along with the atmospheric heat fluxes. The strongest heat fluxes were observed approximately at, or just offshore of, the sea ice edge (Fig. 4.22), which agrees with a previous study in this area (Papritz and Spengler, 2017). The sea ice was closer to the mooring, there were stronger heat fluxes, stronger northerlies and the mixed layers were colder and deeper in the first winter compared to the following winter.

Furthermore, the sea ice extent in the Nordic Seas has been substantially reduced over the past century (Moore *et al.*, 2015). The sea ice loss has occured mostly in the southwestern Nordic Seas, which may be very critical for the formation of deep water in the Iceland Sea. Deep-water formation (with $\sigma_\theta \geq 28.03\,\mathrm{kg/m^3}$) does not occur in the Iceland Sea nowadays, but there may have been periods in the past when the sea ice extended all the way to the Iceland Sea gyre. In that case, the Iceland Sea gyre must have had a more important role in the formation of dense DSOW. Lack of wintertime data in the region prevents us from knowing this for sure (Swift *et al.*,

1980).

Moore *et al.* (2015) found that the heat fluxes were reduced by more than 50% from 1955 to 2015 in the Iceland Sea gyre. The winter mean heat flux was -50 W/m^2 in 2015 (Moore *et al.*, 2015). This value is comparable to the mean heat flux in winter 2017-18 in the Eggvin Offset. The winter mean heat flux found in the Eggvin Offset the first winter was, on the other hand, more comparable with the observations from winter 2015-16 in the western Iceland Sea (-120 W/m^2, Våge *et al.*, 2018). The region observed in Våge *et al.* (2018) was farther to the west than the Eggvin Offset and therefore also the Iceland Sea gyre, thus closer to the sea ice edge and exposed to colder air masses. These comparisons suggest that when the sea ice edge is near, strong heat fluxes are observed, while when the sea ice edge is farther west, the heat fluxes are weaker.

5.4 Dense water transport through the Eggvin Offset

The hypothesis for this thesis was that the Eggvin Offset is an important passage for dense water between the Iceland and Greenland Seas. If this was the case, and if supported by available observations, water advected through the Eggvin Offset, and dense water formed in this channel, would have been a substantial source to the NIJ. However, the velocity measurements from the Eggvin Offset Mooring did not support this hypothesis.

The velocities were relatively weak, as seen from the mooring data and the CTD sections across the channel at different times (Figs. 4.24 and 4.25). The velocities observed from the mooring data were overall directed eastward, especially from December to April for both years and at intermediate and great depths. (Fig. 4.23). The surface layer, on the other hand, was more variable and directed towards the west/northwest. This agrees with the theory of Ekman transport that is perpendicular and at right hand-side of the large-scale winds, which are directed southward in this case.

The velocities were found to be relatively uniform and barotrophic along the southern slope in the channel, where the Eggvin Offset Mooring was deployed (Fig. 4.25). This indicated that

the mooring could represent the southern slope in the channel, from the beginning of the slope to the local maximum depth, 21 km farther north.

The general statement by Brown (2016), that the water flows with shallower water at right-hand side on the Northern Hemisphere, together with the theory of geostrophy and conserved potential vorticity (Marshall and Plumb, 2016), was supported by the mean direction of the velocities from the mooring. The velocities were directed east, towards the Iceland Sea (Section 3.7). Additionally, the Argo float that drifted at 200 m depth from February to May 2018, floated through the channel along the southern slope, eastward, into the Iceland Sea (Fig. 3.2). This strengthens the argument of an eastern flow through the channel.

The above assumptions and considerations are rough, and only used in order to get an indication of the dense-water transport through the channel. The large errors associated with the width of the transports were assessed by estimating minimum and maximum transports. Finally, the transports in the Eggvin Offset were not particularly high, 0.013 Sv [0.007 Sv to 0.015 Sv] for the mixed layer and 0.072 Sv [0.024 Sv to 0.105 Sv] for the deeper transport, compared to the overall mean transport of the NIJ, which has an average transport of 1.4 Sv ± 0.1 Sv (Semper *et al.*, 2019). However, the transport estimates in the Eggvin Offset are significantly different from zero, and the deep-layer transport could potentially contribute with 5% of the NIJ.

Chapter 6

Conclusion

This study has expanded our knowledge of water transformation and circulation in the sparsely sampled northwestern Iceland Sea. Open-ocean convection was observed during both winters the Eggvin Offset Mooring was deployed, and the wintertime mixed layers became sufficiently dense to contribute to the DSOW. Sufficiently dense water to supply the NIJ, and hence the densest component of the DSOW, was not formed in the Eggvin Offset, but almost during the first winter. Such dense water was, however, observed at intermediate and greater depths.

Among the major findings from this study are the differences between winter 2016-17 and winter 2017-18. During the first winter, the mixed-layer depth reached 400 m, while in the following winter it only reached 300 m. The first winter was also colder, had stronger northerly winds, stronger flow, the mooring was closer to the sea ice edge, and it had twice as strong turbulent heat fluxes than the second winter.

Hence, the differences of the water hydrography between the two winters can be explained by the change in the large-scale wind pattern. Strong southerly winds dominated the region in February 2018, which carried warmer air masses towards the Eggvin Offset, and the winter mean northerly winds were weak, especially in the northern region of the Nordic Seas (Fig. 4.16). Both of these wind patterns are linked to sea ice retreat (Section 2.3; Moore, 2016; Langehaug *et al.*, prep). The less extent of sea ice causes weaker heat fluxes in the Eggvin Offset, and thereby less cooling and shallower mixed layers.

Another important feature affecting the evolution of the mixed layer was the position of the Polar Front. The Polar Front, or the lateral extension of Polar Surface Water, was observed to migrate seasonally. Its position was further linked to the large-scale winds and the preconditioning of the water column in the Eggvin Offset.

The transports estimated through Eggvin Offset were significantly different from zero, 0.013 Sv [0.007 Sv to 0.015 Sv] in the mixed layer and 0.072 Sv [0.024 Sv to 0.105 Sv] at depth, but of no significant magnitude. Despite observations of overflow water formed in the channel, the velocities were too low to make the channel an important source to the DSOW, and thereby, to the lower limb of the AMOC. If the period August 2016 to June 2018 is representative for a longer time period, the Eggvin Offset is neither an important pathway, nor source, of dense water to the DSOW.

Chapter 7

Future work

In this study, the oceanic and atmospheric heat fluxes were compared at different stages of the mixed-layer evolution, and some cold-air outbreaks were identified (Figs. 4.18 and 4.19). This can be studied in much more detail, due to the high temporal resolution from the 8 m moored instrument and the hourly ERA5 reanalysis data. A further study of this aspect might hopefully enhance our understanding of the oceanic response to atmospheric forcing in this region. Additionally, it would be of interest to investigate the link between the oceanic heat fluxes, mixed-layer evolution, and the Polar Mesoscale Cyclones (PMC) that occur frequently in the area (Linders, 2009; Condron and Renfrew, 2013).

Case studies of different cold-air outbreak events and corresponding oceanic behavior could also be of interest. For example, 67 PMCs events were observed at or nearby the Eggvin Offset in the time period the mooring was deployed (Denis Sergeev, 2019, personal communication). Nevertheless, a general study of the impact PMCs have on the mixed-layer depths over the winter would be an interesting study. What is the role of the PMCs in preconditioning and cooling the water? Are they more important than the distance to the sea ice edge, or the large-scale wind system? The ongoing global warming might change the track of the PMCs, will that impact the formation of overflow water in the western Nordic Seas?

The lateral and seasonal cycle of the Polar Front is important in order to precondition the water before open-ocean convection could take place. Is it only the northerly winds that impact

the lateral extent of the Polar Front? And, what impact does its position have on the deep-water formation in the Iceland and Greenland Seas? Is much freshwater mixed into the gyres? What amount of surface water is moved east and west with seasons?

The transports in the Eggvin Offset were relatively small. So, when suggested that this channel was not the major connector between the Greenland and Iceland Seas, where does the dense water at depth in the Iceland Sea originate from? Or moreover, where is the dense water in the NIJ formed and how is it transported southward from the Greenland Sea? Eggvin Offset being ticked off the box, at least based on the presented observations, a future study will be to investigate other channels that connect the Greenland to the Iceland Sea.

Bibliography

Amante C, Eakins BW. 2009. ETOPO1 arc-minute global relief model: procedures, data sources and analysis .

Bourke RH, Paquette RG, Blythe RF. 1992. The Jan Mayen current of the Greenland Sea. *Journal of Geophysical Research: Oceans* **97**(C5): 7241–7250.

Brakstad A, Våge K, Håvik L, Moore G. 2019. Water mass transformation in the Greenland Sea during the period 1986–2016. *Journal of Physical Oceanography* **49**(1): 121–140.

Brown J. 2016. *Ocean circulation: prepared by an Open University course team*. Elsevier.

Chafik L, Rossby T. 2019. Volume, heat, and freshwater divergences in the subpolar North Atlantic suggest the Nordic Seas as key to the state of the meridional overturning circulation. *Geophysical Research Letters* **46**(9): 4799–4808.

Condron A, Renfrew IA. 2013. The impact of polar mesoscale storms on northeast Atlantic Ocean circulation. *Nature Geoscience* **6**(1): 34.

Copernicus Climate Change Service (C3S). 2017. ERA5: Fifth generation of ECMWF atmospheric reanalyses of the global climate. URL https://cds.climate.copernicus.eu/cdsapp#!/home.

Darelius E, Fer I, Quadfasel D. 2011. Faroe Bank Channel overflow: mesoscale variability. *Journal of Physical Oceanography* **41**(11): 2137–2154.

Dickson RR, Brown J. 1994. The production of North Atlantic Deep Water: Sources, rates, and pathways. *Journal of Geophysical Research* **99**: 12.

Dickson RR, Meincke J, Malmberg SA, Lee AJ. 1988. The "great salinity anomaly" in the northern North Atlantic 1968–1982. *Progress in Oceanography* **20**(2): 103–151.

Eldevik T, Nilsen JEØ, Iovino D, Anders Olsson K, Sandø AB, Drange H. 2009. Observed sources and variability of Nordic Seas overflow. *Nature Geoscience* **2**(6): 406–410, doi:10.1038/ngeo518, URL http://dx.doi.org/10.1038/ngeo518.

Furevik T, Mauritzen C, Ingvaldsen R. 2007. The flow of Atlantic water to the Nordic Seas and Arctic Ocean. In: *Arctic alpine ecosystems and people in a changing environment*, Springer, pp. 123–146.

Gebbie G, Huybers P. 2010. Total matrix intercomparison: A method for determining the geometry of water-mass pathways. *Journal of Physical Oceanography* **40**(8): 1710–1728.

Hansen C, Skern-Mauritzen M, van der Meeren G, Jähkel A, Drinkwater K. 2016. Set-up of the Nordic and Barents Seas (NoBa) Atlantis model .

Harden B, Renfrew I, Petersen G. 2011. A climatology of wintertime barrier winds off southeast Greenland. *Journal of Climate* **24**(17): 4701–4717.

Harden BE, Pickart RS, Valdimarsson H, Våge K, de Steur L, Richards C, Bahr F, Torres D, Børve E, Jónsson S, *et al.* 2016. Upstream sources of the Denmark Strait Overflow: Observations from a high-resolution mooring array. *Deep Sea Research Part I: Oceanographic Research Papers* **112**: 94–112.

Håvik L, Pickart RS, Våge K, Torres D, Thurnherr AM, Beszczynska-Möller A, Walczowski W, von Appen WJ. 2017. Evolution of the East Greenland Current from Fram Strait to Denmark Strait: synoptic measurements from summer 2012. *Journal of Geophysical Research: Oceans* **122**(3): 1974–1994.

Jonsson S, Valdimarsson H. 2004. A new path for the Denmark Strait Overflow Water from the Iceland Sea to Denmark Strait. *Geophysical Research Letters* **31**(3).

Köhl A, Käse RH, Stammer D, Serra N. 2007. Causes of changes in the Denmark Strait overflow. *Journal of physical oceanography* **37**(6): 1678–1696.

Langehaug HR, Våge K, Brakstad A, Jeansson E, Iliicak M. in prep. Seasonal and interannual variability in freshwater transport to the deep basins of the Nordic Seas in a forced global ocean-sea ice model.

Lenton T, Held H, Kriegler E, Hall J, Lucht W, Rahmstorf S, Schellnhuber H. 2008. Tipping elements in the Earth's climate system. *PNAS; Proceedings of the National Academy of Sciences* **105**(6): 1786–1793.

Linders T. 2009. Polar low interaction with the ocean .

Malmberg SA, Jónsson S. 1997. Timing of deep convection in the Greenland and Iceland Seas. *ICES Journal of Marine Science* **54**(3): 300–309.

Marshall J, Plumb RA. 2016. *Atmosphere, ocean and climate dynamics: an introductory text*. Academic Press.

Marshall J, Schott F. 1999. Open-ocean convection: Observations, theory, and models. *Reviews of Geophysics* **37**(1): 1–64.

Mastropole D, Pickart RS, Valdimarsson H, Våge K, Jochumsen K, Girton J. 2017. On the hydrography of Denmark Strait. *Journal of Geophysical Research: Oceans* **122**(1): 306–321.

Mauritzen C. 1996. Production of dense overflow waters feeding the North Atlantic across the Greenland-Scotland Ridge. Part 1: Evidence for a revised circulation scheme. *Deep Sea Research Part I: Oceanographic Research Papers* **43**(6): 769–806.

McDougall TJ, Barker PM. 2011. Getting started with TEOS-10 and the Gibbs Seawater (GSW) oceanographic toolbox. *SCOR/IAPSO WG* **127**: 1–28.

Messias MJ, Watson A, Johannessen T, Oliver K, Olsson K, Fogelqvist E, Olafsson J, Bacon S, Balle J, Bergman N, *et al.* 2008. The Greenland Sea tracer experiment 1996–2002: horizontal mixing and transport of Greenland Sea intermediate water. *Progress in Oceanography* **78**(1): 85–105.

Moore G. 2012. A new look at Greenland flow distortion and its impact on barrier flow, tip jets and coastal oceanography. *Geophysical research letters* **39**(22).

Moore G. 2016. The December 2015 North Pole warming event and the increasing occurrence of such events. *Scientific Reports* **6**: 39 084.

Moore GWK, Våge K, Pickart RS, Renfrew IA. 2015. Decreasing intensity of open-ocean convection in the Greenland and Iceland seas. *Nature Climate Change* **5**(9): 877.

Nilsen JEØ, Falck E. 2006. Variations of mixed layer properties in the Norwegian Sea for the period 1948–1999. *Progress in Oceanography* **70**(1): 58–90.

Østerhus S, Woodgate R, Turrell B, Quadfasel D, Moritz M, Lee CM, Johnson C, Hansen B, Curry B, Cunningham S, *et al.* 2019. Arctic Mediterranean exchanges: a consistent volume budget and trends in transports from two decades of observations .

Papritz L, Spengler T. 2017. A Lagrangian climatology of wintertime cold air outbreaks in the Irminger and Nordic Seas and their role in shaping air–sea heat fluxes. *Journal of Climate* **30**(8): 2717–2737.

Pickart RS, Spall MA, Torres DJ, Våge K, Valdimarsson H, Nobre C, Moore G, Jonsson S, Mastropole D. 2017. The North Icelandic Jet and its relationship to the North Icelandic Irminger Current. *Journal of Marine Research* **75**(5): 605–639.

Renfrew IA, Moore G. 1999. An extreme cold-air outbreak over the Labrador Sea: Roll vortices and air–sea interaction. *Monthly Weather Review* **127**(10): 2379–2394.

Renfrew IA, Pickart RS, Våge K, Moore GW, Bracegirdle TJ, Elvidge AD, Jeansson E, Lachlan-Cope T, McRaven LT, Papritz L, *et al.* 2019. The Iceland Greenland Seas Project. *Bulletin of the American Meteorological Society* (2019).

Rudels B, Björk G, Nilsson J, Winsor P, Lake I, Nohr C. 2005. The interaction between waters from the Arctic Ocean and the Nordic Seas north of Fram Strait and along the East Greenland Current: results from the Arctic Ocean-02 Oden expedition. *Journal of Marine Systems* **55**(1-2): 1–30.

Rudels B, Fahrbach E, Meincke J, Budéus G, Eriksson P. 2002. The East Greenland Current and its contribution to the Denmark Strait overflow. *ICES Journal of Marine Science* **59**(6): 1133–1154.

Scheffer M, Carpenter S, Foley JA, Folke C, Walker B. 2001. Catastrophic shifts in ecosystems. *Nature* **413**(6856): 591.

Semper S, Våge K, Pickart RS, Valdimarsson H, Torres DJ, Jónsson S. 2019. The emergence of the North Icelandic Jet and its evolution from northeast Iceland to Denmark Strait. *Journal of Physical Oceanography* **49**(10): 2499–2521.

Swift JH, Aagaard K. 1981. Seasonal transitions and water mass formation in the Iceland and Greenland Seas. *Deep Sea Research Part A. Oceanographic Research Papers* **28**(10): 1107 – 1129, doi:https://doi.org/10.1016/0198-0149(81)90050-9, URL http://www.sciencedirect.com/science/article/pii/0198014981900509.

Swift JH, Aagaard K, Malmberg SA. 1980. The contribution of the Denmark strait overflow to the deep North Atlantic. *Deep Sea Research Part A. Oceanographic Research Papers* **27**(1): 29 – 42, doi:https://doi.org/10.1016/0198-0149(80)90070-9, URL http://www.sciencedirect.com/science/article/pii/0198014980900709.

Tan P, Breivik AJ, Trønnes RG, Mjelde R, Azuma R, Eide S. 2017. Crustal structure and origin of the Eggvin Bank west of Jan Mayen, NE Atlantic. *Journal of Geophysical Research: Solid Earth* **122**(1): 43–62.

Tanhua T, Olsson KA, Jeansson E. 2005. Formation of Denmark Strait Overflow Water and its hydro-chemical composition. *Journal of Marine Systems* **57**(3-4): 264–288.

Våge K, Moore GWK, Jónsson S, Valdimarsson H. 2015. Water mass transformation in the Iceland Sea. *Deep Sea Research Part I: Oceanographic Research Papers* **101**: 98–109.

Våge K, Papritz L, Håvik L, Spall MA, Moore GWK. 2018. Ocean convection linked to the recent ice edge retreat along east Greenland. *Nature communications* **9**(1): 1287.

Våge K, Pickart RS, Spall MA, Moore G, Valdimarsson H, Torres DJ, Erofeeva SY, Nilsen JEØ. 2013. Revised circulation scheme north of the Denmark Strait. *Deep Sea Research Part I: Oceanographic Research Papers* **79**: 20–39.

Våge K, Pickart RS, Spall MA, Valdimarsson H, Jónsson S, Torres DJ, Østerhus S, Eldevik T. 2011. Significant role of the North Icelandic Jet in the formation of Denmark Strait Overflow Water. *Nature Geoscience* **4**(10): 723.

Voet G, Quadfasel D, Mork KA, Søiland H. 2010. The mid-depth circulation of the Nordic Seas derived from profiling float observations. *Tellus A: Dynamic Meteorology and Oceanography* **62**(4): 516–529.